8 Bottom hadron decays and mixings

Authors: Y. Aoki, M. Della Morte, E. Lunghi, S. Meinel, C. Monahan, S. Simula, A. Vaquero

The (semi)leptonic decay and mixing processes of $B_{(s)}$ mesons have been playing a crucial role in flavour physics. In particular, they contain important information for the investigation of the $b-d$ unitarity triangle in the Cabibbo-Kobayashi-Maskawa (CKM) matrix, and can be ideal probes of physics beyond the Standard Model. The charged-current decay channels $B^+ \to l^+\nu_l$ and $B^0 \to \pi^- l^+\nu_l$, where l^+ is a charged lepton with ν_l being the corresponding neutrino, are essential in extracting the CKM matrix element $|V_{ub}|$. Similarly, the B to $D^{(*)}$ semileptonic transitions can be used to determine $|V_{cb}|$. The flavour-changing neutral current (FCNC) processes, such as $B \to K^{(*)}\ell^+\ell^-$ and $B_{d(s)} \to \ell^+\ell^-$, occur only beyond the tree level in weak interactions and are suppressed in the Standard Model. Therefore, these processes can be sensitive to new physics, since heavy particles can contribute to the loop diagrams. They are also suitable channels for the extraction of the CKM matrix elements involving the top quark that can appear in the loop. The decays $B \to D^{(*)}\ell\nu$ and $B \to K^{(*)}\ell\ell$ can also be used to test lepton flavour universality by comparing results for $\ell = e$, μ and τ. In particular, anomalies have been seen in the ratios $R(D^{(*)}) = \mathcal{B}(B \to D^{(*)}\tau\nu)/\mathcal{B}(B \to D^{(*)}\ell\nu)_{\ell=e,\mu}$ and $R(K^{(*)}) = \mathcal{B}(B \to K^{(*)}\mu\mu)/\mathcal{B}(B \to K^{(*)}ee)$. In addition, the neutral $B_{d(s)}$-meson mixings are FCNC processes and are dominated by the 1-loop "box" diagrams containing the top quark and the W bosons. Thus, using the experimentally measured neutral $B^0_{d(s)}$-meson oscillation frequencies, $\Delta M_{d(s)}$, and the theoretical calculations for the relevant hadronic mixing matrix elements, one can obtain $|V_{td}|$ and $|V_{ts}|$ in the Standard Model.

At the Large Hadron Collider, decays of b quarks can also be probed with Λ_b and other bottom baryons, which can provide complementary constraints on physics beyond the Standard Model. The most important processes are the charged-current decays $\Lambda_b \to p\ell\bar{\nu}$ and $\Lambda_b \to \Lambda_c\ell\bar{\nu}$, and the neutral-current decay $\Lambda_b \to \Lambda\ell^+\ell^-$.

Accommodating the light quarks and the b quark simultaneously in lattice-QCD computations is a challenging endeavour. To incorporate the pion and the b hadrons with their physical masses, the simulations have to be performed using the lattice size $\hat{L} = L/a \sim \mathcal{O}(10^2)$, where a is the lattice spacing and L is the physical (dimensionful) box size. The most ambitious calculations are now using such volumes; however, many ensembles are smaller. Therefore, in addition to employing Chiral Perturbation Theory for the extrapolations in the light-quark mass, current lattice calculations for quantities involving b hadrons often make use of effective theories that allow one to expand in inverse powers of m_b. In this regard, two general approaches are widely adopted. On the one hand, effective field theories such as Heavy-Quark Effective Theory (HQET) and Nonrelativistic QCD (NRQCD) can be directly implemented in numerical computations. On the other hand, a relativistic quark action can be improved *à la* Symanzik to suppress cutoff errors, and then re-interpreted in a manner that is suitable for heavy-quark physics calculations. This latter strategy is often referred to as the method of the Relativistic Heavy-Quark Action (RHQA). The utilization of such effective theories inevitably introduces systematic uncertainties that are not present in light-quark calculations. These uncertainties can arise from the truncation of the expansion in constructing the effective theories (as in HQET and NRQCD), or from more intricate cutoff effects (as in NRQCD and RHQA). They can also be introduced through more complicated renormalization procedures which often lead to significant systematic effects in matching the lattice operators to their continuum counterparts. For instance, due to the use of different actions for the heavy and

the light quarks, it is more difficult to construct absolutely normalized bottom-light currents.

Complementary to the above "effective theory approaches", another popular method is to simulate the heavy and the light quarks using the same (normally improved) lattice action at several values of the heavy-quark mass m_h with $am_h < 1$ and $m_h < m_b$. This enables one to employ HQET-inspired relations to extrapolate the computed quantities to the physical b mass. When combined with results obtained in the static heavy-quark limit, this approach can be rendered into an interpolation, instead of extrapolation, in m_h. The discretization errors are the main source of the systematic effects in this method, and very small lattice spacings are needed to keep such errors under control.

In recent years, it has also been possible to perform lattice simulations at very fine lattice spacings and treat heavy quarks as fully relativistic fermions without resorting to effective field theories. Such simulations are, of course, very demanding in computing resources.

Because of the challenge described above, the efforts that have been made to obtain reliable, accurate lattice-QCD results for physics of the b quark have been enormous. These efforts include significant theoretical progress in formulating QCD with heavy quarks on the lattice. This aspect is briefly reviewed in Appendix A.1.3 of FLAG 19 [1].

In this section, we summarize the results of the B-meson leptonic decay constants, the neutral B-mixing parameters, and the semileptonic form factors of B mesons and Λ_b baryons, from lattice QCD. To focus on the calculations that have strong phenomenological impact, we limit the review to results based on modern simulations containing dynamical fermions with reasonably light pion masses (below approximately 500 MeV).

Following our review of $B_{(s)}$-meson leptonic decay constants, the neutral B-meson mixing parameters, and semileptonic form factors, we then interpret our results within the context of the Standard Model. We combine our best-determined values of the hadronic matrix elements with the most recent experimentally-measured branching fractions to obtain $|V_{ub}|$ and $|V_{cb}|$, and compare these results to those obtained from inclusive semileptonic B decays.

8.1 Leptonic decay constants f_B and f_{B_s}

The B- and B_s-meson decay constants are crucial inputs for extracting information from leptonic B decays. Charged B mesons can decay to a lepton-neutrino final state through the charged-current weak interaction. On the other hand, neutral $B_{d(s)}$ mesons can decay to a charged-lepton pair via a flavour-changing neutral current (FCNC) process.

In the Standard Model, the decay rate for $B^+ \to \ell^+\nu_\ell$ is described by a formula identical to Eq. (170), with $D_{(s)}$ replaced by B, and the relevant CKM matrix element V_{cq} replaced by V_{ub},

$$\Gamma(B \to \ell\nu_\ell) = \frac{m_B}{8\pi} G_F^2 f_B^2 |V_{ub}|^2 m_\ell^2 \left(1 - \frac{m_\ell^2}{m_B^2}\right)^2 . \tag{203}$$

The only two-body charged-current B-meson decay that has been observed so far is $B^+ \to \tau^+\nu_\tau$, which has been measured by the Belle and Babar collaborations [2, 3]. Both collaborations have reported results with errors around 20%. These measurements can be used to determine $|V_{ub}|$ when combined with lattice-QCD predictions of the corresponding decay constant.

Neutral $B_{d(s)}$-meson decays to a charged-lepton pair $B_{d(s)} \to l^+l^-$ is a FCNC process, and can only occur at one loop in the Standard Model. Hence these processes are expected to be rare, and are sensitive to physics beyond the Standard Model. The corresponding expression

for the branching fraction has the form

$$B(B_q \to \ell^+\ell^-) = \tau_{B_q} \frac{G_F^2}{\pi} Y \left(\frac{\alpha}{4\pi \sin^2 \Theta_W}\right)^2 m_{B_q} f_{B_q}^2 |V_{tb}^* V_{tq}|^2 m_\ell^2 \sqrt{1 - 4\frac{m_\ell^2}{m_B^2}} \,, \tag{204}$$

where the light quark $q = s$ or d, and the function Y includes NLO QCD and electro-weak corrections [4, 5]. Evidence for the $B_s \to \mu^+\mu^-$ decay was first observed by the CMS and the LHCb collaborations, and a combined analysis was presented in 2014 in Ref. [6]. In 2020, the ATLAS, CMS and LHCb collaborations reported their measurements from a preliminary combined analysis as [7]

$$\begin{aligned} B(B_d \to \mu^+\mu^-) &< (1.9) \times 10^{-10} \text{ at } 95\% \text{ CL}, \\ B(B_s \to \mu^+\mu^-) &= (2.69^{+0.37}_{-0.35}) \times 10^{-9}, \end{aligned} \tag{205}$$

which are compatible with the Standard Model predictions within approximately 2 standard deviations [8]. We note that the errors of these results are currently too large to enable a precise determination of $|V_{td}|$ and $|V_{ts}|$.

The decay constants f_{B_q} (with $q = u, d, s$) parameterize the matrix elements of the corresponding axial-vector currents $A^\mu_{bq} = \bar{b}\gamma^\mu\gamma^5 q$ analogously to the definition of f_{D_q} in Sec. 7.1:

$$\langle 0|A^\mu|B_q(p)\rangle = ip_B^\mu f_{B_q} \,. \tag{206}$$

For heavy-light mesons, it is convenient to define and analyse the quantity

$$\Phi_{B_q} \equiv f_{B_q}\sqrt{m_{B_q}} \,, \tag{207}$$

which approaches a constant (up to logarithmic corrections) in the $m_B \to \infty$ limit, because of heavy-quark symmetry. In the following discussion, we denote lattice data for Φ, and the corresponding decay constant f, obtained at a heavy-quark mass m_h and light valence-quark mass m_ℓ as $\Phi_{h\ell}$ and f_{hl}, to differentiate them from the corresponding quantities at the physical b- and light-quark masses.

The $SU(3)$-breaking ratio f_{B_s}/f_B is of phenomenological interest, because many systematic effects can be partially reduced in lattice-QCD calculations of this ratio. The discretization errors, heavy-quark mass tuning effects, and renormalization/matching errors may all be partially reduced. This $SU(3)$-breaking ratio is, however, still sensitive to the chiral extrapolation. Provided the chiral extrapolation is under control, one can then adopt f_{B_s}/f_B as an input in extracting phenomenologically-interesting quantities. In addition, it often happens to be easier to obtain lattice results for f_{B_s} with smaller errors than direct calculations of f_B. Therefore, one can combine the B_s-meson decay constant with the $SU(3)$-breaking ratio to calculate f_B. Such a strategy can lead to better precision in the computation of the B-meson decay constant, and has been adopted by the ETM [9, 10] and the HPQCD collaborations [11]. An alternative strategy, used in Ref. [12], is to obtain the B_s-meson decay constant by combining the D_s-meson decay constant with the ratio f_{B_s}/f_{D_s}.

It is clear that the decay constants for charged and neutral B mesons play different roles in flavour-physics phenomenology. Knowledge of the B^+-meson decay constant f_{B^+} is essential for extracting $|V_{ub}|$ from leptonic B^+ decays. The neutral B-meson decay constants f_{B^0} and f_{B_s} are inputs to searches for new physics in rare leptonic B^0 decays. In view of this, it is desirable to include isospin-breaking effects in lattice computations for these

quantities, and have results for f_{B^+} and f_{B^0}. With the increasing precision of recent lattice calculations, isospin splittings for B-meson decay constants can be significant, and will play an important role in the foreseeable future. A few collaborations have reported f_{B^+} and f_{B^0} separately by taking into account strong isospin effects in the valence sector, and estimated the corrections from electromagnetism. The $N_f = 2 + 1 + 1$ strong isospin-breaking effect was computed in HPQCD 13 [13] (see Tab. 41 in this subsection). However, since only unitary points (with equal sea- and valence-quark masses) were considered in HPQCD 13 [13], this procedure only correctly accounts for the effect from the valence-quark masses, while introducing a spurious sea-quark contribution. The decay constants f_{B^+} and f_{B^0} are also separately reported in FNAL/MILC 17 [14] by taking into account the strong-isospin effect. The new FNAL/MILC results were obtained by keeping the averaged light sea-quark mass fixed when varying the quark masses in their analysis procedure. Their finding indicates that the strong isospin-breaking effects, $f_{B^+} - f_B \sim 0.5$ MeV, could be smaller than those suggested by previous computations. One would have to take into account QED effects in the B-meson leptonic decay rates to properly use these results for extracting phenomenologically relevant information.[1] Currently, errors on the experimental measurements on these decay rates are still very large. In this review, we will therefore concentrate on the isospin-averaged result f_B and the B_s-meson decay constant, as well as the $SU(3)$-breaking ratio f_{B_s}/f_B.

The status of lattice-QCD computations for B-meson decay constants and the $SU(3)$-breaking ratio, using gauge-field ensembles with light dynamical fermions, is summarized in Tabs. 41 and 42, while Figs. 27 and 28 contain the graphical presentation of the collected results and our averages. Most results in these tables and plots have been reviewed in detail in FLAG 19 [1]. Here, we only describe the new results published after January 2019.

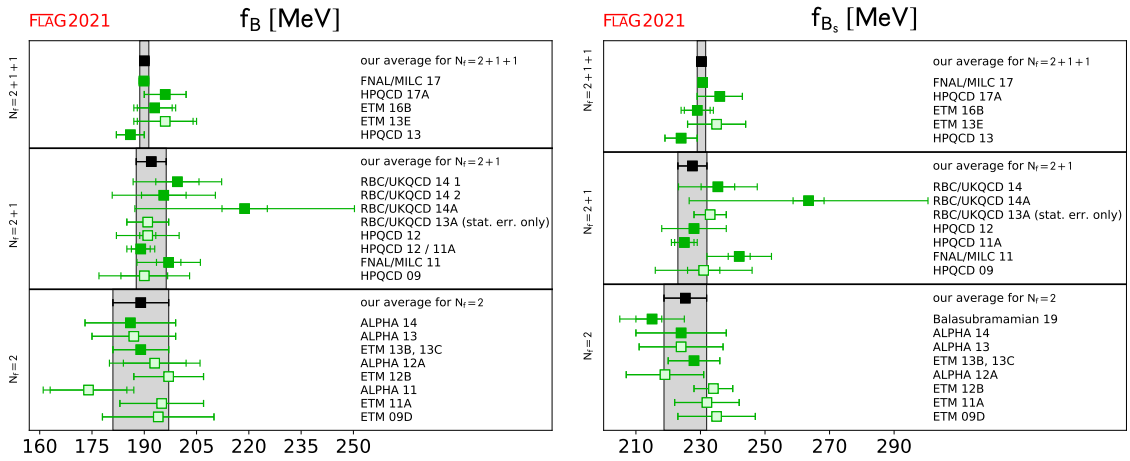

Figure 27: Decay constants of the B and B_s mesons. The values are taken from Tab. 41 (the f_B entry for FNAL/MILC 11 represents f_{B^+}). The significance of the colours is explained in Sec. 2. The black squares and grey bands indicate our averages in Eqs. (208), (211), (214), (209), (212) and (215).

One new $N_f = 2$ calculation of f_{B_s} has appeared after the publication of the previous FLAG review [1]. In Tab. 41, this result is labelled Balasubramamian 19 [12].

In Balasubramamian 19 [12], simulations at three values of the lattice spacing, $a = 0.0751$,

[1] See Ref. [15] for a strategy that has been proposed to account for QED effects.

Collaboration	Ref.	N_f	publication status	continuum extrapolation	chiral extrapolation	finite volume	renormalization/matching	heavy-quark treatment	f_{B^+}	f_{B^0}	f_B	f_{B_s}
FNAL/MILC 17	[14]	2+1+1	A	★	★	★	★	✓	189.4(1.4)	190.5(1.3)	189.9(1.4)	230.7(1.2)
HPQCD 17A	[16]	2+1+1	A	○	★	★	○	✓	–	–	196(6)	236(7)
ETM 16B	[10]	2+1+1	A	★	○	○	○	✓	–	–	193(6)	229(5)
ETM 13E	[17]	2+1+1	C	★	○	○	○	✓	–	–	196(9)	235(9)
HPQCD 13	[13]	2+1+1	A	○	★	★	○	✓	184(4)	188(4)	186(4)	224(5)
RBC/UKQCD 14	[18]	2+1	A	○	○	○	○	✓	195.6(14.9)	199.5(12.6)	–	235.4(12.2)
RBC/UKQCD 14A	[19]	2+1	A	○	○	○	○	✓	–	–	219(31)	264(37)
RBC/UKQCD 13A	[20]	2+1	C	○	○	○	○	✓	–	–	$191(6)^{\diamond}_{\text{stat}}$	$233(5)^{\diamond}_{\text{stat}}$
HPQCD 12	[11]	2+1	A	○	○	○	○	✓	–	–	191(9)	228(10)
HPQCD 12	[11]	2+1	A	○	○	○	○	✓	–	–	$189(4)^{\triangle}$	–
HPQCD 11A	[21]	2+1	A	★	○	★	★	✓	–	–	–	$225(4)^{\nabla}$
FNAL/MILC 11	[22]	2+1	A	○	○	★	○	✓	197(9)	–	–	242(10)
HPQCD 09	[23]	2+1	A	○	○	○	○	✓	–	–	$190(13)^{\bullet}$	$231(15)^{\bullet}$
Balasubramamian 19†	[12]	2	A	★	★	★	○	✓	–	–	–	$215(10)(2)(^{+2}_{-5})$
ALPHA 14	[24]	2	A	★	★	★	★	✓	–	–	186(13)	224(14)
ALPHA 13	[25]	2	C	★	★	★	★	✓	–	–	187(12)(2)	224(13)
ETM 13B, 13C‡	[9, 26]	2	A	★	○	★	○	✓	–	–	189(8)	228(8)
ALPHA 12A	[27]	2	C	★	★	★	★	✓	–	–	193(9)(4)	219(12)
ETM 12B	[28]	2	C	★	○	★	○	✓	–	–	197(10)	234(6)
ALPHA 11	[29]	2	C	★	○	★	★	✓	–	–	174(11)(2)	–
ETM 11A	[30]	2	A	★	○	★	○	✓	–	–	195(12)	232(10)
ETM 09D	[31]	2	A	★	○	○	○	✓	–	–	194(16)	235(12)

$^{\diamond}$Statistical errors only.
$^{\triangle}$Obtained by combining f_{B_s} from HPQCD 11A with f_{B_s}/f_B calculated in this work.
$^{\nabla}$This result uses one ensemble per lattice spacing with light to strange sea-quark mass ratio $m_\ell/m_s \approx 0.2$.
$^{\bullet}$This result uses an old determination of $r_1 = 0.321(5)$ fm from Ref. [32] that has since been superseded.
‡Obtained by combining f_{D_s}, updated in this work, with f_{B_s}/f_{D_s}, calculated in this work.
‡Update of ETM 11A and 12B.

Table 41: Decay constants of the B, B^+, B^0 and B_s mesons (in MeV). Here f_B stands for the mean value of f_{B^+} and f_{B^0}, extrapolated (or interpolated) in the mass of the light valence-quark to the physical value of m_{ud}.

0.0653 and 0.0483 fm were performed with nonperturbatively $\mathcal{O}(a)$-improved Wilson-clover fermions and the Wilson plaquette gauge action. The pion masses in this work range from 194 to 439 MeV, and the lattice sizes are between 2.09 and 4.18 fm. A key feature of this

Collaboration	Ref.	N_f	publication status	continuum extrapolation	chiral extrapolation	finite volume	renormalization/matching	heavy-quark treatment	f_{B_s}/f_{B^+}	f_{B_s}/f_{B^0}	f_{B_s}/f_B
FNAL/MILC 17	[14]	2+1+1	A	★	★	★	★	✓	1.2180(49)	1.2109(41)	–
HPQCD 17A	[16]	2+1+1	A	○	★	★	○	✓	–	–	1.207(7)
ETM 16B	[10]	2+1+1	A	★	○	○	○	✓	–	–	1.184(25)
ETM 13E	[17]	2+1+1	C	★	○	○	○	✓	–	–	1.201(25)
HPQCD 13	[13]	2+1+1	A	○	★	★	○	✓	1.217(8)	1.194(7)	1.205(7)
RBC/UKQCD 18A	[33]	2+1	P	★	★	★	★	✓	–	–	$1.1949(60)(^{+95}_{-175})$
RBC/UKQCD 14	[18]	2+1	A	○	○	○	○	✓	1.223(71)	1.197(50)	–
RBC/UKQCD 14A	[19]	2+1	A	○	○	○	○	✓	–	–	1.193(48)
RBC/UKQCD 13A	[20]	2+1	C	○	○	○	○	✓	–	–	$1.20(2)^{\diamond}_{\text{stat}}$
HPQCD 12	[11]	2+1	A	○	○	○	○	✓	–	–	1.188(18)
FNAL/MILC 11	[22]	2+1	A	○	○	★	○	✓	1.229(26)	–	–
RBC/UKQCD 10C	[34]	2+1	A	■	■	■	○	✓	–	–	1.15(12)
HPQCD 09	[23]	2+1	A	○	○	○	○	✓	–	–	1.226(26)
ALPHA 14	[24]	2	A	★	★	★	★	✓	–	–	1.203(65)
ALPHA 13	[25]	2	C	★	★	★	★	✓	–	–	1.195(61)(20)
ETM 13B, 13C†	[9, 26]	2	A	★	○	★	○	✓	–	–	1.206(24)
ALPHA 12A	[27]	2	C	★	★	★	★	✓	–	–	1.13(6)
ETM 12B	[28]	2	C	★	○	★	○	✓	–	–	1.19(5)
ETM 11A	[30]	2	A	○	○	★	○	✓	–	–	1.19(5)

$^{\diamond}$Statistical errors only.
†Update of ETM 11A and 12B.

Table 42: Ratios of decay constants of the B and B_s mesons (for details see Tab. 41).

calculation is the use of a variant of the ratio method [31], applied for the first time to Wilson-clover fermions. This variant is required because, in contrast to twisted-mass Wilson fermions, there is no simple relationship between the heavy quark pole mass and the bare quark mass. In the application of this approach to the B_s-decay constant, one first computes the quantity $\mathcal{F}_{hq} \equiv f_{hq}/M_{hq}$, where f_{hq} and M_{hq} are the decay constant and mass of the pseudoscalar meson composed of valence (relativistic) heavy quark h and light (or strange) quark q. The matching between the lattice and the continuum heavy-light currents for extracting the above f_{hq} is straightforward because the valence heavy quark is also described by Wilson-clover fermions. In the second step, the ratio $z_q(M_{hq}, \lambda) \equiv [\mathcal{F}_{hq} C_A^{\text{stat}}(M_{h'q}) M_{hq}^{3/2}]/[\mathcal{F}_{h'q} C_A^{\text{stat}}(M_{hq}) M_{h'q}^{3/2}]$ is calculated, where $C_A^{\text{stat}}(M_{hq})$ is the matching coefficient for the (hq)-meson decay constant

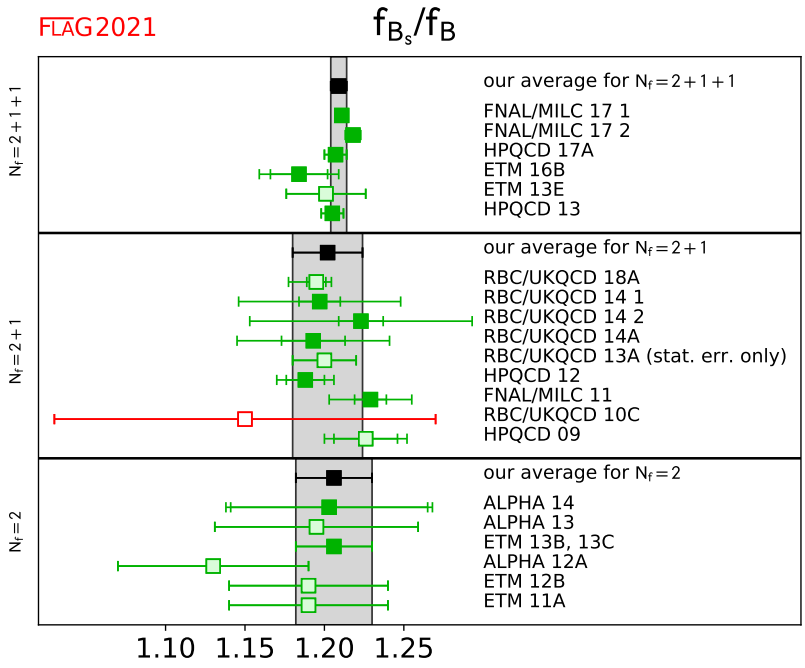

Figure 28: Ratio of the decay constants of the B and B_s mesons. The values are taken from Tab. 42. Results labelled as FNAL/MILC 17 1 and FNAL/MILC 17 2 correspond to those for f_{B_s}/f_{B^0} and f_{B_s}/f_{B^+} reported in FNAL/MILC 17. The significance of the colours is explained in Sec. 2. The black squares and grey bands indicate our averages in Eqs. (210), (213), and (216).

in QCD and its counterpart in HQET, and $M_{hq} = \lambda M_{h'q}$. The authors of Balasubramamian 19 [12] use the NNLO perturbative result of $C_A^{\rm stat}(M_{hq})$ [35–37] and $\lambda = 1.18$. By starting from a "triggering" point with the heavy-meson mass around that of the D_s meson, one can proceed with the calculations in steps, such that M_{hq} is increased by a factor of λ at each step. The authors simulate up to heavy-quark mass around 4.5 GeV, but observed significant $(aM_{H_s})^2$ cutoff effects on ensembles with lattice spacings $a = 0.0751$ and 0.0653 fm and so simulate up to 3.2 GeV on these lattices. In this formulation of the ratio method, the ratio obeys $z_q(M_{hq}, \lambda) \to 1/\sqrt{\lambda}$ in the limit $M_{hq} \to \infty$. Designing the computations in such a way that in the last step M_{hq} is equal to the physical B_s mass, one obtains $f_{B_{(s)}}/f_{D_{(s)}}$. Combining this ratio with results for $f_{D_{(s)}}$, updated with a third lattice spacing, the decay constant of the B_s meson can be extracted. The authors estimated the systematic uncertainty associated with their generic fit form, which combines chiral-continuum extrapolation with heavy quark discretization effects, and quote a single systematic uncertainty. The systematic uncertainty associated with scale-setting is estimated from f_{D_s}.

There have been no new $N_f = 2$ calculations of f_B or f_{B_s}/f_B. Therefore, our averages for these two cases stay the same as those in Ref. [1]. We update our average of f_{B_s} to include

the new calculation of Balasubramamian 19 [12]:

$$N_f = 2: \qquad f_B = 188(7)\ \text{MeV} \qquad \text{Refs. [9, 24]}, \tag{208}$$

$$N_f = 2: \qquad f_{B_s} = 225.3(6.6)\ \text{MeV} \qquad \text{Refs. [9, 12, 24]}, \tag{209}$$

$$N_f = 2: \qquad \frac{f_{B_s}}{f_B} = 1.206(0.023) \qquad \text{Refs. [9, 24]}. \tag{210}$$

One new $N_f = 2+1$ calculation of f_{B_s}/f_B was completed after the publication of the previous FLAG review [1]. In Tab. 42, this result is labelled RBC/UKQCD 18A [33].

The RBC/UKQCD collaboration presented in RBC/UKQCD 18A [33] the ratio of decay constants, f_{B_s}/f_B, using $N_f = 2+1$ dynamical ensembles generated using Domain Wall Fermions (DWF). Three lattice spacings, of $a = 0.114$, 0.0835 and 0.0727 fm, were used, with pion masses ranging from 139 to 431 MeV, and lattice sizes between 2.65 and 5.47 fm. Two different Domain Wall discretizations (Möbius and Shamir) have been used for both valence and sea quarks. These discretizations correspond to two different choices for the DWF kernel. The Möbius DWF are loosely equivalent to Shamir DWF at twice the extension in the fifth dimension [38]. The bare parameters for these discretizations were chosen to lie on the same scaling trajectory, to enable a combined continuum extrapolation. Heavy quark masses between the charm and approximately half the bottom quark mass were used, with a linear extrapolation in $1/m_H$ applied to reach the physical B_s mass, where m_H is the mass of the heavy meson used to set the heavy quark mass. For the central fit, the authors set the heavy quark mass through the pseudoscalar heavy-strange meson H_s, and estimate systematic uncertainties by comparing these results to those obtained with H a heavy-light meson or a heavy-heavy meson. For the quenched heavy quark Möbius DWF are always used, with a domain-wall height slightly different from the one adopted for light valence quarks. The choice helps to keep cutoff effects under control, according to the study in Ref. [39]. The chiral-continuum extrapolations are performed with a Taylor expansion in a^2 and $m_\pi^2 - (m_\pi^{\text{phys}})^2$ and the associated systematic error is estimated by varying the fit function to apply cuts in the pion mass. The corresponding systematic error is estimated as approximately 0.5%, which is roughly equal to the statistical uncertainty and to the systematic uncertainties associated with extrapolation to the physical m_{B_s} mass and with higher-order corrections to the static limit. These latter corrections take the form $\mathcal{O}(\Lambda^2/m_{B_s}^2)$. The error estimate comes from assuming the coefficient of such terms is up to five times larger than the fitted $\mathcal{O}(\Lambda/m_{B_s})$ coefficient. Isospin corrections and heavy-quark discretization effects are estimated to be less than 0.1%.

At time of writing, RBC/UKQCD 18A [33] has not been published and therefore is not included in our average. Thus, our averages for these quantities remain the same as in Ref. [1],

$$N_f = 2+1: \qquad f_B = 192.0(4.3)\ \text{MeV} \qquad \text{Refs. [11, 18, 19, 21, 22]}, \tag{211}$$

$$N_f = 2+1: \qquad f_{B_s} = 228.4(3.7)\ \text{MeV} \qquad \text{Refs. [11, 18, 19, 21, 22]}, \tag{212}$$

$$N_f = 2+1: \qquad \frac{f_{B_s}}{f_B} = 1.201(0.016) \qquad \text{Refs. [11, 18, 19, 22, 33]}. \tag{213}$$

No new $N_f = 2+1+1$ calculations of f_B, f_{B_s}/f_B or $f_{B_{(s)}}$ have appeared since the last

FLAG review. Therefore, our averages for these quantities remain the same as in Ref. [1],

$$N_f = 2+1+1: \qquad f_B = 190.0(1.3)\ \text{MeV} \qquad \text{Refs. [10, 13, 14, 16]}, \tag{214}$$

$$N_f = 2+1+1: \qquad f_{B_s} = 230.3(1.3)\ \text{MeV} \qquad \text{Refs. [10, 13, 14, 16]}, \tag{215}$$

$$N_f = 2+1+1: \qquad \frac{f_{B_s}}{f_B} = 1.209(0.005) \qquad \text{Refs. [10, 13, 14, 16]}. \tag{216}$$

The PDG presented averages for the $N_f = 2+1$ and $N_f = 2+1+1$ lattice-QCD determinations of the isospin-averaged f_B, f_{B_s} and f_{B_s}/f_B in 2020 [40]. The $N_f = 2+1$ and $N_f = 2+1+1$ lattice-computation results used in Ref. [40] are identical to those included in our current work, and the averages quoted in Ref. [40] are those determined in [1].

8.2 Neutral B-meson mixing matrix elements

Neutral B-meson mixing is induced in the Standard Model through 1-loop box diagrams to lowest order in the electroweak theory, similar to those for short-distance effects in neutral kaon mixing. The effective Hamiltonian is given by

$$\mathcal{H}_{\text{eff}}^{\Delta B=2,\text{SM}} = \frac{G_F^2 M_{\text{W}}^2}{16\pi^2}(\mathcal{F}_d^0 \mathcal{Q}_1^d + \mathcal{F}_s^0 \mathcal{Q}_1^s) + \text{h.c.}\,, \tag{217}$$

with

$$\mathcal{Q}_1^q = \left[\bar{b}\gamma_\mu(1-\gamma_5)q\right]\left[\bar{b}\gamma_\mu(1-\gamma_5)q\right], \tag{218}$$

where $q = d$ or s. The short-distance function $\mathcal{F}_q^0$ in Eq. (217) is much simpler compared to the kaon mixing case due to the hierarchy in the CKM matrix elements. Here, only one term is relevant,

$$\mathcal{F}_q^0 = \lambda_{tq}^2 S_0(x_t) \tag{219}$$

where

$$\lambda_{tq} = V_{tq}^* V_{tb}, \tag{220}$$

and where $S_0(x_t)$ is an Inami-Lim function with $x_t = m_t^2/M_W^2$, which describes the basic electroweak loop contributions without QCD [4]. The transition amplitude for B_q^0 with $q = d$ or s can be written as

$$\begin{aligned}\langle \bar{B}_q^0|\mathcal{H}_{\text{eff}}^{\Delta B=2}|B_q^0\rangle =& \frac{G_F^2 M_W^2}{16\pi^2}\left[\lambda_{tq}^2 S_0(x_t)\eta_{2B}\right] \\ &\times \left(\frac{\bar{g}(\mu)^2}{4\pi}\right)^{-\gamma_0/(2\beta_0)} \exp\left\{\int_0^{\bar{g}(\mu)} dg \left(\frac{\gamma(g)}{\beta(g)} + \frac{\gamma_0}{\beta_0 g}\right)\right\} \\ &\times \langle \bar{B}_q^0|Q_{\text{R}}^q(\mu)|B_q^0\rangle + \text{h.c.}\,,\end{aligned} \tag{221}$$

where $Q_{\text{R}}^q(\mu)$ is the renormalized four-fermion operator (usually in the NDR scheme of $\overline{\text{MS}}$). The running coupling $\bar{g}$, the β-function $\beta(g)$, and the anomalous dimension of the four-quark operator $\gamma(g)$ are defined in Eqs. (143) and (144). The product of μ-dependent terms on the second line of Eq. (221) is, of course, μ-independent (up to truncation errors arising from the use of perturbation theory). The explicit expression for the short-distance QCD correction factor η_{2B} (calculated to NLO) can be found in Ref. [41].

For historical reasons the B-meson mixing matrix elements are often parameterized in terms of bag parameters defined as

$$B_{B_q}(\mu) = \frac{\langle \bar{B}^0_q \left| Q^q_{\rm R}(\mu) \right| B^0_q \rangle}{\frac{8}{3} f^2_{B_q} m^2_{\rm B}} \ . \tag{222}$$

The renormalization group independent (RGI) B parameter $\hat{B}$ is defined as in the case of the kaon, and expressed to 2-loop order as

$$\hat{B}_{B_q} = \left(\frac{\bar{g}(\mu)^2}{4\pi} \right)^{-\gamma_0/(2\beta_0)} \left\{ 1 + \frac{\bar{g}(\mu)^2}{(4\pi)^2} \left[\frac{\beta_1\gamma_0 - \beta_0\gamma_1}{2\beta_0^2} \right] \right\} B_{B_q}(\mu) \ , \tag{223}$$

with β_0, β_1, γ_0, and γ_1 defined in Eq. (145). Note, as Eq. (221) is evaluated above the bottom threshold ($m_b < \mu < m_t$), the active number of flavours here is $N_f = 5$.

Nonzero transition amplitudes result in a mass difference between the CP eigenstates of the neutral B-meson system. Writing the mass difference for a B^0_q meson as Δm_q, its Standard Model prediction is

$$\Delta m_q = \frac{G_F^2 m_W^2 m_{B_q}}{6\pi^2} |\lambda_{tq}|^2 S_0(x_t) \eta_{2B} f^2_{B_q} \hat{B}_{B_q}. \tag{224}$$

Experimentally, the mass difference is determined from the oscillation frequency of the CP eigenstates. The frequencies are measured precisely with an error of less than a percent. Many different experiments have measured Δm_d, but the current average [40] is dominated by the LHCb experiment. For Δm_s the experimental average is again dominated by results from LHCb [40] and the precision reached is about one per mille. With these experimental results and lattice-QCD calculations of $f^2_{B_q}\hat{B}_{B_q}$, λ_{tq} can be determined. In lattice-QCD calculations the flavour $SU(3)$-breaking ratio

$$\xi^2 = \frac{f^2_{B_s} B_{B_s}}{f^2_{B_d} B_{B_d}} \tag{225}$$

can be obtained more precisely than the individual B_q-mixing matrix elements because statistical and systematic errors cancel in part. From ξ^2, the ratio $|V_{td}/V_{ts}|$ can be determined and used to constrain the apex of the CKM triangle.

Neutral B-meson mixing, being loop-induced in the Standard Model, is also a sensitive probe of new physics. The most general $\Delta B = 2$ effective Hamiltonian that describes contributions to B-meson mixing in the Standard Model and beyond is given in terms of five local four-fermion operators:

$$\mathcal{H}^{\Delta B=2}_{\rm eff,BSM} = \sum_{q=d,s} \sum_{i=1}^{5} C_i \mathcal{Q}^q_i \ , \tag{226}$$

where $\mathcal{Q}_1$ is defined in Eq. (218) and where

$$\begin{aligned} \mathcal{Q}^q_2 &= \left[\bar{b}(1-\gamma_5)q\right]\left[\bar{b}(1-\gamma_5)q\right], & \mathcal{Q}^q_3 &= \left[\bar{b}^\alpha(1-\gamma_5)q^\beta\right]\left[\bar{b}^\beta(1-\gamma_5)q^\alpha\right], \\ \mathcal{Q}^q_4 &= \left[\bar{b}(1-\gamma_5)q\right]\left[\bar{b}(1+\gamma_5)q\right], & \mathcal{Q}^q_5 &= \left[\bar{b}^\alpha(1-\gamma_5)q^\beta\right]\left[\bar{b}^\beta(1+\gamma_5)q^\alpha\right], \end{aligned} \tag{227}$$

with the superscripts α, β denoting colour indices, which are shown only when they are contracted across the two bilinears. There are three other basis operators in the $\Delta B = 2$ effective Hamiltonian. When evaluated in QCD, however, they give identical matrix elements to the

ones already listed due to parity invariance in QCD. The short-distance Wilson coefficients $\mathcal{C}_i$ depend on the underlying theory and can be calculated perturbatively. In the Standard Model only matrix elements of $\mathcal{Q}_1^q$ contribute to Δm_q, while all operators do, for example, for general SUSY extensions of the Standard Model [42]. The matrix elements or bag parameters for the non-SM operators are also useful to estimate the width difference $\Delta\Gamma_q$ between the CP eigenstates of the neutral B meson in the Standard Model, where combinations of matrix elements of $\mathcal{Q}_1^q$, $\mathcal{Q}_2^q$, and $\mathcal{Q}_3^q$ contribute to $\Delta\Gamma_q$ at $\mathcal{O}(1/m_b)$ [43, 44].

In this section, we report on results from lattice-QCD calculations for the neutral B-meson mixing parameters $\hat{B}_{B_d}$, $\hat{B}_{B_s}$, $f_{B_d}\sqrt{\hat{B}_{B_d}}$, $f_{B_s}\sqrt{\hat{B}_{B_s}}$ and the $SU(3)$-breaking ratios B_{B_s}/B_{B_d} and ξ defined in Eqs. (222), (223), and (225). The results are summarized in Tabs. 43 and 44 and in Figs. 29 and 30. Additional details about the underlying simulations and systematic error estimates are given in Appendix C.6.2. Some collaborations do not provide the RGI quantities $\hat{B}_{B_q}$, but quote instead $B_B(\mu)^{\overline{MS},NDR}$. In such cases, we convert the results using Eq. (223) to the RGI quantities quoted in Tab. 43 with a brief description for each case. More detailed descriptions for these cases are provided in FLAG13 [45]. We do not provide the B-meson matrix elements of the other operators $\mathcal{Q}_{2-5}$ in this report. They have been calculated in Ref. [9] for the $N_f = 2$ case and in Refs. [46, 47] for $N_f = 2+1$.

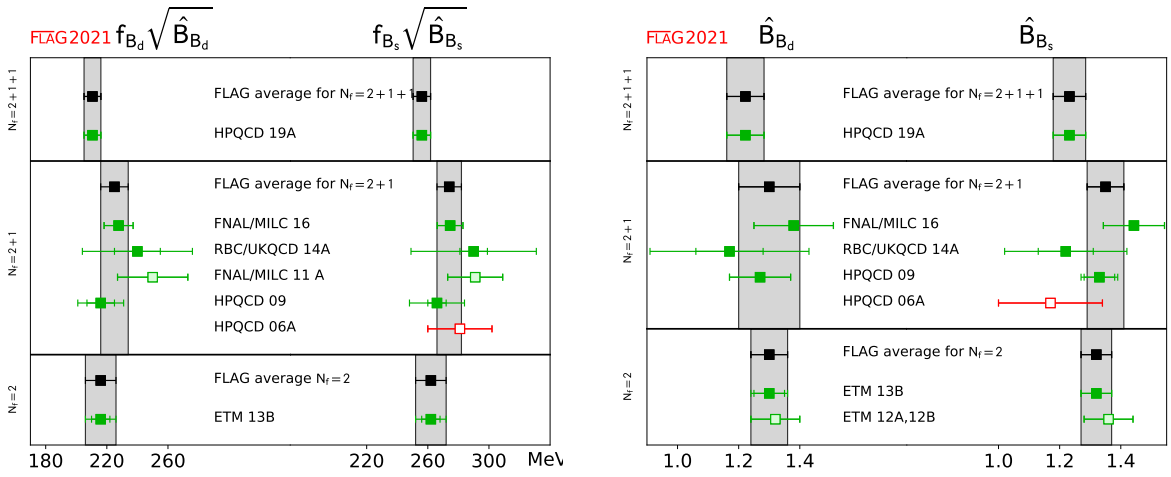

Figure 29: Neutral B- and B_s-meson mixing matrix elements and bag parameters [values in Tab. 43 and Eqs. (228), (231), (234), (229), (232), (235)].

There are no new results for $N_f = 2$ reported after the previous FLAG review. In this category, one work (ETM 13B) [9] passes the quality criteria. A description of this work can be found in the FLAG 13 review [45] where it did not enter the average as it had not appeared in a journal. Because this is the only result available for $N_f = 2$, we quote their values as our estimates

$$N_f = 2: \quad \begin{aligned} f_{B_d}\sqrt{\hat{B}_{b_d}} &= 216(10)\text{MeV} & f_{B_s}\sqrt{\hat{B}_{B_s}} &= 262(10)\text{MeV} & &\text{Ref. [9]}, & (228)\\ \hat{B}_{B_d} &= 1.30(6) & \hat{B}_{B_s} &= 1.32(5) & &\text{Ref. [9]}, & (229)\\ \xi &= 1.225(31) & B_{B_s}/B_{B_d} &= 1.007(21) & &\text{Ref. [9]}. & (230)\end{aligned}$$

For the $N_f = 2+1$ case the RBC/UKQCD collaboration reported their new results on the flavour SU(3) breaking ratio of neutral B-meson mixing parameters in 2018. Their paper [33]

Collaboration	Ref.	N_f	publication status	continuum extrapolation	chiral extrapolation	finite volume	renormalization/matching	heavy-quark treatment	$f_{\mathrm{B_d}}\sqrt{\hat{B}_{\mathrm{B_d}}}$	$f_{\mathrm{B_s}}\sqrt{\hat{B}_{\mathrm{B_s}}}$	$\hat{B}_{\mathrm{B_d}}$	$\hat{B}_{\mathrm{B_s}}$
HPQCD 19A	[48]	2+1+1	A	○	○	★	○	✓	210.6(5.5)	256.1(5.7)	1.222(61)	1.232(53)
FNAL/MILC 16	[47]	2+1	A	★	○	★	○	✓	227.7(9.5)	274.6(8.4)	1.38(12)(6)$^{\odot}$	1.443(88)(48)$^{\odot}$
RBC/UKQCD 14A	[19]	2+1	A	○	○	○	○	✓	240(15)(33)	290(09)(40)	1.17(11)(24)	1.22(06)(19)
FNAL/MILC 11A	[46]	2+1	C	★	○	★	○	✓	250(23)†	291(18)†	–	–
HPQCD 09	[23]	2+1	A	○	○$^{\nabla}$	○	○	✓	216(15)*	266(18)*	1.27(10)*	1.33(6)*
HPQCD 06A	[49]	2+1	A	■	■	★	○	✓	–	281(21)	–	1.17(17)
ETM 13B	[9]	2	A	★	○	○	★	✓	216(6)(8)	262(6)(8)	1.30(5)(3)	1.32(5)(2)
ETM 12A, 12B	[28, 50]	2	C	★	○	○	★	✓	–	–	1.32(8)$^{\diamond}$	1.36(8)$^{\diamond}$

$^{\odot}$ PDG averages of decay constant f_{B^0} and f_{B_s} [51] are used to obtain these values.
† Reported $f_B^2 B$ at $\mu = m_b$ is converted to RGI by multiplying the 2-loop factor 1.517.
$^{\nabla}$ While wrong-spin contributions are not included in the HMrSχPT fits, the effect is expected to be small for these quantities (see description in FLAG 13 [45]).
* This result uses an old determination of $r_1 = 0.321(5)$ fm from Ref. [32] that has since been superseded, which however has only a small effect in the total error budget (see description in FLAG 13 [45]) .
$^{\diamond}$ Reported B at $\mu = m_b = 4.35$ GeV is converted to RGI by multiplying the 2-loop factor 1.521.

Table 43: Neutral B- and B_s-meson mixing matrix elements (in MeV) and bag parameters.

has not been published yet, thus the results will not be included in our averages presented here. Their computation uses ensembles generated by the $2+1$ flavour domain-wall fermion (DWF) formulation. The use of the DWFs also for the heavy quarks makes the renormalization structure simple. Because of the chiral symmetry, the mixing is the same as in the continuum theory. The operators for standard model mixing matrix elements are multiplicatively renormalized. Since they only report the SU(3) breaking ratio, the renormalization of the operators is not needed. The lattice spacings employed are not as fine as some of the recent results reported here. But, by applying successive stout link smearings in the heavy DWF, the reach to heavy mass is improved, which allows them to simulate up to half of the physical bottom mass. Two ensembles are of physical ud quark mass at $a = 0.11$ and 0.09 fm, and there is yet another ensemble off the physical point but with finer lattice spacing, $a = 0.07$ fm. This is the first computation using physical light-quark mass for these quantities, which yields a drastic reduction of the chiral extrapolation error.

The results that enter our averages for $N_f = 2+1$ are FNAL/MILC 16 [47], which had been included in the averages at FLAG 19 [1], RBC/UKQCD 14A [19], included in the averages at FLAG 16 [53], and HPQCD 09 [23] for which a description is available in FLAG 13 [45]. Thus, the averages for $N_f = 2+1$ are unchanged:

Collaboration	Ref.	N_f	publication status	continuum extrapolation	chiral extrapolation	finite volume	renormalization/matching	heavy-quark treatment	ξ	$B_{\mathrm{B_s}}/B_{\mathrm{B_d}}$
HPQCD 19A	[48]	2+1+1	A	○	○	★	○	✓	1.216(16)	1.008(25)
RBC/UKQCD 18A	[33]	2+1	P	★	★	★	★	✓	1.1939(67)$(^{+95}_{-177})$	0.9984(45)$(^{+80}_{-63})$
FNAL/MILC 16	[47]	2+1	A	★	○	★	○	✓	1.206(18)	1.033(31)(26)$^{\odot}$
RBC/UKQCD 14A	[19]	2+1	A	○	○	○	○	✓	1.208(41)(52)	1.028(60)(49)
FNAL/MILC 12	[52]	2+1	A	○	○	★	○	✓	1.268(63)	1.06(11)
RBC/UKQCD 10C	[34]	2+1	A	■	■	■	○	✓	1.13(12)	–
HPQCD 09	[23]	2+1	A	○	○$^{\nabla}$	○	○	✓	1.258(33)	1.05(7)
ETM 13B	[9]	2	A	★	○	○	★	✓	1.225(16)(14)(22)	1.007(15)(14)
ETM 12A, 12B	[28, 50]	2	C	★	○	○	★	✓	1.21(6)	1.03(2)

$^{\odot}$ PDG average of the ratio of decay constants f_{B_s}/f_{B^0} [51] is used to obtain the value.
$^{\nabla}$ Wrong-spin contributions are not included in the HMrSχPT fits. As the effect may not be negligible, these results are excluded from the average (see description in FLAG 13 [45]).

Table 44: Results for $SU(3)$-breaking ratios of neutral B_d- and B_s-meson mixing matrix elements and bag parameters.

$N_f = 2+1$:

$$f_{B_d}\sqrt{\hat{B}_{B_d}} = 225(9)\,\mathrm{MeV} \qquad f_{B_s}\sqrt{\hat{B}_{B_s}} = 274(8)\,\mathrm{MeV} \qquad \text{Refs. [19, 23, 47]}, \tag{231}$$

$$\hat{B}_{B_d} = 1.30(10) \qquad \hat{B}_{B_s} = 1.35(6) \qquad \text{Refs. [19, 23, 47]}, \tag{232}$$

$$\xi = 1.206(17) \qquad B_{B_s}/B_{B_d} = 1.032(38) \qquad \text{Refs. [19, 47]}. \tag{233}$$

Here all the above equations have not been changed from the FLAG 19. The averages were obtained using the nested averaging scheme described in Sec. 2.3.2, due to a nested correlation structure among the results. Details are discussed in the FLAG 19 report [1].

We have the first $N_f = 2+1+1$ calculation for these quantities by the HPQCD collaboration HPQCD 19A [48], using the MILC collaboration's HISQ ensembles. The lattice spacings used are 0.15, 0.12 and 0.09 fm, among which the mass of the Nambu-Goldstone pion (lightest in the staggered taste multiplets) is as small as 130 MeV for two coarser lattices. However, the smallest root-mean-squared pion mass through all taste multiplets is 241 MeV, which is a similar size as the FNAL/MILC 16 result [47] with $N_f = 2+1$ and makes the rating on the chiral extrapolation a green circle. The heavy quark formulation used is non-relativistic QCD (NRQCD). The NRQCD action employed is improved from that used in older calculations,

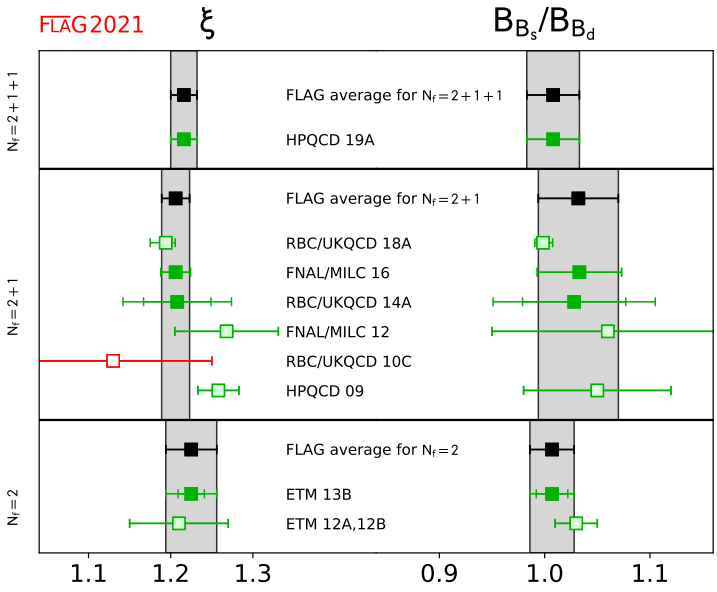

Figure 30: The $SU(3)$-breaking quantities ξ and B_{B_s}/B_{B_d} [values in Tab. 44 and Eqs. (230), (233), (236)].

especially by including one-loop radiative corrections to most of the coefficients of the $\mathcal{O}(v_b^4)$ terms [54]. The b-quark mass is pre-tuned with the spin-averaged kinetic mass of the Υ and η_b states. Therefore, there is no need for extrapolation or interpolation on the b-quark mass. The HISQ-NRQCD four-quark operators are matched through $\mathcal{O}(1/M)$ and renormalized to one-loop, which includes the effects of $\mathcal{O}(\alpha_s)$, $\mathcal{O}(\Lambda_{\rm QCD}/M)$, $\mathcal{O}(\alpha_s/aM)$, and $\mathcal{O}(\alpha_s\,\Lambda_{\rm QCD}/M)$. The remaining error is dominated by $\mathcal{O}(\alpha_s\Lambda_{\rm QCD}/M)$ 2.9% and $\mathcal{O}(\alpha_s^2)$ 2.1% for individual bag parameters. The bag parameters are the primary quantities calculated in this work. The mixing matrix elements are obtained by combining the so-obtained bag parameters with the B-meson decay constants calculated by Fermilab-MILC collaboration (FNAL/MILC 17 [14]).

Because this is the only result available for $N_f = 2+1+1$, we quote their values as the FLAG estimates

$N_f = 2+1+1$:

$$f_{B_d}\sqrt{\hat{B}_{b_d}} = 210.6(5.5)\ \text{MeV} \qquad f_{B_s}\sqrt{\hat{B}_{B_s}} = 256.1(5.7)\ \text{MeV} \qquad \text{Ref. [48]}, \tag{234}$$

$$\hat{B}_{B_d} = 1.222(61) \qquad \hat{B}_{B_s} = 1.232(53) \qquad \text{Ref. [48]}, \tag{235}$$

$$\xi = 1.216(16) \qquad B_{B_s}/B_{B_d} = 1.008(25) \qquad \text{Ref. [48]}. \tag{236}$$

We note that the above results within same N_f (e.g., those in Eqs. (234-236)) are all correlated with each other, due to the use of the same gauge field ensembles for different quantities. The results are also correlated with the averages obtained in Sec. 8.1 and shown in Eqs. (208)–(210) for $N_f = 2$, Eqs. (211)–(213) for $N_f = 2+1$ and Eqs. (214)–(216) for $N_f = 2+1+1$. This is because the calculations of B-meson decay constants and mixing quantities are performed

on the same (or on similar) sets of ensembles, and results obtained by a given collaboration use the same actions and setups. These correlations must be considered when using our averages as inputs to unitarity triangle (UT) fits. For this reason, if one were for example to estimate $f_{B_s}\sqrt{\hat{B}_s}$ from the separate averages of f_{B_s} (Eq. (212)) and $\hat{B}_s$ (Eq. (232)) for $N_f = 2+1$, one would obtain a value about one standard deviation below the one quoted above in Eq. (231). While these two estimates lead to compatible results, giving us confidence that all uncertainties have been properly addressed, we do not recommend combining averages this way, as many correlations would have to be taken into account to properly assess the errors. We recommend instead using the numbers quoted above. In the future, as more independent calculations enter the averages, correlations between the lattice-QCD inputs to UT fits will become less significant.

8.3 Semileptonic form factors for B decays to light flavours

The Standard Model differential rate for the decay $B_{(s)} \to P\ell\nu$ involving a quark-level $b \to u$ transition is given, at leading order in the weak interaction, by a formula analogous to the one for D decays in Eq. (182), but with $D \to B_{(s)}$ and the relevant CKM matrix element $|V_{cq}| \to |V_{ub}|$:

$$\begin{aligned}\frac{d\Gamma(B_{(s)} \to P\ell\nu)}{dq^2} =& \frac{G_F^2|V_{ub}|^2}{24\pi^3}\frac{(q^2-m_\ell^2)^2\sqrt{E_P^2-m_P^2}}{q^4 m_{B_{(s)}}^2} \\ &\times\left[\left(1+\frac{m_\ell^2}{2q^2}\right) m_{B_{(s)}}^2 (E_P^2-m_P^2)|f_+(q^2)|^2 \right. \\ &\left. +\frac{3m_\ell^2}{8q^2}(m_{B_{(s)}}^2-m_P^2)^2|f_0(q^2)|^2\right]. \end{aligned} \tag{237}$$

Again, for $\ell = e, \mu$ the contribution from the scalar form factor f_0 can be neglected, and one has a similar expression to Eq. (184), which, in principle, allows for a direct extraction of $|V_{ub}|$ by matching theoretical predictions to experimental data. However, while for D (or K) decays the entire physical range $0 \le q^2 \le q^2_{\rm max}$ can be covered with moderate momenta accessible to lattice simulations, in $B \to \pi\ell\nu$ decays one has $q^2_{\rm max} \sim 26$ GeV^2 and only part of the full kinematic range is reachable. As a consequence, obtaining $|V_{ub}|$ from $B \to \pi\ell\nu$ is more complicated than obtaining $|V_{cd(s)}|$ from semileptonic D-meson decays.

In practice, lattice computations are restricted to large values of the momentum transfer q^2 (see Sec. 7.2) where statistical and momentum-dependent discretization errors can be controlled,[2] which in existing calculations roughly cover the upper third of the kinematically allowed q^2 range. Since, on the other hand, the decay rate is suppressed by phase space at large q^2, most of the semileptonic $B \to \pi$ events are observed in experiment at lower values of q^2, leading to more accurate experimental results for the binned differential rate in that region.[3] It is, therefore, a challenge to find a window of intermediate values of q^2 at which both the experimental and lattice results can be reliably evaluated.

[2]The variance of hadron correlation functions at nonzero three-momentum is dominated at large Euclidean times by zero-momentum multiparticle states [55]; therefore the noise-to-signal grows more rapidly than for the vanishing three-momentum case.

[3]Upcoming data from Belle II are expected to significantly improve the precision of experimental results, in particular, for larger values of q^2.

State-of-the-art determinations of CKM matrix elements, say, e.g., $|V_{ub}|$, are obtained from joint fits to lattice and experimental results, keeping the relative normalization $|V_{ub}|^2$ as a free parameter. This requires, in particular, that both experimental and lattice data for the q^2-dependence be parameterized by fitting data to specific ansätze, with the ultimate aim of minimizing the systematic uncertainties involved. This plays a key role in assessing the systematic uncertainties of CKM determinations, and will be discussed extensively in this section. A detailed discussion of the parameterization of form factors as a function of q^2 can be found in Appendix B.1.

8.3.1 Form factors for $B \to \pi\ell\nu$

The semileptonic decay process $B \to \pi\ell\nu$ enables determination of the CKM matrix element $|V_{ub}|$ within the Standard Model via Eq. (237). Early results for $B \to \pi\ell\nu$ form factors came from the HPQCD [56] and FNAL/MILC [57] collaborations. Our 2016 review featured a significantly extended calculation of $B \to \pi\ell\nu$ from FNAL/MILC [58] and a new computation from RBC/UKQCD [59]. In 2022, the JLQCD collaboration published another new calculation using Möbius Domain Wall fermions [60]. FNAL/MILC and RBC/UKQCD continue working on further new calculations of the $B \to \pi$ form factors and have reported on their progress at the annual Lattice conferences and the 2020 Asia-Pacific Symposium for Lattice Field Theory. The results are preliminary or blinded, so not yet ready for inclusion in this review. FNAL/MILC is using $N_f = 2+1+1$ HISQ ensembles with $a \approx 0.15$, 0.12, 0.088 fm, 0.057 fm, with Goldstone pion mass down to its physical value [61, 62]. The RBC/UKQCD Collaborations have added a new Möbius-domain-wall-fermion ensemble with $a \approx 0.07$ fm and $m_\pi \approx 230$ MeV to their analysis [63]. In addition, HPQCD using MILC ensembles had published the first $N_f = 2+1+1$ results for the $B \to \pi\ell\nu$ scalar form factor, working at zero recoil ($q^2 = q^2_{\rm max}$) and pion masses down to the physical value [64]; this adds to previous reports on ongoing work to upgrade their 2006 computation [65, 66]. Since this latter result has no immediate impact on current $|V_{ub}|$ determinations, which come from the vector-form-factor-dominated decay channels into light leptons, we will from now on concentrate on the $N_f = 2+1$ determinations of the q^2-dependence of $B \to \pi$ form factors.

Both the HPQCD and the FNAL/MILC computations of $B \to \pi\ell\nu$ amplitudes use ensembles of gauge configurations with $N_f = 2+1$ flavours of rooted staggered quarks produced by the MILC collaboration; however, the latest FNAL/MILC work makes a much more extensive use of the currently available ensembles, both in terms of lattice spacings and light-quark masses. HPQCD have results at two values of the lattice spacing ($a \approx 0.12$, 0.09 fm), while FNAL/MILC employs four values ($a \approx 0.12$, 0.09, 0.06, 0.045 fm). Lattice-discretization effects are estimated within heavy-meson rooted staggered chiral perturbation theory (HMrSχPT) in the FNAL/MILC computation, while HPQCD quotes the results at $a \approx 0.12$ fm as central values and uses the $a \approx 0.09$ fm results to quote an uncertainty. The relative scale is fixed in both cases through the quark-antiquark potential-derived ratio r_1/a. HPQCD set the absolute scale through the Υ $2S$–$1S$ splitting, while FNAL/MILC uses a combination of f_π and the same Υ splitting, as described in Ref. [22]. The spatial extent of the lattices employed by HPQCD is $L \simeq 2.4$ fm, save for the lightest mass point (at $a \approx 0.09$ fm) for which $L \simeq 2.9$ fm. FNAL/MILC, on the other hand, uses extents up to $L \simeq 5.8$ fm, in order to allow for light-pion masses while keeping finite-volume effects under control. Indeed, while in the 2006 HPQCD work the lightest RMS pion mass is 400 MeV, the latest FNAL/MILC work includes pions as light as 165 MeV—in both cases the bound

$m_\pi L \gtrsim 3.8$ is kept. Other than the qualitatively different range of MILC ensembles used in the two computations, the main difference between HPQCD and FNAL/MILC lies in the treatment of heavy quarks. HPQCD uses the NRQCD formalism, with a 1-loop matching of the relevant currents to the ones in the relativistic theory. FNAL/MILC employs the clover action with the Fermilab interpretation, with a mostly nonperturbative renormalization of the relevant currents, within which the overall renormalization factor of the heavy-light current is written as a product of the square roots of the renormalization factors of the light-light and heavy-heavy temporal vector currents (which are determined nonperturbatively) and a residual factor that is computed using 1-loop perturbation theory. (See Tab. 45; full details about the computations are provided in tables in Appendix C.6.3.)

The RBC/UKQCD computation is based on $N_f = 2 + 1$ DWF ensembles at two values of the lattice spacing ($a \approx 0.12,\ 0.09$ fm), and pion masses in a narrow interval ranging from slightly above 400 MeV to slightly below 300 MeV, keeping $m_\pi L \gtrsim 4$. The scale is set using the Ω^- baryon mass. Discretization effects coming from the light sector are estimated in the 1% ballpark using HMχPT supplemented with effective higher-order interactions to describe cutoff effects. The b quark is treated using the Columbia RHQ action, with a mostly nonperturbative renormalization of the relevant currents. Discretization effects coming from the heavy sector are estimated with power-counting arguments to be below 2%.

The JLQCD collaboration is using Möbius Domain Wall fermions, including for the heavy quark, with $a \approx 0.08$, 0.055, and 0.044 fm and pion masses down to 230 MeV. The relative scales are set using the gradient-flow time $t_0^{1/2}/a$, with the absolute scale $t_0^{1/2}$ taken from Ref. [67]. All ensembles have $m_\pi L \gtrsim 4.0$. The bare heavy-quark masses satisfy $am_Q < 0.7$ and reach from the charm mass up to 2.44 times the charm mass. The form factors are extrapolated linearly in $1/m_Q$ to the bottom mass. For the lower range of the quark masses, the vector current is renormalized using a factor $Z_{V_{qq}}$ obtained from position-space current-current correlators. For heavier quark masses, $\sqrt{Z_{V_{QQ}} Z_{V_{qq}}}$ is used, where $Z_{V_{QQ}}$ is the renormalization factor of the flavor-conserving temporal vector current, determined using charge conservation.

Given the large kinematical range available in the $B \to \pi$ transition, chiral extrapolations are an important source of systematic uncertainty: apart from the eventual need to reach physical pion masses in the extrapolation, the applicability of χPT is not guaranteed for large values of the pion energy E_π. Indeed, in all computations E_π reaches values in the 1 GeV ballpark, and chiral extrapolation systematics is the dominant source of errors. FNAL/MILC uses $SU(2)$ NLO HMrSχPT for the continuum-chiral extrapolation, supplemented by NNLO analytic terms and hard-pion χPT terms [68];[4] systematic uncertainties are estimated through an extensive study of the effects of varying the specific fit ansatz and/or data range. RBC/UKQCD and JLQCD use $SU(2)$ hard-pion HMχPT to perform their combined continuum-chiral extrapolations, and obtain estimates for systematic uncertainties by varying the ansätze and ranges used in fits. HPQCD performs chiral extrapolations using HMrSχPT formulae, and estimates systematic uncertainties by comparing the result with the ones from fits to a linear behaviour in the light-quark mass, continuum HMχPT, and partially quenched HMrSχPT formulae (including also data with different sea and valence light-quark masses).

[4] It is important to stress the finding in Ref. [69] that the factorization of chiral logs in hard-pion χPT breaks down, implying that it does not fulfill the expected requisites for a proper effective field theory. Its use to model the mass dependence of form factors can thus be questioned.

Collaboration	Ref.	N_f	publication status	continuum extrapolation	chiral extrapolation	finite volume	renormalization	heavy-quark treatment	z-parameterization
JLQCD 22	[60]	2+1	A	★	○	★	★	✓	BCL
FNAL/MILC 15	[58]	2+1	A	★	○	★	○	✓	BCL
RBC/UKQCD 15	[59]	2+1	A	○	○	○	○	✓	BCL
HPQCD 06	[56]	2+1	A	○	○	○	○	✓	n/a

Table 45: Results for the $B \to \pi\ell\nu$ semileptonic form factor.

FNAL/MILC, RBC/UKQCD, and JLQCD describe the q^2-dependence of f_+ and f_0 by applying a BCL parameterization to the form factors extrapolated to the continuum limit, within the range of values of q^2 covered by data. (A discussion of the various parameterizations can be found in Appendix B.1.) RBC/UKQCD and JLQCD generate synthetic data for the form factors at some values of q^2 (evenly spaced in z) from the continuous function of q^2 obtained from the joint chiral-continuum extrapolation, which are then used as input for the fits. After having checked that the kinematical constraint $f_+(0) = f_0(0)$ is satisfied within errors by the extrapolation to $q^2 = 0$ of the results of separate fits, this constraint is imposed to improve fit quality. In the case of FNAL/MILC, rather than producing synthetic data a functional method is used to extract the z-parameterization directly from the fit functions employed in the continuum-chiral extrapolation. In the case of HPQCD, the parameterization of the q^2-dependence of form factors is somewhat intertwined with chiral extrapolations: a set of fiducial values $\{E_\pi^{(n)}\}$ is fixed for each value of the light-quark mass, and $f_{+,0}$ are interpolated to each of the $E_\pi^{(n)}$; chiral extrapolations are then performed at fixed E_π (i.e., m_π and q^2 are varied subject to E_π=constant). The interpolation is performed using a Ball-Zwicky (BZ) ansatz [70]. The q^2-dependence of the resulting form factors in the chiral limit is then described by means of a BZ ansatz, which is cross-checked against Becirevic-Kaidalov (BK) [71], Richard Hill (RH) [72], and Boyd-Grinstein-Lebed (BGL) [73] parameterizations (see Appendix B.1), finding agreement within the quoted uncertainties. Unfortunately, the correlation matrix for the values of the form factors at different q^2 is not provided, which severely limits the possibilities of combining them with other computations into a global z-parameterization.

The different ways in which the current results are presented do not allow a straightforward averaging procedure. RBC/UKQCD only provides synthetic values of f_+ and f_0 at a few values of q^2 as an illustration of their results, and FNAL/MILC does not quote synthetic values at all. In both cases, full results for BCL z-parameterizations defined by Eq. (533) are quoted. In the case of HPQCD 06, unfortunately, a fit to a BCL z-parameterization is not possible, as discussed above.

In order to combine these form factor calculations, we start from sets of synthetic data

for several q^2 values. HPQCD, RBC/UKQCD, and JLQCD directly provide this information; FNAL/MILC present only fits to a BCL z-parameterization from which we can easily generate an equivalent set of form factor values. It is important to note that in both the RBC/UKQCD and JLQCD synthetic data and the FNAL/MILC z-parameterization fits the kinematic constraint at $q^2 = 0$ is automatically included (in the FNAL/MILC case the constraint is manifest in an exact degeneracy of the (a_n^+, a_n^0) covariance matrix). Due to these considerations, in our opinion, the most accurate procedure is to perform a simultaneous fit to all synthetic data for the vector and scalar form factors. Unfortunately, the absence of information on the correlation in the HPQCD result between the vector and scalar form factors even at a single q^2 point makes it impossible to include consistently this calculation in the overall fit. In fact, the HPQCD and FNAL/MILC statistical uncertainties are highly correlated (because they are based on overlapping subsets of MILC $N_f = 2 + 1$ ensembles) and, without knowledge of the $f_+ - f_0$ correlation we are unable to construct the HPQCD-FNAL/MILC off-diagonal entries of the overall covariance matrix.

In conclusion, we will present as our best result a combined vector and scalar form factor fit to the FNAL/MILC, RBC/UKQCD, and JLQCD results that we treat as completely uncorrelated.

The resulting data set is then fitted to the BCL parameterization in Eqs. (533) and (534). We assess the systematic uncertainty due to truncating the series expansion by considering fits to different orders in z. In Fig. 31 (left), we show $(1 - q^2/m_{B^*}^2) f_+(q^2)$ and $f_0(q^2)$ versus z; Fig. 31 (right) shows the full form factors versus q^2. The fit has $\chi^2/\text{dof} = 43.6/12$ with $N^+ = N^0 = 3$. The poor quality of the fit is caused by slight tensions between the results from the different collaborations; in particular in the slopes of f_0, which are very constrained due to strong correlations between data points. We have therefore rescaled the uncertainties of the z parameters by $\sqrt{\chi^2/\text{dof}} = 1.9$. We point out that tensions in the form factors, especially in f_0, might be an artifact associated with the basis of form factors employed to take the continuum limit, as explained in Appendix B.1. The outcome of the five-parameter $N^+ = N^0 = 3$ BCL fit to the FNAL/MILC, RBC/UKQCD, and JLQCD calculations is shown in Tab. 46.

The fit shown in Tab. 46 can therefore be used as the averaged FLAG result for the lattice-computed form factor $f_+(q^2)$. The coefficient a_3^+ can be obtained from the values for a_0^+–a_2^+ using Eq. (532). The coefficient a_2^0 can be obtained from all other coefficients imposing the $f_+(q^2 = 0) = f_0(q^2 = 0)$ constraint. We emphasize that future lattice-QCD calculations of semileptonic form factors should publish their full statistical and systematic correlation matrices to enable others to use the data. It is also preferable to present a set of synthetic form factors data equivalent to the z-fit results, since this allows for an independent analysis that avoids further assumptions about the compatibility of the procedures to arrive at a given z-parameterization.[5] It is also preferable to present covariance/correlation matrices with enough significant digits to calculate correctly all their eigenvalues.

8.3.2 Form factors for $B_s \to K\ell\nu$

Similar to $B \to \pi\ell\nu$, measurements of $B_s \to K\ell\nu$ decay rates enable determinations of the CKM matrix element $|V_{ub}|$ within the Standard Model via Eq. (237). From the lattice point of view, the two channels are very similar. As a matter of fact, $B_s \to K\ell\nu$ is actually

[5] Note that generating synthetic data is a trivial task, but less so is choosing the number of required points and the q^2 values that lead to an optimal description of the form factors.

$B \to \pi$ ($N_f = 2+1$)

	Central Values	Correlation Matrix				
a_0^+	0.423 (21)	1	-0.00466	-0.0749	0.402	0.0920
a_1^+	−0.507 (93)	-0.00466	1	0.498	-0.0556	0.659
a_2^+	−0.75 (34)	-0.0749	0.498	1	-0.152	0.677
a_0^0	0.561 (24)	0.402	-0.0556	-0.152	1	-0.548
a_1^0	−1.42 (11)	0.0920	0.659	0.677	-0.548	1

Table 46: Coefficients and correlation matrix for the $N^+ = N^0 = 3$ z-expansion fit of the $B \to \pi$ form factors f_+ and f_0. The coefficient a_2^0 is fixed by the $f_+(q^2 = 0) = f_0(q^2 = 0)$ constraint. The chi-square per degree of freedom is $\chi^2/\text{dof} = 43.6/12$ and the errors on the z-parameters have been rescaled by $\sqrt{\chi^2/\text{dof}} = 1.9$. The lattice calculations that enter this fit are taken from FNAL/MILC 15 [58], RBC/UKQCD 15 [59] and JLQCD 22 [60]. The parameterizations are defined in Eqs. (533) and (534).

somewhat simpler, in that the kaon mass region is easily accessed by all simulations making the systematic uncertainties related to chiral extrapolation smaller.

At the time of our FLAG 19 review [1], results for $B_s \to K\ell\nu$ form factors were provided by HPQCD [74] and RBC/UKQCD [59] for both form factors f_+ and f_0, in both cases using $N_f = 2+1$ dynamical configurations. HPQCD has recently emphasized the value of using ratios of form factors for the processes $B_s \to K\ell\nu$ and $B_s \to D_s\ell\nu$ for the determination of $|V_{ub}/V_{cb}|$ [75]. In the FLAG Review 19 [1], FNAL/MILC preliminary results had been reported for both $N_f = 2+1$ [76] and $N_f = 2+1+1$ [61], but were not included in the average due to their non-final status. The $N_f = 2+1$ results have since been published [77]; we, therefore, include them in the average here. Moreover, in this web update, we replace the RBC/UKQCD 15 [59] results for the $B_s \to K$ form factors by the superseding results of RBC/UKQCD 23 [78].

The HPQCD computation uses ensembles of gauge configurations with $N_f = 2+1$ flavours of asqtad rooted staggered quarks produced by the MILC collaboration at two values of the lattice spacing ($a \approx 0.12,\ 0.09$ fm), for three and two different sea-pion masses, respectively, down to a value of 260 MeV. The b quark is treated within the NRQCD formalism, with a 1-loop matching of the relevant currents to the ones in the relativistic theory, omitting terms of $\mathcal{O}(\alpha_s\Lambda_{\rm QCD}/m_b)$. The HISQ action is used for the valence s quark. The continuum-chiral extrapolation is combined with the description of the q^2-dependence of the form factors into a modified z-expansion (cf. Appendix B.1) that formally coincides in the continuum with the BCL ansatz. The dependence of form factors on the pion energy and quark masses is fitted to a 1-loop ansatz inspired by hard-pion χPT [68], that factorizes out the chiral logarithms describing soft physics.

The FNAL/MILC computation coincides with HPQCD's in using ensembles of gauge configurations with $N_f = 2+1$ flavours of asqtad rooted staggered quarks produced by the MILC collaboration, but only one ensemble is shared, and a different valence regularization is employed; we will thus treat the two results as fully independent from the statistics point of view. FNAL/MILC uses three values of the lattice spacing ($a \approx 0.12,\ 0.09,\ 0.06$ fm); only one value of the sea pion mass and the volume is available at the extreme values of the lattice

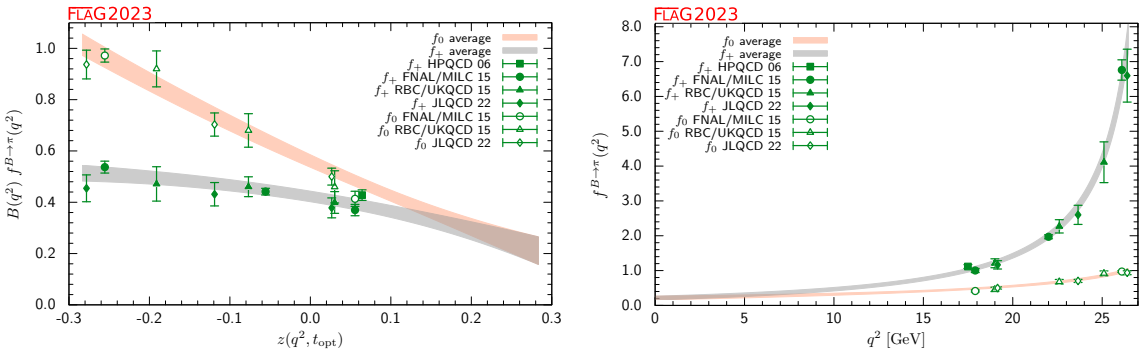

Figure 31: The form factors $f_+(q^2)$ and $f_0(q^2)$ for $B \to \pi\ell\nu$ plotted versus z (left panel) and q^2 (right panel). In the left plot, we removed the Blaschke factors. See text for a discussion of the data set. The grey and salmon bands display our preferred $N^+ = N^0 = 3$ BCL fit (five parameters).

spacing, while four different masses and volumes are considered at $a = 0.09$ fm. Heavy quarks are treated within the Fermilab approach. HMrSχPT expansion is used at next-to-leading order in $SU(2)$ and leading order in $1/M_B$, including next-to-next-to-leading-order (NNLO) analytic and generic discretization terms, to perform continuum-chiral extrapolations. Hard kaons are assumed to decouple, i.e., their effect is reabsorbed in the $SU(2)$ LECs. Continuum- and chiral-extrapolated values of the form factors are fitted to a z-parametrization imposing the kinematical constraint $f_+(0) = f_0(0)$. See Tab. 47 and the tables in Appendix C.6.3 for full details.

The RBC/UKQCD 15 computation had been published together with the $B \to \pi\ell\nu$ computation discussed in Sec. 8.3.1, all technical details being practically identical. The RBC/UKQCD 23 computation (which considers $B_s \to K\ell\nu$ only) differs from RBC/UKQCD 15 by the addition of one new ensemble with a third, finer lattice spacing that also has a lower pion mass than the other ensembles, updated scale setting and updated tuning of m_s and of the RHQ parameters, and a change of the form-factor basis in which the chiral-continuum extrapolation is performed (previously: $f_\parallel$ and $f_\perp$, now: f_+ and f_0). Reference [78] furthermore uses a new method to perform extrapolations of the form factors to the full q^2 range with unitarity bounds, taking into account that the dispersive integral ranges only of an arc of the unit circle instead of the full circle [79, 80]. However, we do not use these extrapolations in performing our average and instead use the synthetic data points provided in Ref. [78].

In order to combine the results for the q^2 dependence of the form factors from the three collaborations, we will follow a similar approach to the one adopted above for $B \to \pi\ell\nu$, and produce synthetic data from the preferred fits quoted in the papers (or use the synthetic data provided in the paper), to obtain a dataset to which a joint fit can be performed. Note that the kinematic constraint at $q^2 = 0$ is included in all three cases; we will impose it in our fit as well, since the synthetic data will implicitly depend on that fitting choice. However, it is worth mentioning that the systematic uncertainty of the resulting extrapolated value $f_+(0) = f_0(0)$ can be fairly large, the main reason being the required long extrapolation from the high-q^2 region covered by lattice data. While we stress that the average far away

Collaboration	Ref.	N_f	publication status	continuum extrapolation	chiral extrapolation	finite volume	renormalization	heavy-quark treatment	z-parameterization
RBC/UKQCD 23*	[78]	2+1	A	★	○	★	○	✓	BGL§
FNAL/MILC 19	[77]	2+1	A	★	○	★	○	✓	BCL
RBC/UKQCD 15	[59]	2+1	A	○	○	○	○	✓	BCL
HPQCD 14	[74]	2+1	A	○	○	○	○	✓	BCL†

* Supersedes RBC/UKQCD 15.
§ generalized as discussed in Ref. [79].
† Results from modified z-expansion.

Table 47: Summary of lattice calculations of the $B_s \to K\ell\nu$ semileptonic form factors.

from the high-q^2 region has to be used carefully, it is possible that increasing the number of z coefficients beyond what is sufficient for a good description of the lattice data and using unitarity constraints to control the size of additional terms, might yield fits with a more stable extrapolation at very low q^2. We plan to include said unitarity analysis into the next edition of the FLAG review. It is, however, important to emphasize that joint fits with experimental data, where the latter accurately map the q^2 region, are expected to be safe.

Our fits employ a BCL ansatz with $t_+ = (M_B + M_\pi)^2$ and $t_0 = t_+ - \sqrt{t_+(t_+ - t-)}$, with $t_- = (M_{B_s} - M_K)^2$. Our pole factors will contain a single pole in both the vector and scalar channels, for which we take the mass values $M_{B^*} = 5.32465$ GeV and $M_{B^*(0^+)} = 5.68$ GeV.[6] The constraint $f_+(0) = f_0(0)$ is imposed by expressing the coefficient $b^0_{N^0-1}$ in terms of all others. The outcome of the seven-parameter $N^+ = N^0 = 4$ BCL fit, which we quote as our preferred result, is shown in Tab. 48. The fit has a chi-square per degree of freedom $\chi^2/\text{dof} = 3.82$. Following the PDG recommendation, we rescale the whole covariance matrix by χ^2/dof: the errors on the z-parameters are increased by $\sqrt{\chi^2/\text{dof}} = 1.95$ and the correlation matrix is unaffected. The parameters shown in Tab. 48 provide the averaged FLAG results for the lattice-computed form factors $f_+(q^2)$ and $f_0(q^2)$. The coefficient a_4^+ can be obtained from the values for a_0^+–a_3^+ using Eq. (532). The fit is illustrated in Fig. 32.[7] As can be seen in Fig. 32, the large value of χ^2/dof is caused by a significant tension between the lattice results from the different collaborations for f_0. Compared to the 2021 FLAG fit that used RBC/UKQCD 15, the tension has increased as the RBC/UKQCD results for f_0 have shifted

[6] These are the values used in the FNAL/MILC determination, while HPQCD and RBC/UKQCD use $M_{B^*(0+)} = 5.6794(10)$ GeV and $M_{B^*(0+)} = 5.63$ GeV, respectively. They also employ different values of t_+ and t_0 than employed here, which again coincide with FNAL/MILC's choice.

[7] Note that in FLAG 19 [1] we had adopted the threshold $t_+ = (M_{B_s} + M_K)^2$ rather than $t_+ = (M_B + M_\pi)^2$. This change impacted the z-range which the physical q^2 interval maps onto. We also point out that, in the FLAG 19 version of Fig. 32, the three synthetic f_0 data points from HPQCD were plotted incorrectly, but this did not affect the fit.

$B_s \to K$ ($N_f = 2+1$)

	Central Values	Correlation Matrix						
a_0^+	0.370(21)	1.	0.2781	−0.3169	−0.3576	0.6130	0.3421	0.2826
a_1^+	−0.68(10)	0.2781	1.	0.3672	0.1117	0.4733	0.8487	0.8141
a_2^+	0.55(48)	−0.3169	0.3672	1.	0.8195	0.3323	0.6614	0.6838
a_3^+	2.11(83)	−0.3576	0.1117	0.8195	1.	0.2350	0.4482	0.4877
a_0^0	0.234(10)	0.6130	0.4733	0.3323	0.2350	1.	0.6544	0.5189
a_1^0	0.135(86)	0.3421	0.8487	0.6614	0.4482	0.6544	1.	0.9440
a_2^0	0.20(35)	0.2826	0.8141	0.6838	0.4877	0.5189	0.9440	1.

Table 48: Coefficients and correlation matrix for the $N^+ = N^0 = 4$ z-expansion of the $B_s \to K$ form factors f_+ and f_0. The coefficient a_3^0 is fixed by the $f_+(q^2 = 0) = f_0(q^2 = 0)$ constrain. The chi-square per degree of freedom is $\chi^2/\text{dof} = 3.82$ and the errors on the z-parameters have been rescaled by $\sqrt{\chi^2/\text{dof}} = 1.95$.

upward. The tension indicates that the uncertainties have been underestimated in at least some of the calculations. One possible, at least partial, explanation was offered by the authors of RBC/UKQCD 23 [78], who found that the results for f_0 shift upward when performing the chiral/continuum extrapolation directly for f_0 and f_+ rather than $f_\parallel$ and $f_\perp$ as was done in RBC/UKQCD 15 and FNAL/MILC 19. Using f_0 and f_+ is argued to be the better choice because these form factors have definite J^P quantum numbers for the bound states producing poles in q^2, and the chiral-continuum extrapolation fit functions include these poles. More details on the problems associated with taking the chiral/continuum extrapolation in the $f_\parallel$ and $f_\perp$ basis can be found in Appendix B.1.

We will conclude by pointing out progress in the application of the npHQET method to the extraction of semileptonic form factors, reported for $B_s \to K$ transitions in Ref. [81], which extends the work of Ref. [82]. This is a methodological study based on CLS $N_f = 2$ ensembles at two different values of the lattice spacing and pion masses, and full $1/m_b$ corrections are incorporated within the npHQET framework. Emphasis is on the role of excited states in the extraction of the bare form factors, which are shown to pose an impediment to reaching precisions better than a few percent.

8.3.3 Form factors for rare and radiative B-semileptonic decays to light flavours

Lattice-QCD input is also available for some exclusive semileptonic decay channels involving neutral-current $b \to q$ transitions at the quark level, where $q = d, s$. Being forbidden at tree level in the SM, these processes allow for stringent tests of potential new physics; simple examples are $B \to K^*\gamma$, $B \to K^{(*)}\ell^+\ell^-$, or $B \to \pi\ell^+\ell^-$ where the B meson (and therefore the light meson in the final state) can be either neutral or charged.

The corresponding SM effective weak Hamiltonian is considerably more complicated than the one for the tree-level processes discussed above: after integrating out the top quark and the W boson, as many as ten dimension-six operators formed by the product of two hadronic currents or one hadronic and one leptonic current appear.[8] Three of the latter, coming from

[8] See, e.g., Ref. [83] and references therein.

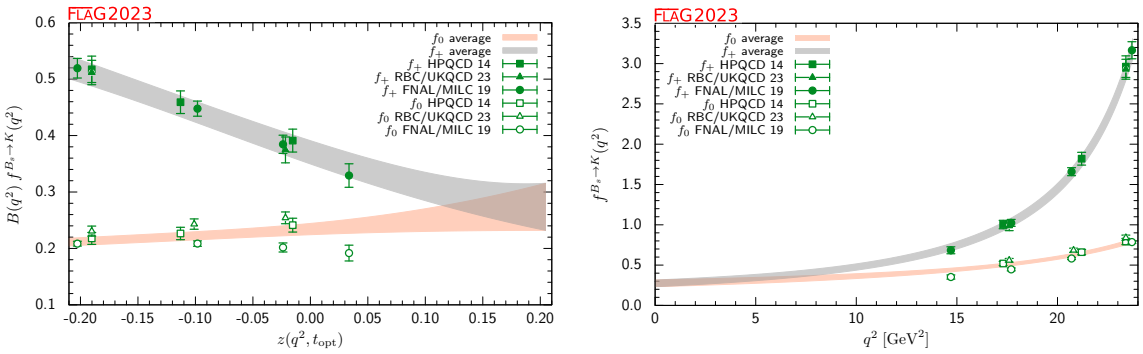

Figure 32: The form factors $f_+(q^2)$ and $f_0(q^2)$ for $B_s \to K\ell\nu$ plotted versus z (left panel) and q^2 (right panel). In the left plot, we remove the Blaschke factors. See text for a discussion of the data sets. The grey and salmon bands display our preferred $N^+ = N^0 = 4$ BCL fit (seven parameters).

Collaboration	Ref.	N_f	publication status	continuum extrapolation	chiral extrapolation	finite volume	renormalization	heavy-quark treatment	z-parameterization
FNAL/MILC 15D	[85]	2+1	A	★	○	★	○	✓	BCL
HPQCD 13E	[86]	2+1	A	○	○	○	○	✓	BCL

Table 49: Summary of lattice calculations of the $B \to K$ semileptonic form factors.

penguin and box diagrams, dominate at short distances and have matrix elements that, up to small QED corrections, are given entirely in terms of $B \to (\pi, K, K^*)$ form factors. The matrix elements of the remaining seven operators can be expressed, up to power corrections whose size is still unclear, in terms of form factors, decay constants and light-cone distribution amplitudes (for the π, K, K^* and B mesons) by employing OPE arguments (at large di-lepton invariant mass) and results from Soft Collinear Effective Theory (at small di-lepton invariant mass). In conclusion, the most important contributions to all of these decays are expected to come from matrix elements of current operators (vector, tensor, and axial-vector) between one-hadron states, which in turn can be parameterized in terms of a number of form factors (see Ref. [84] for a complete description).

In channels with pseudoscalar mesons in the final state, the level of sophistication of lattice calculations is similar to the $B \to \pi$ case and there are results for the vector, scalar, and tensor form factors for $B \to K\ell^+\ell^-$ decays by HPQCD [86], and more recent results for both $B \to \pi\ell^+\ell^-$ [87] and $B \to K\ell^+\ell^-$ [85] from FNAL/MILC. Full details about these two calculations are provided in Tab. 49 and in Appendix C.6.4. Both computations employ

$B \to \pi$ ($N_f = 2+1$)

	Central Values	Correlation Matrix			
a_0^T	0.393(17)	1.000	0.400	0.204	0.166
a_1^T	−0.65(23)	0.400	1.000	0.862	0.806
a_2^T	−0.6(1.5)	0.204	0.862	1.000	0.989
a_3^T	0.1(2.8)	0.166	0.806	0.989	1.000

Table 50: Coefficients and correlation matrix for the $N^+ = N^0 = 3$ z-expansion of the $B \to \pi$ form factor f_T.

MILC $N_f = 2+1$ asqtad ensembles. HPQCD [88] and FNAL/MILC [89] have also companion papers in which they calculate the Standard Model predictions for the differential branching fractions and other observables and compare to experiment. The HPQCD computation employs NRQCD b quarks and HISQ valence light quarks, and parameterizes the form factors over the full kinematic range using a model-independent z-expansion as in Appendix B.1, including the covariance matrix of the fit coefficients. In the case of the (separate) FNAL/MILC computations, both of them use Fermilab b quarks and asqtad light quarks, and a BCL z-parameterization of the form factors.

Reference [87] includes results for the tensor form factor for $B \to \pi\ell^+\ell^-$ not included in previous publications on the vector and scalar form factors [58]. Nineteen ensembles from four lattice spacings are used to control continuum and chiral extrapolations. The results for $N_z = 4$ z-expansion of the tensor form factor and its correlations with the expansions for the vector and scalar form factors, which we consider the FLAG estimate, are shown in Tab. 50. Partial decay widths for decay into light leptons or $\tau^+\tau^-$ are presented as a function of q^2. The former is compared with results from LHCb [90], while the latter is a prediction.

The averaging of the HPQCD and FNAL/MILC results for the $B \to K$ form factors is similar to our treatment of the $B \to \pi$ and $B_s \to K$ form factors. In this case, even though the statistical uncertainties are partially correlated because of some overlap between the adopted sets of MILC ensembles, we choose to treat the two calculations as independent. The reason is that, in $B \to K$, statistical uncertainties are subdominant and cannot be easily extracted from the results presented by HPQCD and FNAL/MILC. Both collaborations provide only the outcome of a simultaneous z-fit to the vector, scalar and tensor form factors, that we use to generate appropriate synthetic data. We then impose the kinematic constraint $f_+(q^2 = 0) = f_0(q^2 = 0)$ and fit to ($N^+ = N^0 = N^T = 3$) BCL parameterization. The functional forms of the form factors that we use are identical to those adopted in Ref. [89].[9] The results of the fit are presented in Tab. 51. The fit is illustrated in Fig. 33. Note that the average for the f_T form factor appears to prefer the FNAL/MILC synthetic data. This happens because we perform a correlated fit of the three form factors simultaneously (both FNAL/MILC and HPQCD present covariance matrices that include correlations between all form factors). We checked that the average for the f_T form factor, obtained neglecting correlations with f_0 and f_+, is a little lower and lies in between the two data sets. There is still a noticeable tension between the FNAL/MILC and HPQCD data for the tensor form

[9] Note in particular that not much is known about the sub-threshold poles for the scalar form factor. FNAL/MILC includes one pole at the B^*_{s0} mass as taken from the calculation in Ref. [91].

$B \to K$ ($N_f = 2+1$)

	Central Values	Correlation Matrix							
a_0^+	0.471 (14)	1	0.513	0.128	0.773	0.594	0.613	0.267	0.118
a_1^+	−0.74 (16)	0.513	1	0.668	0.795	0.966	0.212	0.396	0.263
a_2^+	0.32 (71)	0.128	0.668	1	0.632	0.768	-0.104	0.0440	0.187
a_0^0	0.301 (10)	0.773	0.795	0.632	1	0.864	0.393	0.244	0.200
a_1^0	0.40 (15)	0.594	0.966	0.768	0.864	1	0.235	0.333	0.253
a_0^T	0.455 (21)	0.613	0.212	-0.104	0.393	0.235	1	0.711	0.608
a_1^T	−1.00 (31)	0.267	0.396	0.0440	0.244	0.333	0.711	1	0.903
a_2^T	−0.9 (1.3)	0.118	0.263	0.187	0.200	0.253	0.608	0.903	1

Table 51: Coefficients and correlation matrix for the $N^+ = N^0 = N^T = 3$ z-expansion of the $B \to K$ form factors f_+, f_0 and f_T. The coefficient a_2^0 is fixed by the $f_+(q^2 = 0) = f_0(q^2 = 0)$ constraint. The chi-square per degree of freedom is $\chi^2/\text{dof} = 1.86$ and the errors on the z-parameters have been rescaled by $\sqrt{\chi^2/\text{dof}} = 1.36$.

factor; indeed, a standalone fit to these data results in $\chi^2_{\text{red}} = 7.2/3 = 2.4$, while a similar standalone joint fit to f_+ and f_0 has $\chi^2_{\text{red}} = 9.2/7 = 1.3$. Finally, the global fit that is shown in the figure has $\chi^2_{\text{red}} = 18.6/10 = 1.86$.

Lattice computations of form factors in channels with a vector meson in the final state face extra challenges with respect to the case of a pseudoscalar meson: the state is unstable, and the extraction of the relevant matrix element from correlation functions is significantly more complicated; χPT cannot be used as a guide to extrapolate results at unphysically heavy pion masses to the chiral limit. While field-theory procedures to take resonance effects into account are available [92–102], they have not yet been implemented in the existing preliminary computations, which therefore suffer from uncontrolled systematic errors in calculations of weak decay form factors into unstable vector meson final states, such as the K^* or ρ mesons.[10]

As a consequence of the complexity of the problem, the level of maturity of these computations is significantly below the one present for pseudoscalar form factors. Therefore, we only provide a short guide to the existing results. Horgan *et al.* have obtained the seven form factors governing $B \to K^* \ell^+ \ell^-$ (as well as those for $B_s \to \phi\, \ell^+ \ell^-$ and for the charged-current decay $B_s \to K^* \ell \nu$) in Ref. [103] using NRQCD b quarks and asqtad staggered light quarks. In this work, they use a modified z-expansion to simultaneously extrapolate to the physical light-quark masses and fit the q^2-dependence. As discussed above, the unstable nature of the vector mesons was not taken into account. Horgan *et al.* use their form-factor results to calculate the differential branching fractions and angular distributions and discuss the implications for phenomenology in a companion paper [104]. An update of the form factor fits that enforces endpoint relations and also provides the full correlation matrices can be found in Ref. [105]. Finally, preliminary results on $B \to K^* \ell^+ \ell^-$ and $B_s \to \phi \ell^+ \ell^-$ by RBC/UKQCD have been reported in Refs. [106–108].

[10] In cases such as $B \to D^*$ transitions, that will be discussed below, this is much less of a practical problem due to the very narrow nature of the resonance.

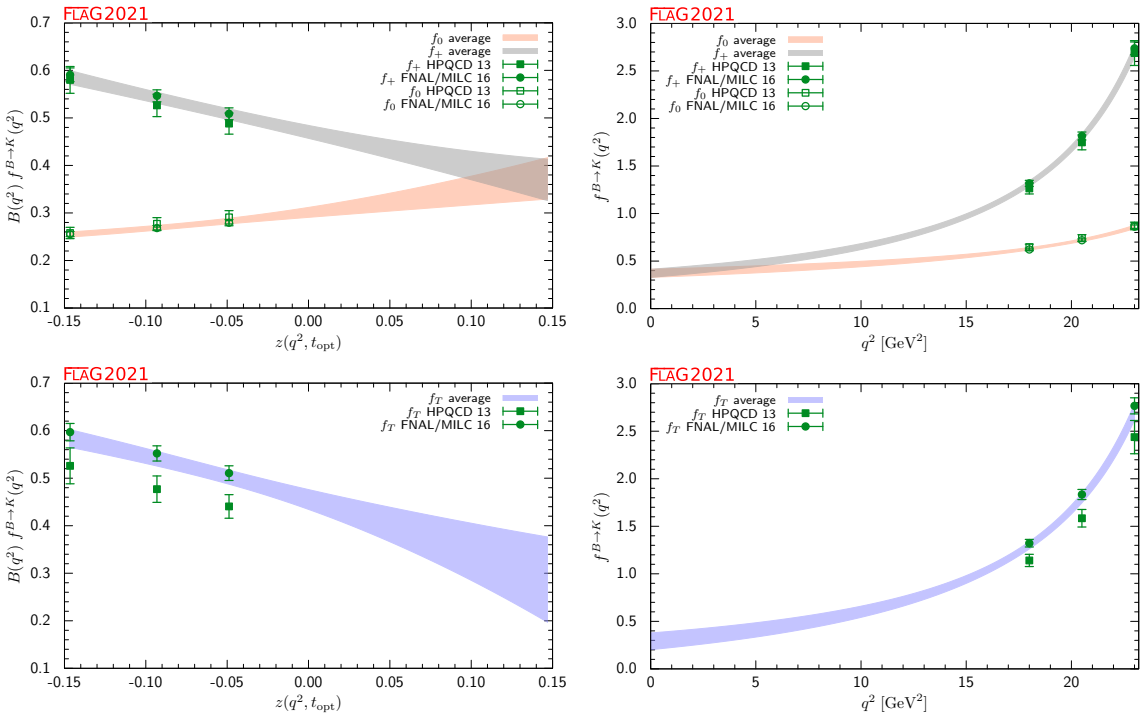

Figure 33: The $B \to K$ form factors $f_+(q^2)$, $f_0(q^2)$ and $f_T(q^2)$ plotted versus z (left panels) and q^2 (right panels). In the plots as a function of z, we remove the Blaschke factors. See text for a discussion of the data sets. The grey, salmon and blue bands display our preferred $N^+ = N^0 = N^T = 3$ BCL fit (eight parameters).

8.4 Semileptonic form factors for $B_{(s)} \to D_{(s)}\ell\nu$ and $B_{(s)} \to D^*_{(s)}\ell\nu$

The semileptonic processes $B_{(s)} \to D_{(s)}\ell\nu$ and $B_{(s)} \to D^*_{(s)}\ell\nu$ have been studied extensively by experimentalists and theorists over the years. They allow for the determination of the CKM matrix element $|V_{cb}|$, an extremely important parameter of the Standard Model. The matrix element V_{cb} appears in many quantities that serve as inputs to CKM unitarity triangle analyses and reducing its uncertainties is of paramount importance. For example, when ϵ_K, the measure of indirect CP violation in the neutral kaon system, is written in terms of the parameters ρ and η that specify the apex of the unitarity triangle, a factor of $|V_{cb}|^4$ multiplies the dominant term. As a result, the errors coming from $|V_{cb}|$ (and not those from B_K) are now the dominant uncertainty in the Standard Model (SM) prediction for this quantity.

The decay rate for $B \to D\ell\nu$ can be parameterized in terms of vector and scalar form factors in the same way as, e.g., $B \to \pi\ell\nu$ (see Sec. 8.3). The decay rate for $B \to D^*\ell\nu$ is different because the final-state hadron is spin-1. There are four form factors used to describe the vector and axial-vector current matrix elements that are needed to calculate this decay. We define the 4-velocity of the meson P as $v_P = p_P/m_P$ and the polarization vector of the D^* as ϵ. When the light lepton $\ell = e$, or μ, it is traditional to use $w = v_B \cdot v_{D^{(*)}}$ rather than q^2 as the variable upon which the form factors depend. Then, the form factors h_V and h_{A_i}, with $i = 1$, 2 or 3 are defined by

$$\langle D^*|V_\mu|B\rangle = \sqrt{m_B m_{D^*}}h_V(w)\varepsilon_{\mu\nu\alpha\beta}\epsilon^{*\nu}v^\alpha_{D^*}v^\beta_B\,, \tag{238}$$

$$\langle D^*|A_\mu|B\rangle = i\sqrt{m_B m_{D^*}}\left[h_{A_1}(w)(1+w)\epsilon^{*\mu} - h_{A_2}(w)\epsilon^*\cdot v_B v_{B\mu} - h_{A_3}(w)\epsilon^*\cdot v_B v_{D^*\mu}\right]. \tag{239}$$

The differential decay rates can then be written as[11]

$$\frac{d\Gamma_{B^-\to D^0\ell^-\bar\nu}}{dw} = \frac{G_F^2 m_D^3}{48\pi^3}(m_B+m_D)^2(w^2-1)^{3/2}|\eta_{\rm EW}|^2|V_{cb}|^2|\mathcal{G}(w)|^2, \tag{240}$$

$$\frac{d\Gamma_{B^-\to D^{0*}\ell^-\bar\nu}}{dw} = \frac{G_F^2 m_{D^*}^3}{4\pi^3}(m_B-m_{D^*})^2(w^2-1)^{1/2}|\eta_{\rm EW}|^2|V_{cb}|^2\chi(w)|\mathcal{F}(w)|^2, \tag{241}$$

where $w = v_B \cdot v_{D^{(*)}}$ (depending on whether the final-state meson is D or D^*) and $\eta_{\rm EW} = 1.0066$ is the 1-loop electroweak correction [109]. The function $\chi(w)$ in Eq. (241) depends on the recoil w and the meson masses, and reduces to unity at zero recoil [83].[12] These formulas do not include terms that are proportional to the lepton mass squared, which can be neglected for $\ell = e, \mu$. Further details of the definitions of $\mathcal{F}$ and $\mathcal{G}$ (which can be expressed in terms of the form factors h_V and h_{A_i}) may be found, e.g., in Ref. [83]. Until recently, most unquenched lattice calculations for $B \to D^*\ell\nu$ and $B \to D\ell\nu$ decays focused on the form

[11] These are the only meson decay channels dealt with in this review where we apply the Sirlin correction factor η_{EW}, that incorporates leading-order, structure-independent corrections. This is in keeping with common practice. While including η_{EW} in the analysis of $b \to c$ transitions is nearly universal in the literature, this is not so in other flavour-changing decays. It is worth stressing that this is just part of the expected corrections —cf. the discussion of QED corrections in the sections of this review dealing with light meson decay— and therefore its inclusion is largely arbitrary, insofar as a precise control of the full corrections, including the structure-dependent ones, is unavailable for a given channel. It is also necessary to remark, on the other hand, that different practices contribute to a small ambiguity in the comparison of CKM matrix elements determined from different decays, precisely of the order of the typically neglected electromagnetic corrections.

[12] The reason to keep the factor $\chi(w)$ outside the combination of form factors that defines $\mathcal{F}(w)$ is conventional, and inspired by the heavy-quark limit. One particular consequence of this notation is that at zero recoil $\mathcal{F}(1) = h_{A_1}(1)$.

factors at zero recoil $\mathcal{F}^{B\to D^*}(1)$ and $\mathcal{G}^{B\to D}(1)$; these can then be combined with experimental input to extract $|V_{cb}|$. aThe main reasons for concentrating on the zero recoil point are that (i) the decay rate then depends on a single form factor, and (ii) for $B \to D^*\ell\nu$, there are no $\mathcal{O}(\Lambda_{QCD}/m_Q)$ contributions due to Luke's theorem [110]. Further, the zero recoil form factor can be computed via a double ratio in which most of the current renormalization cancels and heavy-quark discretization errors are suppressed by an additional power of Λ_{QCD}/m_Q. Recent work on $B \to D^{(*)}\ell\nu$ transitions has started to explore the dependence of the relevant form factors on the momentum transfer, using a similar methodology to the one employed in $B \to \pi\ell\nu$ transitions; see Sec. 8.3 for a detailed discussion.

Early computations of the form factors for $B \to D\ell\nu$ decays include $N_f = 2+1$ results by FNAL/MILC [111, 112] for $\mathcal{G}^{B\to D}(1)$ and the $N_f = 2$ study by Atoui *et al.* [113], that in addition to providing $\mathcal{G}^{B\to D}(1)$ explored the $w > 1$ region. This latter work also provided the first results for $B_s \to D_s\ell\nu$ amplitudes, again including information about the momentum-transfer dependence. The first published unquenched results for $\mathcal{F}^{B\to D^*}(1)$, obtained by FNAL/MILC, date from 2008 [114]. In 2014 and 2015, significant progress was achieved in $N_f = 2+1$ computations: the FNAL/MILC value for $\mathcal{F}^{B\to D^*}(1)$ was updated in Ref. [115], and full results for $B \to D\ell\nu$ at $w \geq 1$ were published by FNAL/MILC [116] and HPQCD [117]. These works also provided full results for the scalar form factor, allowing analysis of the decay with a final-state τ. In the FLAG 19 review [1], we included new results for $B_s \to D_s\ell\nu$ form factors over the full kinematic range for $N_f = 2+1$ from HPQCD [118, 119], and for $B_{(s)} \to D^*_{(s)}\ell\nu$ form factors at zero recoil with $N_f = 2+1+1$ also from HPQCD [120, 121]. Most recently, HPQCD published further new calculations of the $B_s \to D_s^*$ form factor at zero recoil [122] and of the $B_s \to D_s$ form factors in the full kinematic range [123], now using MILC's HISQ $N_f = 2+1+1$ ensembles and using the HISQ action also for the b quark, reaching up to $m_b = 4m_c$ (unrenormalized mass) in their finest ensemble. Both of these calculations have recently been used by LHCb to determine $|V_{cb}|$ [124, 125], as discussed further in Sec. 8.9. HPQCD also extended their zero recoil analysis of $B_s \to D_s^*$ to the full recoil range, using the ensembles as in their $B_s \to D_s\ell\nu$ analysis, but with a small increase in statistics [126]. The last breakthrough in the field came from the FNAL/MILC collaboration, that recently published a complete calculation of the $B \to D^*$ form factors at nonzero recoil [127]. The HPQCD and the JLQCD collaborations are also working on this channel, as well as on improving their existing $B \to D$ calculations, and have presented preliminary results at nonzero recoil in several conferences [128, 129]. Improved calculations of the $B \to D$ and $B_s \to D_s$ form factors are also underway by RBC/UKQCD [63].

In the discussion below, we mainly concentrate on the latest generation of results, which supersedes previous $N_f = 2+1$ determinations and allows for an extraction of $|V_{cb}|$ that incorporates information about the q^2-dependence of the decay rate (cf. Sec. 8.9).

8.4.1 $B_{(s)} \to D_{(s)}$ decays

We will first discuss the $N_f = 2+1$ computations of $B \to D\ell\nu$ by FNAL/MILC and HPQCD mentioned above, both based on MILC asqtad ensembles. Full details about all the computations are provided in Tab. 54 and in the tables in Appendix C.6.5.

The FNAL/MILC study [116] employs ensembles at four values of the lattice spacing ranging between approximately 0.045 fm and 0.12 fm, and several values of the light-quark mass corresponding to pions with RMS masses ranging between 260 MeV and 670 MeV (with

just one ensemble with $M_\pi^{\rm RMS} \simeq 330$ MeV at the finest lattice spacing). The b and c quarks are treated using the Fermilab approach. The quantities directly studied are the form factors $h_\pm$ defined by

$$\frac{\langle D(p_D)|i\bar{c}\gamma_\mu b|B(p_B)\rangle}{\sqrt{m_D m_B}} = h_+(w)(v_B+v_D)_\mu + h_-(w)(v_B-v_D)_\mu\,, \tag{242}$$

which are related to the standard vector and scalar form factors by

$$f_+(q^2) = \frac{1}{2\sqrt{r}}\left[(1+r)h_+(w) - (1-r)h_-(w)\right], \tag{243}$$

$$f_0(q^2) = \sqrt{r}\left[\frac{1+w}{1+r}h_+(w) + \frac{1-w}{1-r}h_-(w)\right], \tag{244}$$

with $r = m_D/m_B$. (Recall that $q^2 = (p_B - p_D)^2 = m_B^2 + m_D^2 - 2w m_B m_D$.) The hadronic form factor relevant for experiment, $\mathcal{G}(w)$, is then obtained from the relation $\mathcal{G}(w) = \sqrt{4r} f_+(q^2)/(1+r)$. The form factors are obtained from double ratios of three-point functions in which the flavour-conserving current renormalization factors cancel. The remaining matching factor to the flavour-changing normalized current is estimated with 1-loop lattice perturbation theory. In order to obtain $h_\pm(w)$, a joint continuum-chiral fit is performed to an ansatz that contains the light-quark mass and lattice-spacing dependence predicted by next-to-leading order HMrSχPT, and the leading dependence on m_c predicted by the heavy-quark expansion ($1/m_c^2$ for h_+ and $1/m_c$ for h_-). The w-dependence, which allows for an interpolation in w, is given by analytic terms up to $(1-w)^2$, as well as a contribution from the logarithm proportional to $g^2_{D^*D\pi}$. The total resulting systematic error, determined as a function of w and quoted at the representative point $w = 1.16$ as 1.2% for f_+ and 1.1% for f_0, dominates the final error budget for the form factors. After f_+ and f_0 have been determined as functions of w within the interval of values of q^2 covered by the computation, synthetic data points are generated to be subsequently fitted to a z-expansion of the BGL form, cf. Sec. 8.3, with pole factors set to unity. This in turn enables one to determine $|V_{cb}|$ from a joint fit of this z-expansion and experimental data. The value of the zero-recoil form factor resulting from the z-expansion is

$$\mathcal{G}^{B\to D}(1) = 1.054(4)_{\rm stat}(8)_{\rm sys}\,. \tag{245}$$

The HPQCD computations [117, 119] use ensembles at two values of the lattice spacing, $a = 0.09,\ 0.12$ fm, and two and three values of light-quark masses, respectively. The b quark is treated using NRQCD, while for the c quark the HISQ action is used. The form factors studied, extracted from suitable three-point functions, are

$$\langle D_{(s)}(p_{D_{(s)}})|V^0|B_{(s)}\rangle = \sqrt{2M_{B_{(s)}}}f_\parallel^{(s)}\,, \qquad \langle D_{(s)}(p_{D_{(s)}})|V^k|B_{(s)}\rangle = \sqrt{2M_{B_{(s)}}}p^k_{D_{(s)}} f_\perp^{(s)}\,, \tag{246}$$

where V_μ is the relevant vector current and the $B_{(s)}$ rest frame is chosen. The standard vector and scalar form factors are retrieved as

$$f_+^{(s)} = \frac{1}{\sqrt{2M_{B_{(s)}}}}\left[f_\parallel^{(s)} + (M_{B_{(s)}} - E_{D_{(s)}})f_\perp^{(s)}\right], \tag{247}$$

$$f_0^{(s)} = \frac{\sqrt{2M_{B_{(s)}}}}{M^2_{B_{(s)}} - M^2_{D_{(s)}}}\left[(M_{B_{(s)}} - E_{D_{(s)}})f_\parallel^{(s)} + (M^2_{B_{(s)}} - E^2_{D_{(s)}})f_\perp^{(s)}\right]. \tag{248}$$

The currents in the effective theory are matched at 1-loop to their continuum counterparts. Results for the form factors are then fitted to a modified BCL z-expansion ansatz, that takes into account simultaneously the lattice spacing, light-quark masses, and q^2-dependence. For the mass dependence, NLO chiral logarithms are included, in the form obtained in hard-pion χPT (see footnote 33). As in the case of the FNAL/MILC computation, once f_+ and f_0 have been determined as functions of q^2, $|V_{cb}|$ can be determined from a joint fit of this z-expansion and experimental data. The papers quote for the zero-recoil vector form factor the result

$$\mathcal{G}^{B\to D}(1) = 1.035(40) \qquad \mathcal{G}^{B_s\to D_s}(1) = 1.068(40)\,. \tag{249}$$

The HPQCD and FNAL/MILC results for $B \to D$ differ by less than half a standard deviation (assuming they are uncorrelated, which they are not as some of the ensembles are common) primarily because of lower precision of the former result. The HPQCD central value is smaller by 1.8 of the FNAL/MILC standard deviations than the FNAL/MILC value. The dominant source of errors in the $|V_{cb}|$ determination by HPQCD are discretization effects and the systematic uncertainty associated with the perturbative matching.

In order to combine the form factor determinations of HPQCD and FNAL/MILC into a lattice average, we proceed in a similar way as with $B \to \pi\ell\nu$ and $B_s \to K\ell\nu$ above. FNAL/MILC quotes synthetic values for each form factor at three values of w (or, alternatively, q^2) with a full correlation matrix, which we take directly as input. In the case of HPQCD, we use their preferred modified z-expansion parameterization to produce synthetic values of the form factors at five different values of q^2 (three for f_+ and two for f_0). This leaves us with a total of six (five) data points in the kinematical range $w \in [1.00, 1.11]$ for the form factor f_+ (f_0). As in the case of $B \to \pi\ell\nu$, we conservatively assume a 100% correlation of statistical uncertainties between HPQCD and FNAL/MILC. We then fit this data set to a BCL ansatz, using $t_+ = (M_{B^0} + M_{D^\pm})^2 \simeq 51.12$ GeV^2 and $t_0 = (M_{B^0} + M_{D^\pm})(\sqrt{M_{B^0}} - \sqrt{M_{D^\pm}})^2 \simeq 6.19$ GeV^2. In our fits, pole factors have been set to unity, i.e., we do not take into account the effect of sub-threshold poles, which is then implicitly absorbed into the series coefficients. The reason for this is our imperfect knowledge of the relevant resonance spectrum in this channel, which does not allow us to decide the precise number of poles needed.[13] This, in turn, implies that unitarity bounds do not rigorously apply, which has to be taken into account when interpreting the results (cf. Appendix B.1).

With a procedure similar to what we adopted for the $B \to \pi$ and $B_s \to K$ cases, we impose the kinematic constraint at $q^2 = 0$ by expressing the $a^0_{N^0-1}$ coefficient in the z-expansion of f_0 in terms of all the other coefficients. As mentioned above, FNAL/MILC provides synthetic data for f_+ and f_0 including correlations; HPQCD presents the result of simultaneous z-fits to the two form factors including all correlations, thus enabling us to generate a complete set of synthetic data for f_+ and f_0. Since both calculations are based on MILC ensembles, we then reconstruct the off-diagonal HPQCD-FNAL/MILC entries of the covariance matrix by conservatively assuming that statistical uncertainties are 100% correlated. The Fermilab/MILC (HPQCD) statistical error is 58% (31%) of the total error for every f_+ value, and 64% (49%) for every f_0 one. Using this information we can easily build the off-diagonal block of the overall covariance matrix (e.g., the covariance between $[f_+(q_1^2)]_{\rm FNAL}$ and $[f_0(q_2^2)]_{\rm HPQCD}$ is $(\delta[f_+(q_1^2)]_{\rm FNAL} \times 0.58)\,(\delta[f_0(q_2^2)]_{\rm HPQCD} \times 0.49)$, where δf is the total error).

[13] As noted above, this is the same approach adopted by FNAL/MILC in their fits to a BGL ansatz. HPQCD, meanwhile, uses one single pole in the pole factors that enter their modified z-expansion, using their spectral studies to fix the value of the relevant resonance masses.

$B \to D$ ($N_f = 2+1$)

a_n^i	Central Values	Correlation Matrix				
a_0^+	0.896 (10)	1	0.423	-0.231	0.958	0.596
a_1^+	-7.94 (20)	0.423	1	0.325	0.498	0.919
a_2^+	51.4 (3.2)	-0.231	0.325	1	-0.146	0.317
a_0^0	0.7821 (81)	0.958	0.498	-0.146	1	0.593
a_1^0	-3.28 (20)	0.596	0.919	0.317	0.593	1

Table 52: Coefficients and correlation matrix for the $N^+ = N^0 = 3$ z-expansion of the $B \to D$ form factors f_+ and f_0. The chi-square per degree of freedom is $\chi^2/\text{dof} = 4.6/6 = 0.77$. The lattice calculations that enter this fit are taken from FNAL/MILC [116] and HPQCD [117].

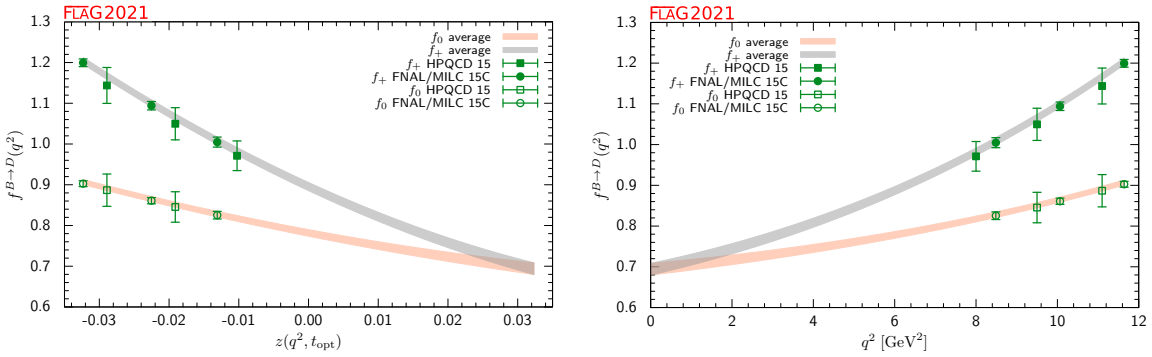

Figure 34: The form factors $f_+(q^2)$ and $f_0(q^2)$ for $B \to D\ell\nu$ plotted versus z (left panel) and q^2 (right panel). See text for a discussion of the data sets. The grey and salmon bands display our preferred $N^+ = N^0 = 3$ BCL fit (five parameters).

For our central value, we choose an $N^+ = N^0 = 3$ BCL fit, shown in Tab. 52. The coefficient a_3^+ can be obtained from the values for a_0^+–a_2^+ using Eq. (532). We find $\chi^2/\text{dof} = 4.6/6 = 0.77$. The fit, which is dominated by the FNAL/MILC calculation, is illustrated in Fig. 34.

Reference [113] is the only existing $N_f = 2$ work on $B \to D\ell\nu$ transitions, that furthermore provided the first available results for $B_s \to D_s\ell\nu$. This computation uses the publicly available ETM configurations obtained with the twisted-mass QCD action at maximal twist. Four values of the lattice spacing, ranging between 0.054 fm and 0.098 fm, are considered, with physical box lengths ranging between 1.7 fm and 2.7 fm. At two values of the lattice spacing two different physical volumes are available. Charged-pion masses range between ≈ 270 MeV and ≈ 490 MeV, with two or three masses available per lattice spacing and volume, save for the $a \approx 0.054$ fm point at which only one light mass is available for each of the two volumes. The strange- and heavy-valence quarks are also treated with maximally twisted-mass QCD.

The quantities of interest are again the form factors $h_\pm$ defined above. In order to control discretization effects from the heavy quarks, a strategy similar to the one employed by the ETM collaboration in their studies of B-meson decay constants (cf. Sec. 8.1) is employed: the value of $\mathcal{G}(w)$ is computed at a fixed value of m_c and several values of a heavier quark mass

$m_h^{(k)} = \lambda^k m_c$, where λ is a fixed scaling parameter, and step-scaling functions are built as

$$\Sigma_k(w) = \frac{\mathcal{G}(w, \lambda^{k+1} m_c, m_c, a^2)}{\mathcal{G}(w, \lambda^k m_c, m_c, a^2)} \,. \tag{250}$$

Each ratio is extrapolated to the continuum limit, $\sigma_k(w) = \lim_{a\to 0} \Sigma_k(w)$. One then exploits the fact that the $m_h \to \infty$ limit of the step-scaling is fixed. In particular, it is easy to find from the heavy-quark expansion that $\lim_{m_h\to\infty} \sigma(1) = 1$. In this way, the physical result at the b-quark mass can be reached by interpolating $\sigma(w)$ between the charm region (where the computation can be carried out with controlled systematics) and the known static limit value.

In practice, the values of m_c and m_s are fixed at each value of the lattice spacing such that the experimental kaon and D_s masses are reached at the physical point, as determined in Ref. [130]. For the scaling parameter, $\lambda = 1.176$ is chosen, and eight scaling steps are performed, reaching $m_h/m_c = 1.176^9 \simeq 4.30$, approximately corresponding to the ratio of the physical b- and c-masses in the $\overline{\text{MS}}$ scheme at 2 GeV. All observables are obtained from ratios that do not require (re)normalization. The ansatz for the continuum and chiral extrapolation of Σ_k contains a constant and linear terms in m_{sea} and a^2. Twisted boundary conditions in space are used for valence-quark fields for better momentum resolution. Applying this strategy, the form factors are finally obtained at four reference values of w between 1.004 and 1.062, and, after a slight extrapolation to $w = 1$, the result is

$$\mathcal{G}^{B_s\to D_s}(1) = 1.052(46) \,. \tag{251}$$

The authors also provide values for the form factor relevant for the meson states with light-valence quarks, obtained from a similar analysis to the one described above for the $B_s \to D_s$ case. Values are quoted from fits with and without a linear m_{sea}/m_s term in the chiral extrapolation. The result in the former case, which safely covers systematic uncertainties, is

$$\mathcal{G}^{B\to D}(1) = 1.033(95) \,. \tag{252}$$

Given the identical strategy, and the small sensitivity of the ratios used in their method to the light valence- and sea-quark masses, we assign this result the same ratings in Tab. 54 as those for their calculation of $\mathcal{G}^{B_s\to D_s}(1)$. Currently, the precision of this calculation is not competitive with that of $N_f = 2 + 1$ works, but this is due largely to the small number of configurations analyzed by Atoui *et al.* The viability of their method has been clearly demonstrated, however, which leaves significant room for improvement on the errors of both the $B \to D$ and $B_s \to D_s$ form factors with this approach by including either additional two-flavour data or analysing more recent ensembles with $N_f > 2$.

Atoui *et al.* also study the scalar and tensor form factors, as well as the momentum-transfer dependence of $f_{+,0}$. The value of the ratio $f_0(q^2)/f_+(q^2)$ is provided at a reference value of q^2 as a proxy for the slope of $\mathcal{G}(w)$ around the zero-recoil limit.

Let us finally discuss the most recent results for $B_s \to D_s$ form factors, obtained by the HPQCD collaboration using MILC's $N_f = 2 + 1 + 1$ ensembles in Ref. [123]. Three values of the lattice spacing are used, including a very fine ensemble at $a \simeq 0.044$ fm; the pion mass is kept fixed at around 300 MeV, and in addition at the coarser $a \simeq 0.09$ fm lattice an ensemble with the physical pion mass is included. The scalar current needs no renormalization because of the PCVC relation, while the vector current is nonperturbatively normalized by imposing a condition based on the PCVC relation at zero recoil. Heavy quarks are treated in a fully

$B_s \to D_s$ ($N_f = 2+1+1$)

a_n^i	Central Values	Correlation Matrix					
a_0^0	0.666(12)	1	0.62004	0.03149	1	0.03973	0.00122
a_1^0	-0.26(25)	0.62004	1	0.36842	0.62004	0.12945	0.00002
a_2^0	-0.1(1.8)	0.03149	0.36842	1	0.03149	0.22854	-0.00168
a_0^+	-0.075(12)	1	0.62004	0.03149	1	0.03973	0.00122
a_1^+	-3.24(45)	0.03973	0.12945	0.22854	0.03973	1	0.11086
a_2^+	0.7(2.0)	0.00122	0.00002	-0.00168	0.00122	0.11086	1

Table 53: Coefficients and correlation matrix for the z-expansion of the $B_s \to D_s$ form factors f_+ and f_0. These results are a reproduction of Table VIII of Ref. [123].

relativistic fashion through the use of the HISQ regularization, employing bare values of the quark mass up to $am_h = 0.8$ for the extrapolation to the physical b point.

Results for the form factors are fitted to a modified z-expansion ansatz, based on a BCL ansatz with a Blaschke factor containing one sub-threshold pole, tuned to reproduce the lattice-spacing and heavy-quark-mass-dependent mass of the corresponding resonance. The final error budget is equally dominated by statistics and the combined effect of the continuum and heavy quark mass extrapolations, which correspond to 1.1% and 1.2% uncertainties, respectively, for the scalar form factor at zero recoil. The total uncertainty of the latter is thus below 2%, which remains true in the whole q^2 range. The uncertainty of f_+ is somewhat larger, starting at around 2% at $q^2 = 0$ and increasing up to around 3.5% at zero recoil.

One important matter of concern with this computation is the use of the $a \simeq 0.044$ fm ensemble with periodic boundary conditions, which suffers from severe topology freezing. Other than possible implications for statistical uncertainties, the lack of topology fluctuations are expected to significantly enhance finite-volume effects, which are no longer exponential in $m_\pi L$, but become power-like in the spatial volume. The authors neglect the impact of finite-volume effects in the computation, with a twofold argument: for the two coarser lattice spacings, the impact of pion-mass-related corrections on the heavy-meson states involved is presumably negligible; and, for the finest ensemble, the estimate of finite-volume effects on the D_s decay constant obtained in Ref. [131] turns out to be very small, a result which is presumed to extend to form factors. It is however unclear whether the latter argument would really hold, since the computation in Ref. [131] does show that the expected effect is heavily observable-dependent, reaching, e.g., more than 1% for f_D. We have, therefore, concluded that our standard criteria for finite-volume effects cannot be applied at the finest lattice spacing, and opted to assign ○ rating to them.

We thus proceed to quote the final result of HPQCD 19 as the FLAG estimate for the $N_f = 2+1+1$ $B_s \to D_s$ form factors. The preferred fit is a constrained BCL form with the imposition of the kinematical constraint $f_+(0) = f_0(0)$, carried through z^2 for f_0 and z^3 for f_+. Both form factors contain just one sub-threshold pole, to which the masses $M_{B_c^*} = 6.329$ GeV and $M_{B_{c0}} = 6.704$ GeV, respectively, have been assigned. The fit parameters and covariance matrix, quoted in Table VIII of Ref. [123], are reproduced in Table 53.

8.4.2 Lepton-flavour-universality ratios $R(D^{(*)})$ and $R(D_s^{(*)})$

The availability of results for the scalar form factor f_0 for $B \to D\ell\nu$ amplitudes allows us to study interesting observables that involve the decay in the τ channel. One such quantity is the ratio

$$R(D) = \frac{\mathcal{B}(B \to D\tau\nu)}{\mathcal{B}(B \to D\ell\nu)} \quad \text{with} \quad \ell = e, \mu\,, \tag{253}$$

which, in the Standard Model, depends only on the form factors and hadron and lepton masses. Indeed, the recent availability of experimental results for $R(D)$ has made this quantity particularly relevant in the search for possible physics beyond the Standard Model. The most recent HFLAV average reads [132]:

$$R(D)_{\rm exp} = 0.340(27)(13)\,. \tag{254}$$

Using the FLAG average of the $B \to D$ form factors discussed above and presented in Table 52, we find $R(D)^{\rm FLAG}_{\rm lat} = 0.2934(38)$. The ratio $R(D)$ requires the integral of the branching ratios for $\ell = e, \mu, \tau$ over the whole phase space. Since lattice simulations are sensitive mostly to relatively large q^2 values, lattice-only calculations of $R(D)$ rely on the extrapolation of the form factors to low q^2 and are especially sensitive to the choice of parameterization. In order to estimate this source of systematics, we repeated the fit using the parameterization adopted by HPQCD in Ref. [117]. The main difference with respect to our default paremeterization is the inclusion of Blaschke factors for the form factors f_+ and f_0 located at $M_+ = M_{B_c^*} = 6.330(9)$ GeV and $M_0 = 6.420(9)$ GeV; additionally, the parameter t_0 is set to $(m_B - m_D)^2$. Using five coefficients ($a^+_{1,2,3}$ and $a^0_{1,2}$ with a^0_3 fixed by the $f_+(q^2 = 0) = f_0(q^2 = 0)$ condition) we find $R(D)^{\rm HPQCD}_{\rm lat} = 0.3009(38)$ which deviates from $R(D)^{\rm FLAG}_{\rm lat}$ by 1.4 σ. To take this potential source of systematic uncertainty into account we rescale accordingly the uncertainty of our default fit and obtain:

$$R(D)_{\rm lat} = 0.2934(53)\,, \qquad N_f = 2+1 \text{ (our average)}. \tag{255}$$

After including the $B \to D\ell\nu$ ($\ell = e, \mu$) data in the fit, as discussed at the end of Sec. 8.9, we obtain the following combined lattice plus experiment result:

$$R(D)_{\rm lat+exp} = 0.2951(31)\,, \qquad N_f = 2+1 \text{ (our average)}. \tag{256}$$

HPQCD also computes values for $R(D_s)$, the analog of $R(D)$ with both heavy-light mesons containing a strange quark. The earlier calculation using NRQCD b quarks gives

$$R(D_s)_{\rm lat} = 0.301(6)\,, \qquad N_f = 2+1 \ [119]. \tag{257}$$

The newer calculation with HISQ b quarks yields the somewhat more precise value

$$R(D_s)_{\rm lat} = 0.2987(46)\,, \qquad N_f = 2+1+1 \ [123]. \tag{258}$$

A similar ratio $R(D^*)$ can be considered for $B \to D^*$ transitions. As a matter of fact, the experimental value of $R(D^*)$ is significantly more precise than the one of $R(D)$. As of today, the only complete, unquenched calculation of the $B \to D^*$ form factors that has been published is Ref. [127], by the FNAL/MILC collaboration, that reports

$$R(D^*)_{\rm lat} = 0.265(13)\,, \qquad N_f = 2+1 \ [127]. \tag{259}$$

But there are other efforts to be considered, by the JLQCD and the HPQCD collaborations, that have already presented preliminary results in Refs. [129] and [128], respectively.

There is a growing interest in the $B_s \to D_s^* \ell\nu$ channel, both from the theoretical and the experimental side. The only available calculation right now comes from the HPQCD collaboration [126], giving,

$$R(D_s^*)_{\rm lat} = 0.2490(60)_{\rm latt}(35)_{\rm EM}\,, \qquad N_f = 2+1+1 \ [126], \tag{260}$$

where the first error comes from the lattice calculation, and the second error is an estimate of electromagnetic effects.

8.4.3 Fragmentation fraction ratio f_s/f_d

Another area of immediate interest in searches for physics beyond the Standard Model is the measurement of $B_s \to \mu^+\mu^-$ decays, recently studied at the LHC. One of the inputs required by the LHCb analysis is the ratio of B_q meson ($q = d, s$) fragmentation fractions f_s/f_d, where f_q is the probability that a q quark hadronizes into a B_q. This ratio can be measured by writing it as a product of ratios that involve experimentally measurable quantities, cf. Refs. [133, 134]. One of the factors is the ratio $f_0^{(s)}(M_\pi^2)/f_0^{(d)}(M_K^2)$ of scalar form factors for the corresponding semileptonic meson decay, which is where lattice input becomes useful.

A dedicated $N_f = 2+1$ study by FNAL/MILC[14] [135] addresses the ratios of scalar form factors $f_0^{(q)}(q^2)$, and quotes:

$$f_0^{(s)}(M_\pi^2)/f_0^{(d)}(M_K^2) = 1.046(44)(15), \qquad f_0^{(s)}(M_\pi^2)/f_0^{(d)}(M_\pi^2) = 1.054(47)(17), \tag{261}$$

where the first error is statistical and the second systematic. The more recent results from HPQCD [119] are:

$$f_0^{(s)}(M_\pi^2)/f_0^{(d)}(M_K^2) = 1.000(62), \qquad f_0^{(s)}(M_\pi^2)/f_0^{(d)}(M_\pi^2) = 1.006(62). \tag{262}$$

Results from both groups lead to fragmentation fraction ratios f_s/f_d that are consistent with LHCb's measurements via other methods [134].

8.4.4 $B_{(s)} \to D_{(s)}^*$ decays

The most precise computation of the zero-recoil form factors needed for the determination of $|V_{cb}|$ from exclusive B semileptonic decays comes from the $B \to D^* \ell\nu$ form factor at zero recoil $\mathcal{F}^{B\to D^*}(1)$, calculated by the FNAL/MILC collaboration. The original computation, published in Ref. [114], was updated [115] by employing a much more extensive set of gauge ensembles and increasing the statistics of the ensembles originally considered, while preserving the analysis strategy. Later on, the same setup was used to calculate the same form factors away from the zero recoil point [127]. Other collaborations are also working on nonzero recoil results, mainly HPQCD [128] and JLQCD [129].

References [115] and [127] use the MILC $N_f = 2+1$ ensembles. The bottom and charm quarks are simulated using the clover action with the Fermilab interpretation and light quarks are treated via the asqtad staggered fermion action. Recalling the definition of the form factors

[14] This work also provided a value for $R(D)$, now superseded by Ref. [116].

in Eq. (239), at zero recoil $\mathcal{F}^{B\to D^*}(1)$ reduces to a single form factor $h_{A_1}(1)$ coming from the axial-vector current

$$\langle D^*(v,\epsilon')|\mathcal{A}_\mu|\overline{B}(v)\rangle = i\sqrt{2m_B 2m_{D^*}}\;\epsilon'^*_\mu h_{A_1}(1), \tag{263}$$

where ϵ' is the polarization of the D^*. The form factor is accessed through a ratio of three-point correlators, viz.,

$$\mathcal{R}_{A_1} = \frac{\langle D^*|\bar{c}\gamma_j\gamma_5 b|\overline{B}\rangle\;\langle\overline{B}|\bar{b}\gamma_j\gamma_5 c|D^*\rangle}{\langle D^*|\bar{c}\gamma_4 c|D^*\rangle\;\langle\overline{B}|\bar{b}\gamma_4 b|\overline{B}\rangle} = |h_{A_1}(1)|^2. \tag{264}$$

There are several strategies to calculate the form factor h_{A_1} away from the zero recoil point. The FNAL/MILC collaboration generalizes Eq. (264) to nonzero momentum. The HPQCD and JLQCD collaborations compute $h_{A_1}(1)$ and the ratio

$$\mathcal{Q}_{A_1} = \frac{\langle D^*(p',\varepsilon')|\bar{c}\gamma_j\gamma_5 b|\overline{B}(p)\rangle}{\langle D^*(p,\varepsilon')|\bar{c}\gamma_j\gamma_5 b|\overline{B}(p)\rangle}, \tag{265}$$

which gives $h_{A_1}(w)/h_{A_1}(1)$ times other factors that must be removed. Simulation data of the FNAL/MILC calculation is obtained on MILC ensembles with five lattice spacings, ranging from $a \approx 0.15$ fm to $a \approx 0.045$ fm, and as many as five values of the light-quark masses per ensemble (though just one at the finest lattice spacing). Results are then extrapolated to the physical, continuum/chiral, limit employing staggered χPT.

The D^* meson is not a stable particle in QCD and decays predominantly into a D plus a pion. Nevertheless, heavy-light meson χPT can be applied to extrapolate lattice simulation results for the $B \to D^*\ell\nu$ form factor to the physical light-quark mass. The D^* width is quite narrow, 0.096 MeV for the $D^{*\pm}(2010)$ and less than 2.1 MeV for the $D^{*0}(2007)$, making this system much more stable and long lived than the ρ or the K^* systems. The fact that the $D^* - D$ mass difference is close to the pion mass leads to the well-known "cusp" in $\mathcal{R}_{A_1}$ just above the physical pion mass [136–138]. This cusp makes the chiral extrapolation sensitive to values used in the χPT formulas for the $D^*D\pi$ coupling $g_{D^*D\pi}$. In order to take this sensitivity into account, the FNAL/MILC collaboration includes this coupling in their fits as an input prior $g_{D^*D\pi} = 0.53 \pm 0.08$, resulting in an increase of 0.3% in the total uncertainty for $h_{A_1}(1)$ in Ref. [115]. The FNAL/MILC calculation at nonzero recoil uses the same prior, but the effect on the final result is not specified.

The final value presented in Ref. [127], which supersedes that of Ref. [115], is

$$N_f = 2+1: \quad \mathcal{F}^{B\to D^*}(1) = 0.909(17)\,, \tag{266}$$

making up a total error of 1.9%, up from the 1.4% of Ref. [115] due to more conservative choices. The largest systematic uncertainty comes from discretization errors followed by effects of higher-order corrections in the chiral perturbation theory ansatz.

In 2017, the HPQCD collaboration has published the first study of $B_{(s)} \to D^*_{(s)}\ell\nu$ form factors at zero recoil for $N_f = 2+1+1$ using eight MILC ensembles with lattice spacing $a \approx 0.15$ fm, 0.12 fm, and 0.09 fm [121]. There are three ensembles with varying light-quark masses for the two coarser lattice spacings and two choices of light-quark mass for the finest lattice spacing. In each case, there is one ensemble for which the light-quark mass is very close to the physical value. The b quark is treated using NRQCD and the light quarks are treated using the HISQ action. The resulting zero-recoil form factors are:

$$N_f = 2+1+1: \quad \mathcal{F}^{B\to D^*}(1) = 0.895(10)(24)\,, \qquad \mathcal{F}^{B_s\to D^*_s}(1) = 0.883(12)(28)\,. \tag{267}$$

In 2019, the HPQCD collaboration published a new $N_f = 2+1+1$ calculation of the $B_s \to D_s^*$ form factor at zero recoil, now using the HISQ action also for the b quark [122]. The lattice methodology and ensembles used are the same as in their 2019 calculation of the $B_s \to D_s$ form factors [123], which was discussed in detail in Sec. 8.4.1. The resulting form factor is:

$$N_f = 2+1+1: \quad \mathcal{F}^{B_s \to D_s^*}(1) = 0.9020(96)(90)\,. \tag{268}$$

The calculations in Refs. [121, 122] use different b-quark actions and share only two ensambles at $a = 0.09$ fm and can be considered essentially independent, yielding the average:

$$N_f = 2+1+1: \quad \mathcal{F}^{B_s \to D_s^*}(1) = 0.899(12)\,, \qquad \text{our average.} \tag{269}$$

The HPQCD and JLQCD collaborations are also devoting their efforts to determine the full momentum dependence of $B_{(s)} \to D_{(s)}^* \ell\nu$ form factors, and preprints for both calculations are already available. JLQCD efforts are based on $N_f = 2+1$ Möbius domain-wall ensembles and a relativistic heavy quark action. The latest status update can be found in Ref. [129]. The HPQCD computation, Ref. [128], is based on $N_f = 2+1+1$ HISQ ensembles, and uses the same regularization for heavy quarks. This calculation, once finalized, will supersede the existing HPQCD results in the $B_s \to D_s^*$ channel presented in Ref. [122]. Upon publication of both works, we intend to include full details for them in an upcoming intermediate update of this section.

8.5 Semileptonic form factors for $B_c \to (\eta_c, J/\psi)\ell\nu$ decays

In a recent publication, HPQCD 20B [139] provided the first full determination of $B_c \to J/\psi$ form factors, extending earlier preliminary work that also covered $B_c \to \eta_c$, Refs. [140, 141]. While the latter employed both NRQCD and HISQ actions for the valence b quark, and the HISQ action for the c quark, in HPQCD 20B the HISQ action is used throughout for all flavors. The setup is the same as for the $B_s \to D_s$ computation discussed above, HPQCD 19; we refer to the entries for the latter paper in summary tables for details. The flavor singlet nature of the final state means that there are contributions to the relevant three-point functions from disconnected Wick contractions, which are not discussed in the paper.

There are however some relevant differences with $B_s \to D_s$ decays. In the J/ψ case, since the hadron in the final state has vector quantum numbers, the description of the hadronic amplitude requires four independent form factors V, A_0, A_1, A_2. Specifically,

$$\begin{aligned}
\langle J/\psi(p',\lambda)|\bar{c}\gamma^\mu b|B_c^-(p)\rangle =& \frac{2iV(q^2)}{M_{B_c}+M_{J/\psi}}\varepsilon^{\mu\nu\rho\sigma}\epsilon^*_\nu(p',\lambda)p'_\rho p_\sigma\,,\\
\langle J/\psi(p',\lambda)|\bar{c}\gamma^\mu\gamma^5 b|B_c^-(p)\rangle =& 2M_{J/\psi}A_0(q^2)\frac{\epsilon^*(p',\lambda)\cdot q}{q^2}q^\mu\\
&+(M_{B_c}+M_{J/\psi})A_1(q^2)\left[\epsilon^{*\mu}(p',\lambda)-\frac{\epsilon^*(p',\lambda)\cdot q}{q^2}q^\mu\right]\\
&-A_2(q^2)\frac{\epsilon^*(p',\lambda)\cdot q}{M_{B_c}+M_{J/\psi}}\left[p^\mu+p'^\mu-\frac{M_{B_c}^2-M_{J/\psi}^2}{q^2}q^\mu\right],
\end{aligned} \tag{270}$$

where ϵ_μ is the polarization vector of the J/ψ state. The computed form factors are fitted to a z-parameterization-inspired ansatz, where coefficients are modified to model the lattice-spacing and the heavy- and light-mass dependences, for a total of 280 fit parameters. In

the continuum and at physical kinematics only 16 parameters survive, as each form factor is parameterized by an expression of the form

$$F(q^2) = \frac{1}{P(q^2)} \sum_{n=0}^{3} a_n z^n \,, \tag{271}$$

where the pole factor is given by

$$P(q^2) = \prod_k z(q^2, M_k^2) \tag{272}$$

with $\{M_k\}$ a different set of pole energies below the BD^* threshold for each set of J^P quantum numbers, taken from a mixture of experimental results, lattice determinations, and model estimates. The values used (in GeV) are

$$\begin{aligned} 0^- &: \ 6.275,\ 6.872,\ 7.25; \\ 1^- &: \ 6.335,\ 6.926,\ 7.02,\ 7.28; \\ 1^+ &: \ 6.745,\ 6.75,\ 7.15,\ 7.15. \end{aligned} \tag{273}$$

The outcome of the fit, that we quote as a FLAG estimate, is

	a_0	a_1	a_2	a_3
V	0.1057(55)	-0.746(92)	0.10(98)	0.006(1.000)
$A0$	0.1006(37)	-0.731(72)	0.30(90)	-0.02(1.00)
$A1$	0.0553(19)	-0.266(40)	0.31(70)	0.11(99)
$A2$	0.0511(91)	-0.22(19)	-0.36(82)	-0.05(1.00)

The correlation matrix for the coefficients is provided in Tables XIX-XXVII of Ref. [139]

8.6 Semileptonic form factors for $\Lambda_b \to (p, \Lambda_c^{(*)})\ell\bar{\nu}$ decays

The $b \to c\ell\bar{\nu}$ and $b \to u\ell\bar{\nu}$ transitions can also be probed in decays of Λ_b baryons. With the LHCb experiment, the final state of $\Lambda_b \to p\mu\bar{\nu}$ is easier to identify than that of $B \to \pi\mu\bar{\nu}$ [142], and the first determination of $|V_{ub}|/|V_{cb}|$ at the Large Hadron Collider was performed using a ratio of $\Lambda_b \to p\mu\bar{\nu}$ and $\Lambda_b \to \Lambda_c\mu\bar{\nu}$ decay rates [143] (cf. Sec. 8.10).

The amplitudes of the decays $\Lambda_b \to p\ell\bar{\nu}$ and $\Lambda_b \to \Lambda_c\ell\bar{\nu}$ receive contributions from both the vector and the axial-vector components of the current in the matrix elements $\langle p|\bar{u}\gamma^\mu(\mathbf{1} - \gamma_5)b|\Lambda_b\rangle$ and $\langle\Lambda_c|\bar{c}\gamma^\mu(\mathbf{1} - \gamma_5)b|\Lambda_b\rangle$. The matrix elements split into three form factors f_+, f_0, $f_\perp$ mediated by the vector component of the current, and another three form factors g_+, g_0, $g_\perp$ mediated by the axial-vector component—see, e.g., Ref. [144] for a complete description. Given the sensitivity to all Dirac structures, measurements of the baryonic decay rates also provides useful complementary constraints on right-handed couplings beyond the Standard Model [143].

To date, only one unquenched lattice-QCD computation of the $\Lambda_b \to p$ and $\Lambda_b \to \Lambda_c$ form factors with physical heavy-quark masses has been published: Detmold 15 [145]. This computation uses RBC/UKQCD $N_f = 2 + 1$ DWF ensembles, and treats the b and c quarks within the Columbia RHQ approach. The renormalization of the currents is carried out using a mostly nonperturbative method, with residual matching factors computed at one loop.

Two values of the lattice spacing ($a \approx 0.11,\ 0.085$ fm) are considered, with the absolute scale set from the $\Upsilon(2S)$–$\Upsilon(1S)$ splitting. Sea pion masses lie in a narrow interval ranging from slightly above 400 MeV to slightly below 300 MeV, keeping $m_\pi L \gtrsim 4$; however, lighter pion masses are considered in the valence DWF action for the u, d quarks. The lowest valence-valence pion mass is 227(3) MeV, which leads to a ■ rating of finite-volume effects. Results for the form factors are obtained from suitable three-point functions, and fitted to a modified z-expansion ansatz that combines the q^2-dependence with the chiral and continuum extrapolations. The main results of the paper are the predictions (errors are statistical and systematic, respectively)

$$\zeta_{p\mu\bar{\nu}}(15\text{GeV}^2) \equiv \frac{1}{|V_{ub}|^2}\int_{15\ \text{GeV}^2}^{q^2_{\text{max}}} \frac{\mathrm{d}\Gamma(\Lambda_b \to p\mu^-\bar{\nu}_\mu)}{\mathrm{d}q^2}\,\mathrm{d}q^2 \qquad = 12.31(76)(77)\ \text{ps}^{-1}\,, \tag{274}$$

$$\zeta_{\Lambda_c\mu\bar{\nu}}(7\text{GeV}^2) \equiv \frac{1}{|V_{cb}|^2}\int_{7\ \text{GeV}^2}^{q^2_{\text{max}}} \frac{\mathrm{d}\Gamma(\Lambda_b \to \Lambda_c\mu^-\bar{\nu}_\mu)}{\mathrm{d}q^2}\,\mathrm{d}q^2 \qquad = 8.37(16)(34)\ \text{ps}^{-1}\,, \tag{275}$$

$$\frac{\zeta_{p\mu\bar{\nu}}(15\text{GeV}^2)}{\zeta_{\Lambda_c\mu\bar{\nu}}(7\text{GeV}^2)} = 1.471(95)(109)\,, \tag{276}$$

which are the input for the LHCb analysis. Predictions for the total rates in all possible lepton channels, as well as for ratios similar to $R(D)$ (cf. Sec. 8.4) between the τ and light-lepton channels are also available, in particular,

$$R(\Lambda_c) = \frac{\Gamma(\Lambda_b \to \Lambda_c\,\tau^-\bar{\nu}_\tau)}{\Gamma(\Lambda_b \to \Lambda_c\,\mu^-\bar{\nu}_\mu)} = 0.3328(74)(70). \tag{277}$$

Datta 2017 [146] additionally includes results for the $\Lambda_b \to \Lambda_c$ tensor form factors h_+, $h_\perp$, $\widetilde{h}_+$, $\widetilde{h}_\perp$, based on the same lattice computation as Detmold 15 [145]. The main focus of Datta 2017 is the phenomenology of the $\Lambda_b \to \Lambda_c\tau\overline{\nu}_\tau$ decay and how it can be used to constrain contributions from beyond the Standard Model physics. Unlike in the case of the vector and axial-vector currents, the residual matching factors of the tensor currents are set to their tree-level value. While the matching systematic uncertainty is augmented to take this fact into account, the procedure implies that the tensor current retains an uncanceled logarithmic divergence at $\mathcal{O}(\alpha_s)$.

Recently, first lattice calculations have also been completed for Λ_b semileptonic decays to negative-parity baryons in the final state. Such calculations are substantially more challenging and have not yet reached the same level of precision. Meinel 21 [147] considers the decays $\Lambda_b \to \Lambda_c^*(2595)\ell\bar{\nu}$ and $\Lambda_b \to \Lambda_c^*(2625)\ell\bar{\nu}$, where the $\Lambda_c^*(2595)$ and $\Lambda_c^*(2625)$ are the lightest charm baryons with isospin 0 and $J^P = \frac{1}{2}^-$ and $J^P = \frac{3}{2}^-$, respectively. These decay modes may eventually provide new opportunities to test lepton-flavor universality at the LHC, but are also very interesting from a theoretical point of view. The lattice results for the form factors may help tighten dispersive constraints in global analyses of $b \to c$ semileptonic decays [148], and may provide new insights into the internal structure of the negative-parity heavy baryons and their description in heavy-quark-effective-theory. The $\Lambda_c^*(2595)$ and $\Lambda_c^*(2625)$ are very narrow resonances decaying through the strong interaction into $\Lambda_c\pi\pi$. The strong decays are neglected in Meinel 21 [147]. The calculation was performed using the same lattice actions as previously for $\Lambda_b \to \Lambda_c$, albeit with newly tuned RHQ parameters. Only three ensembles are used, with $a \approx 0.11,\ 0.08$ fm and pion masses in the range from approximately 300 to 430 MeV, with valence-quark masses equal to the sea-quark masses. Chiral-continuum

extrapolations linear in m_π^2 and a^2 are performed, with systematic uncertainties estimated using higher-order fits. Finite-volume effects and effects associated with the strong decays of the Λ_c^*'s are not quantified. The calculation is done in the Λ_c^* rest frame, where the cubic symmetry is sufficient to avoid mixing with unwanted lower-mass states. As a consequence, the calculation is limited to a small kinematic region near the zero-recoil point $w = 1$. On each ensemble, lattice data were produced for two values of $w - 1$ of approximately 0.01 and 0.03. The final results for the form factors are parameterized as linear functions of $w - 1$ and can be found in Meinel 21 [147] and associated supplemental files.

8.7 Semileptonic form factors for $\Lambda_b \to \Lambda^{(*)}\ell\ell$

The decays $\Lambda_b \to \Lambda\ell^+\ell^-$ are mediated by the same underlying $b \to s\ell^+\ell^-$ FCNC transition as, for example, $B \to K\ell^+\ell^-$ and $B \to K^*\ell^+\ell^-$, and can therefore provide additional information on the hints for physics beyond the Standard Model seen in the meson decays. The Λ baryon in the final state decays through the weak interaction into $p\pi^-$ (or $n\pi^0$), leading to a wealth of angular observables even for unpolarized Λ_b. When including the effects of a nonzero Λ_b polarization, $\Lambda_b \to \Lambda(\to p\pi^-)\ell^+\ell^-$ decays are characterized by five angles leading to 34 angular observables [149], which have been measured by LHCb in the bin $q^2 \in [15, 20]\,\text{GeV}^2$ [150]. Given that the Λ is stable under the strong interactions, the $\Lambda_b \to \Lambda$ form factors parametrizing the matrix elements of local $\bar{s}\Gamma b$ currents can be calculated on the lattice with high precision using standard methods. Of course, the process $\Lambda_b \to \Lambda\ell^+\ell^-$ also receives contributions from nonlocal matrix elements of four-quark and quark-gluon operators in the weak effective Hamiltonian combined with the electromagnetic current. As with the mesonic $b \to s\ell^+\ell^-$ decays, these contributions cannot easily be calculated on the lattice and one relies on other theoretical tools for them, including the local OPE at high q^2 and a light-cone OPE / QCD factorization at low q^2.

Following an early calculation with static b quarks [151], Detmold 16 [152] provides results for all ten relativistic $\Lambda_b \to \Lambda$ form factors parametrizing the matrix elements of the local vector, axial-vector and tensor $b \to s$ currents. The lattice setup is identical to that used in the 2015 calculation of the $\Lambda_b \to p$ form factors in Detmold 15 [145], and similar considerations as in the previous section thus apply. The lattice data cover the upper 60% of the q^2 range, and the form factors are extrapolated to the full q^2 range using BCL z-expansion fits. This extrapolation is done simultaneously with the chiral and continuum extrapolations. The caveat regarding the renormalization of the tensor currents also applies here.

Reference [153] uses the lattice results for the $\Lambda_b \to \Lambda$ form factors together with the experimental results for $\Lambda_b \to \Lambda(\to p\pi^-)\mu^+\mu^-$ from LHCb [150, 154] to perform fits of the $b \to s\mu^+\mu^-$ Wilson coefficients and of the Λ_b polarization parameter. Given the uncertainties (which are still dominated by experiment), the results for the Wilson coefficients are presently consistent both with the Standard-Model values and with the deviations seen in global fits that include all mesonic decays [155, 156].

As with the $b \to c$ semileptonic form factors, a first lattice calculation, Meinel 2020 [157], was also recently completed for a $b \to s$ transition to a negative-parity baryon in the final state, in this case the $\Lambda^*(1520)$ with $J^P = \frac{3}{2}^-$ (no calculation has yet been published for the strange $J^P = \frac{1}{2}^-$ final states, which would be the broader and even more challenging $\Lambda^*(1405)/\Lambda^*(1380)$ [40]). The $\Lambda^*(1520)$ decays primarily to $pK^-/n\bar{K}^0$, $\Sigma\pi$, and $\Lambda\pi\pi$ with a total width of 15.6 ± 1.0 MeV [40] . The analysis of the lattice data again neglects the strong decays and does not quantify finite-volume effects, and is again limited to a small kinematic

region near $q^2_{\rm max}$.

Collaboration	Ref.	N_f	publication status	continuum extrapolation	chiral extrapolation	finite volume	renormalization	heavy-quark treatment	$w = 1$ form factor / ratio	
HPQCD 15, HPQCD 17	[117, 119]	2+1	A	○	○	○	○	✓	$\mathcal{G}^{B\to D}(1)$	1.035(40)
FNAL/MILC 15C	[116]	2+1	A	★	○	★	○	✓	$\mathcal{G}^{B\to D}(1)$	1.054(4)(8)
Atoui 13	[113]	2	A	★	○	★	—	✓	$\mathcal{G}^{B\to D}(1)$	1.033(95)
HPQCD 19	[123]	2+1+1	A	★	○	○*	✓	✓	$\mathcal{G}^{B_s\to D_s}(1)$	1.071(37)
HPQCD 15, HPQCD 17	[117, 119]	2+1	A	○	○	○	○	✓	$\mathcal{G}^{B_s\to D_s}(1)$	1.068(40)
Atoui 13	[113]	2	A	★	○	★	—	✓	$\mathcal{G}^{B_s\to D_s}(1)$	1.052(46)
HPQCD 17B	[121]	2+1+1	A	○	★	★	○	✓	$\mathcal{F}^{B\to D^*}(1)$	0.895(10)(24)
FNAL/MILC 22	[127]	2+1	A	★	○	★	○	✓	$\mathcal{F}^{B\to D^*}(1)$	0.909(17)
HPQCD 17B	[121]	2+1+1	A	○	★	★	○	✓	$\mathcal{F}^{B_s\to D_s^*}(1)$	0.883(12)(28)
HPQCD 19B	[122]	2+1+1	A	★	○	○*	✓	✓	$\mathcal{F}^{B_s\to D_s^*}(1)$	0.9020(96)(90)
HPQCD 15, HPQCD 17	[117, 119]	2+1	A	○	○	○	○	✓	$\mathcal{G}^{B_s\to D_s}(1)$	1.068(40)
HPQCD 20B	[139]	2+1+1	A	★	○	○*	✓	✓	n/a	n/a
HPQCD 15, HPQCD 17	[117, 119]	2+1	A	○	○	○	○	✓	$R(D)$	0.300(8)
FNAL/MILC 15C	[116]	2+1	A	★	○	★	○	✓	$R(D)$	0.299(11)
FNAL/MILC 22	[127]	2+1	A	★	○	★	○	✓	$R(D^*)$	0.265(13)

* The rationale for assigning a ○ rating is discussed in the text.

Table 54: Lattice results for mesonic processes involving $b \to c$ transitions.

Process	Collaboration	Ref.	N_f	publication status	continuum extrapolation	chiral extrapolation	finite volume	renormalization	heavy-quark treatment
$\Lambda_b \to \Lambda_c^*(2625)\,\ell^-\bar{\nu}_\ell$	Meinel 21	[147]	2+1	A	○	○	■	○	✓
$\Lambda_b \to \Lambda_c^*(2595)\,\ell^-\bar{\nu}_\ell$	Meinel 21	[147]	2+1	A	○	○	■	○	✓
$\Lambda_b \to \Lambda^*(1520)\,\ell^+\ell^-$	Meinel 20	[157]	2+1	A	○	○	■	○	✓
$\Lambda_b \to \Lambda\,\ell^+\ell^-$	Detmold 16	[152]	2+1	A	○	○	■	○	✓
$\Lambda_b \to p\,\ell^-\bar{\nu}_\ell$	Detmold 15	[145]	2+1	A	○	○	■	○	✓
$\Lambda_b \to \Lambda_c\,\ell^-\bar{\nu}_\ell$	Detmold 15, Datta 17	[145, 146]	2+1	A	○	○	■	○	✓

Table 55: Summary of computations of bottom baryon semileptonic form factors (see also Refs. [151, 158] for calculations with static b quarks). The rationale for the ■ rating of finite-volume effects in Meinel 20 and 21 (despite meeting the ○ criterion based on the minimum pion mass) is that the unstable nature of the final-state baryons was neglected in the analysis.

8.8 Determination of $|V_{ub}|$

We now use the lattice-determined Standard Model transition amplitudes for leptonic (Sec. 8.1) and semileptonic (Sec. 8.3) B-meson decays to obtain exclusive determinations of the CKM matrix element $|V_{ub}|$. In this section, we describe the aspect of our work that involves experimental input for the relevant charged-current exclusive decay processes. The relevant formulae are Eqs. (203) and (237). Among leptonic channels the only input comes from $B \to \tau\nu_\tau$, since the rates for decays to e and μ have not yet been measured. In the semileptonic case, we only consider $B \to \pi\ell\nu$ transitions (experimentally measured for $\ell = e, \mu$).

We first investigate the determination of $|V_{ub}|$ through the $B \to \tau\nu_\tau$ transition. This is the only experimentally measured leptonic decay channel of the charged B meson. The experimental measurements of the branching fraction of this channel, $B(B^- \to \tau^-\bar{\nu})$, have not been updated since the publication of the FLAG Review in 2016 [53]. The status of the experimental results for this branching fraction, summarized in Tab. 56, is unchanged from FLAG Review 16 [53]. Our corresponding values of $|V_{ub}|$ are unchanged from FLAG Review 19 [1].

Collaboration	Tagging method	$B(B^- \to \tau^-\bar{\nu}) \times 10^4$
Belle [159]	Hadronic	$0.72^{+0.27}_{-0.25} \pm 0.11$
Belle [3]	Semileptonic	$1.25 \pm 0.28 \pm 0.27$
BaBar [2]	Hadronic	$1.83^{+0.53}_{-0.49} \pm 0.24$
BaBar [160]	Semileptonic	$1.7 \pm 0.8 \pm 0.2$

Table 56: Experimental measurements for $B(B^- \to \tau^-\bar{\nu})$. The first error on each result is statistical, while the second error is systematic.

It is obvious that all the measurements listed in Tab. 56 have significance smaller than 5σ, and the large uncertainties are dominated by statistical errors. These measurements lead to the averages of experimental measurements for $B(B^- \to \tau\bar{\nu})$ [2, 3],

$$B(B^- \to \tau\bar{\nu}) \times 10^4 = 0.91 \pm 0.22 \text{ from Belle}, \quad (278)$$
$$= 1.79 \pm 0.48 \text{ from BaBar}, \quad (279)$$
$$= 1.06 \pm 0.33 \text{ average}, \quad (280)$$

where, following our standard procedure we perform a weighted average and rescale the uncertainty by the square root of the reduced chi-squared. Note that the Particle Data Group [51] did not inflate the uncertainty in the calculation of the averaged branching ratio.

Combining the results in Eqs. (278–280) with the experimental measurements of the mass of the τ-lepton and the B-meson lifetime and mass we get

$$|V_{ub}| f_B = 0.72 \pm 0.09 \text{ MeV from Belle}, \quad (281)$$
$$= 1.01 \pm 0.14 \text{ MeV from BaBar}, \quad (282)$$
$$= 0.77 \pm 0.12 \text{ MeV average}, \quad (283)$$

which can be used to extract $|V_{ub}|$, viz.,

$$N_f = 2 \qquad \text{Belle } B \to \tau\nu_\tau : \qquad |V_{ub}| = 3.83(14)(48) \times 10^{-3}\,, \tag{284}$$
$$N_f = 2+1 \qquad \text{Belle } B \to \tau\nu_\tau : \qquad |V_{ub}| = 3.75(8)(47) \times 10^{-3}\,, \tag{285}$$
$$N_f = 2+1+1 \qquad \text{Belle } B \to \tau\nu_\tau : \qquad |V_{ub}| = 3.79(3)(47) \times 10^{-3}\,; \tag{286}$$

$$N_f = 2 \qquad \text{Babar } B \to \tau\nu_\tau : \qquad |V_{ub}| = 5.37(20)(74) \times 10^{-3}\,, \tag{287}$$
$$N_f = 2+1 \qquad \text{Babar } B \to \tau\nu_\tau : \qquad |V_{ub}| = 5.26(12)(73) \times 10^{-3}\,, \tag{288}$$
$$N_f = 2+1+1 \qquad \text{Babar } B \to \tau\nu_\tau : \qquad |V_{ub}| = 5.32(4)(74) \times 10^{-3}\,, \tag{289}$$

$$N_f = 2 \qquad \text{average } B \to \tau\nu_\tau : \qquad |V_{ub}| = 4.10(15)(64) \times 10^{-3}\,, \tag{290}$$
$$N_f = 2+1 \qquad \text{average } B \to \tau\nu_\tau : \qquad |V_{ub}| = 4.01(9)(63) \times 10^{-3}\,, \tag{291}$$
$$N_f = 2+1+1 \qquad \text{average } B \to \tau\nu_\tau : \qquad |V_{ub}| = 4.05(3)(64) \times 10^{-3}\,, \tag{292}$$

where the first error comes from the uncertainty in f_B and the second comes from experiment.

Let us now turn our attention to semileptonic decays. The experimental value of $|V_{ub}|f_+(q^2)$ can be extracted from the measured branching fractions for $B^0 \to \pi^\pm \ell\nu$ and/or $B^\pm \to \pi^0 \ell\nu$ applying Eq. (237);[15] $|V_{ub}|$ can then be determined by performing fits to the constrained BCL z-parameterization of the form factor $f_+(q^2)$ given in Eq. (533). This can be done in two ways: one option is to perform separate fits to lattice and experimental results, and extract the value of $|V_{ub}|$ from the ratio of the respective a_0 coefficients; a second option is to perform a simultaneous fit to lattice and experimental data, leaving their relative normalization $|V_{ub}|$ as a free parameter. We adopt the second strategy, because it combines the lattice and experimental input in a more efficient way, leading to a smaller uncertainty on $|V_{ub}|$.

The available state-of-the-art experimental input consists of five data sets: three untagged measurements by BaBar (6-bin [161] and 12-bin [162]) and Belle [163], all of which assume isospin symmetry and provide combined $B^0 \to \pi^-$ and $B^+ \to \pi^0$ data; and the two tagged Belle measurements of $\bar{B}^0 \to \pi^+$ (13-bin) and $B^- \to \pi^0$ (7-bin) [164]. Including all of them, along with the available information about cross-correlations, will allow us to obtain a meaningful final error estimate.[16] The lattice input data set will be the same discussed in Sec. 8.3.

We perform a constrained BCL fit of the vector and scalar form factors (this is necessary in order to take into account the $f_+(q^2 = 0) = f_0(q^2 = 0)$ constraint) together with the combined experimental data sets. We find that the error on $|V_{ub}|$ stabilizes for $N^+ = N^0 = 3$. The result of the combined fit is presented in Tab. 57. The fit has a chi-square per degree of freedom $\chi^2/\text{dof} = 116.7/62 = 1.88$. Following the PDG recommendation we rescale the whole covariance matrix by χ^2/dof: the errors on the z-parameters are increased by $\sqrt{\chi^2/\text{dof}} = 1.37$ and the correlation matrix is unaffected.

In Fig. 35, we show both the lattice and experimental data for $(1 - q^2/m_{B^*}^2)f_+(q^2)$ as a function of $z(q^2)$, together with our preferred fit; experimental data has been rescaled by the resulting value for $|V_{ub}|^2$. It is worth noting the good consistency between the form factor shapes from lattice and experimental data. This can be quantified, e.g., by computing the

[15] Since $\ell = e, \mu$ the contribution from the scalar form factor in Eq. (237) is negligible.
[16] See, e.g., Sec. V.D of Ref. [58] for a detailed discussion.

$B \to \pi\ell\nu$ ($N_f = 2+1$)

	Central Values	Correlation Matrix					
$\lvert V_{ub}\rvert \times 10^3$	3.64 (16)	1	-0.812	-0.108	0.128	-0.326	-0.151
a_0^+	0.425 (15)	-0.812	1	-0.188	-0.309	0.409	0.00926
a_1^+	−0.441 (39)	-0.108	-0.188	1	-0.498	-0.0343	0.150
a_2^+	−0.52 (13)	0.128	-0.309	-0.498	1	-0.190	0.128
a_0^0	0.560 (17)	-0.326	0.409	-0.0343	-0.190	1	-0.772
a_1^0	−1.346 (53)	-0.151	0.00926	0.150	0.128	-0.772	1

Table 57: $|V_{ub}|$, coefficients for the $N^+ = N^0 = N^T = 3$ z-expansion of the $B \to \pi$ form factors f_+ and f_0, and their correlation matrix. The chi-square per degree of freedom is $\chi^2/\text{dof} = 116.7/62 = 1.88$ and the errors on the fit parameters have been rescaled by $\sqrt{\chi^2/\text{dof}} = 1.37$. The lattice calculations that enter this fit are taken from FNAL/MILC [58], RBC/UKQCD [59] and JLQCD [60]. The experimental inputs are taken from BaBar [161, 162] and Belle [163, 164].

ratio of the two leading coefficients in the constrained BCL parameterization: the fit to lattice form factors yields $a_1^+/a_0^+ = -1.20(23)$ (cf. the results presented in Sec. 8.3.1), while the above lattice+experiment fit yields $a_1^+/a_0^+ = -1.039(94)$.

We plot the values of $|V_{ub}|$ we have obtained in Fig. 38, where the GGOU [165] determination through inclusive decays, $|V_{ub}|_{\text{incl}} = (4.32 \pm 0.12_{\text{exp}} \pm 0.13_{\text{theo}} \pm 0.23_{\Delta BF}) \times 10^{-3}$ [40, 166] (the ΔBF error has been added in Ref. [40] to account for the spread in results obtained using different theoretical models), is also shown for comparison.[17] In this plot, the tension between the BaBar and the Belle measurements of $B(B^- \to \tau^- \bar{\nu})$ is manifest. As discussed above, it is for this reason that we do not extract $|V_{ub}|$ through the average of results for this branching fraction from these two collaborations. In fact, this means that a reliable determination of $|V_{ub}|$ using information from leptonic B-meson decays is still absent; the situation will only clearly improve with the more precise experimental data expected from Belle II [167, 168]. The value for $|V_{ub}|$ obtained from semileptonic B decays for $N_f = 2+1$, on the other hand, is significantly more precise than both the leptonic and the inclusive determinations, and exhibits a $\sim 1.7\sigma$ tension with the latter.

8.9 Determination of $|V_{cb}|$

We will now use the lattice-QCD results for the $B \to D^{(*)}\ell\nu$ form factors in order to obtain determinations of the CKM matrix element $|V_{cb}|$ in the Standard Model. The relevant formulae are given in Eq. (241).

Let us summarize the lattice input that satisfies FLAG requirements for the control of systematic uncertainties, discussed in Sec. 8.4. In the (experimentally more precise) $B \to D^*\ell\nu$ channel, there is only one $N_f = 2+1$ lattice computation of the relevant form factor $\mathcal{F}^{B\to D^*}$ at zero recoil. Concerning the $B \to D\ell\nu$ channel, for $N_f = 2$ there is one determination of the

[17] Note that a recent Belle measurement of partial $B \to X_u\ell^+\nu_\ell$ branching fractions which superseeds their previous result and which yields the somewhat lower value $|V_{ub}| = 4.10(9)(22)(15)\times 10^{-3}$, has not been included in the HFLAV average yet.

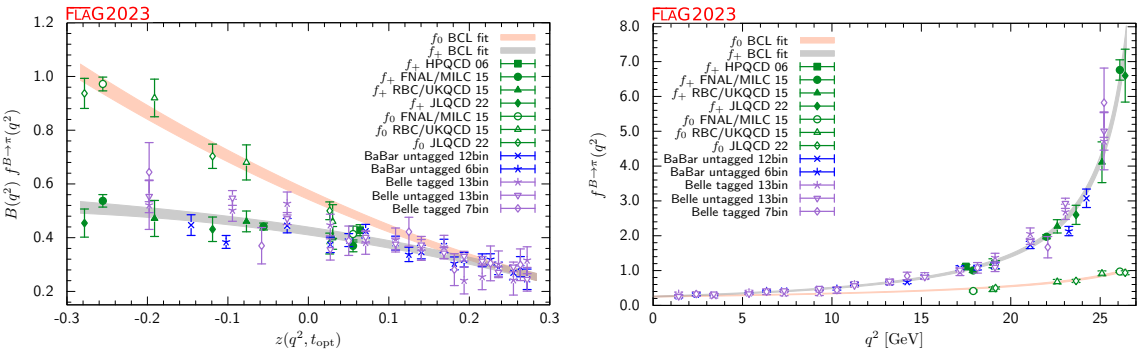

Figure 35: Lattice and experimental data for $f_+^{B\to\pi}(q^2)$ and $f_0^{B\to\pi}(q^2)$ versus z (left panel) and q^2 (right panel). Experimental data has been rescaled by the value for $|V_{ub}|$ found from the joint fit. Green symbols denote lattice-QCD points included in the fit, while blue and indigo points show experimental data divided by the value of $|V_{ub}|$ obtained from the fit. The grey and orange bands display the preferred $N^+ = N^0 = 3$ BCL fit (five z-parameters and $|V_{ub}|$).

relevant form factor $\mathcal{G}^{B\to D}$ at zero recoil, while for $N_f = 2+1$ there are two determinations of the $B \to D$ form factor as a function of the recoil parameter in roughly the lowest third of the kinematically allowed region. In this latter case, it is possible to replicate the analysis carried out for $|V_{ub}|$ in Sec. 8.8, and perform a joint fit to lattice and experimental data; in the former, the value of $|V_{cb}|$ has to be extracted by matching to the experimental value for $\mathcal{F}^{B\to D^*}(1)\eta_{\rm EW}|V_{cb}|$ and $\mathcal{G}^{B\to D}(1)\eta_{\rm EW}|V_{cb}|$.

The latest experimental average by HFLAV [132] for the $B \to D^*$ form factor at zero recoil makes use of the CLN [169] parameterization of the $B \to D^*$ form factor and is

$$[\mathcal{F}^{B\to D^*}(1)\eta_{\rm EW}|V_{cb}|]_{\rm CLN,HFLAV} = 35.61(43)\times 10^{-3}\,. \tag{293}$$

Recent experimental measurements of the $B \to D^*\ell\nu$ branching ratio presented by the BaBar [170], Belle [171, 172] and Belle-II [173] collaborations in which, as suggested in Refs. [174–176], the impact of the form factor parameterization has been studied by comparing the CLN [169] and BGL [73, 177] ansätze. The fit results using the two parameterizations are now consistent. In light of the fact that the BGL parameterization has a much stronger theoretical standing than the CLN one and that it imposes less stringent constraints on the shape of the form factors, we do not consider the CLN determination any further and focus on the BGL fit. Using the BGL fits presented by the BaBar [170], Belle [171, 172] and Belle-II [173] collaborations and assuming a conservative 50% correlation between the untagged [171] and tagged [172] Belle measurements, we obtain the following average:[18]

$$[\mathcal{F}^{B\to D^*}(1)\eta_{\rm EW}|V_{cb}|]_{\rm BGL,\,exp} = 36.07(51)\times 10^{-3}\,, \tag{294}$$

where a PDG rescaling factor of 1.35 has been applied. Given the fact that the two determinations in Eqs. (293) and (294) are quite compatible and that the BGL parameterization is

[18] Note that the BGL fit employed by Belle uses very few z parameters and that this could lead to an underestimation of the error on $[\mathcal{F}^{B\to D^*}(1)\eta_{\rm EW}|V_{cb}|$. See Ref. [178] for a thorough review of this point.

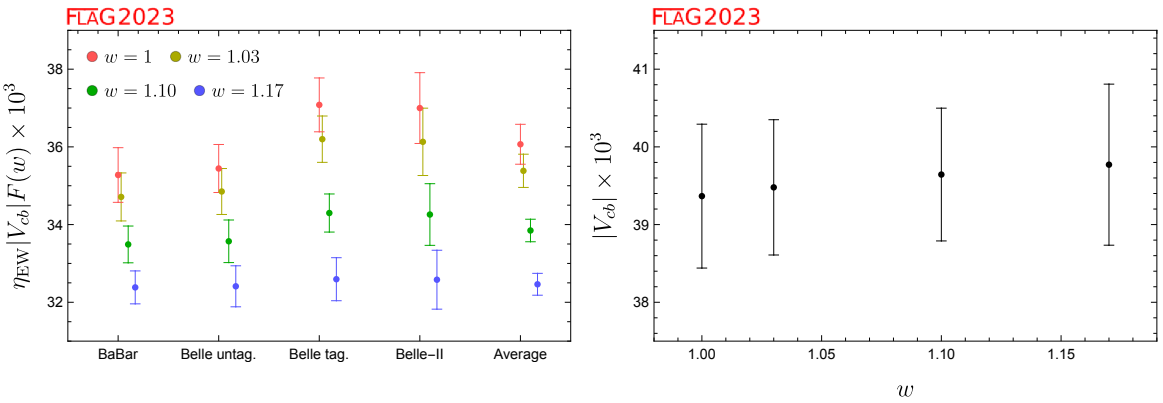

Figure 36: Extractions of $\eta_{\rm EW}|V_{cb}|\mathcal{F}(w)$ from the BaBar [170], Belle [171, 172] and Belle-II [173] measurements of the $B \to D^*\ell\nu$ branching ratio at several recoil points (left panel) and corresponding determinations of $|V_{cb}|$ using the Fermilab/MILC results for $\mathcal{F}^{B\to D^*}(w)$ [115, 127].

on firmer theoretical ground, in the following we present the determination of $|V_{cb}|$ obtained from Eq. (294). We refer to the discussion presented at the end of Sec. 8.8 of the previous edition of this review [1] for further comments on the CLN and BGL parameterizations.

By using $\eta_{\rm EW} = 1.00662$ [19] and the $N_f = 2+1$ lattice value for $\mathcal{F}^{B\to D^*}(1)$ in Eq. (266) [20], we thus extract the average

$$N_f = 2+1 \qquad [B \to D^*\ell\nu]_{\rm BGL}: \qquad |V_{cb}| = 39.37(74)(56) \times 10^{-3}\,, \tag{295}$$

where the first uncertainty comes from the lattice computation and the second from the experimental input. As a consistency check of the extraction of $|V_{cb}|$ using experimental and lattice information extrapolated to a single recoil point, we have repeated the analysis for $w = 1.03$, 1.10 and 1.17. The result of this exercise is presented in two panels of figure 36. It is apparent that the extractions of $|V_{cb}|$ at different recoil points are perfectly compatible with each other (the standard deviation of the four central values is 0.18 and is much smaller than the error on the individual determinations). The small systematic slope of the four determinations is a consequence of the tension between the experimental and lattice determinations of the shape of form factor $\mathcal{F}(w)$. Note that these four determinations of $|V_{cb}|$ are essentially 100% correlated and should not be averaged; a detail study of the extraction of $|V_{cb}|$ which fully takes into account the several measured angular distributions will be presented in the forthcoming version of the FLAG report.

For the zero-recoil $B \to D$ form factor, HFLAV [132] quotes

$$\text{HFLAV:} \qquad \mathcal{G}^{B\to D}(1)\eta_{\rm EW}|V_{cb}| = 41.57(45)(89) \times 10^{-3}\,, \tag{296}$$

[19] Note that this determination does not include the electromagnetic Coulomb correction roughly estimated in Ref. [115]. Currently the numerical impact of this correction is negligible.

[20] In light of our policy not to average $N_f = 2+1$ and $N_f = 2+1+1$ calculations and of the controversy over the use of the CLN vs. BGL parameterizations, we prefer to simply use only the more precise $N_f = 2+1$ determination of $\mathcal{F}^{B\to D^*}(1)$ in Eq. (266) for the extraction of V_{cb}.

$B \to D\ell\nu$ ($N_f = 2+1$)

	Central Values	Correlation Matrix					
$\lvert V_{cb}\rvert \times 10^3$	40.0 (1.0)	1.00	-0.525	-0.339	0.0487	-0.521	-0.433
a_0^+	0.8946 (94)	-0.525	1.00	0.303	-0.351	0.953	0.529
a_1^+	-8.03 (16)	-0.339	0.303	1.00	0.203	0.375	0.876
a_2^+	50.1 (3.1)	0.0487	-0.351	0.203	1.00	-0.276	0.196
a_0^0	0.7804 (75)	-0.521	0.953	0.375	-0.276	1.0	0.502
a_1^0	-3.38 (16)	-0.433	0.529	0.876	0.196	0.502	1.0

Table 58: $|V_{cb}|$, coefficients for the $N^+ = N^0$ z-expansion of the $B \to D$ form factors f_+ and f_0, and their correlation matrix. The coefficient a_2^0 is fixed by the $f_+(q^2 = 0) = f_0(q^2 = 0)$ constrain. The chi-square per degree of freedom is $\chi^2/\text{dof} = 20.0/25 = 0.80$. The lattice calculations that enter this fit are taken from FNAL/MILC [116] and HPQCD [117]. The experimental inputs are taken from BaBar [180] and Belle [669].

yielding the following average for $N_f = 2$:

$$N_f = 2 \qquad B \to D\ell\nu : \qquad |V_{cb}| = 40.0(3.7)(1.0) \times 10^{-3}\,, \tag{297}$$

where the first uncertainty comes from the lattice computation and the second from the experimental input.

Finally, for $N_f = 2+1$ we perform, as discussed above, a joint fit to the available lattice data, discussed in Sec. 8.4, and state-of-the-art experimental determinations. In this case, we will combine the aforementioned Belle measurement [669], which provides partial integrated decay rates in 10 bins in the recoil parameter w, with the 2010 BaBar data set in Ref. [180], which quotes the value of $\mathcal{G}^{B\to D}(w)\eta_{\rm EW}|V_{cb}|$ for ten values of w.[21] The fit is dominated by the more precise Belle data; given this, and the fact that only partial correlations among systematic uncertainties are to be expected, we will treat both data sets as uncorrelated.[22]

A constrained ($N^+ = N^0 = 3$) BCL fit using the same ansatz as for lattice-only data in Sec. 8.4, yields our average, which we present in Tab. 58. The chi-square per degree of freedom is $\chi^2/\text{dof} = 20.0/25 = 0.80$. The fit is illustrated in Fig. 37. In passing, we note that, if correlations between the FNAL/MILC and HPQCD calculations are neglected, the $|V_{cb}|$ central value rises to 40.3×10^{-3} in nice agreement with the results presented in Ref. [181].

Before discussing the combination of the above $|V_{cb}|$ results, we note that the LHCb Collaboration recently reported the first determination of $|V_{cb}|$ at the Large Hadron Collider using $B_s \to D_s^-\mu^+\nu_\mu$ and $B_s \to D_s^{*-}\mu^+\nu_\mu$ decays [124, 125]. The differential decay rates, in combination with the $N_f = 2+1+1$ HPQCD 19 [123] and HPQCD 19B [122] lattice results for $f_+^{B_s\to D_s}$ and $\mathcal{F}^{B_s\to D_s^*}(1)$, were analyzed using either the CLN or BGL form-factor parameterizations. The result for $|V_{cb}|$ from the BGL fit is [125]

$$|V_{cb}| = (41.7 \pm 0.8 \pm 0.9 \pm 1.1) \times 10^{-3} \qquad B_s \to D_s^{(*)-}\mu^+\nu_\mu,\ \text{BGL, LHCb}\,. \tag{298}$$

[21] We thank Marcello Rotondo for providing the ten bins result of the BaBar analysis.

[22] We have checked that results using just one experimental data set are compatible within 1σ. In the case of BaBar, we have taken into account the introduction of some EW corrections in the data.

	from	$\lvert V_{cb}\rvert \times 10^3$
our average for $N_f = 2+1$ (BGL)	$B \to D^* \ell\nu$	39.37(74)(56)
our average for $N_f = 2+1$	$B \to D \ell\nu$	40.0(1.0)
our average for $N_f = 2+1$ (BGL)	$B \to (D, D^*)\ell\nu$	39.66(69)
our average for $N_f = 2$	$B \to D \ell\nu$	40.0(3.7)(1.0)
LHCb result for $N_f = 2+1+1$ (BGL)	$B_s \to D_s^{(*)} \ell\nu$	41.7(0.8)(0.9)(1.1)
Bordone et al.	$B \to X_c \ell\nu$	42.16(51)

Table 59: Results for $|V_{cb}|$. When two errors are quoted in our averages, the first one comes from the lattice form factor, and the second from the experimental measurement. The LHCb result using $B_s \to D_s^{(*)}\ell\nu$ decays [122–125], as well as the inclusive average obtained in the kinetic scheme from Ref. [184] are shown for comparison.

The LHCb analysis used ratios to the reference decay modes $B^0 \to D^- \mu^+ \nu_\mu$ and $B^0 \to D^{*-} \mu^+ \nu_\mu$, whose branching fractions are used as input in the form of the Particle Data Group averages of measurements by other experiments [182]. The result (298) is therefore correlated with the determinations of $|V_{cb}|$ from $B \to D$ and $B \to D^*$ semileptonic decays. Given the challenges involved in performing our own fit to the LHCb data, we do not, at present, include the LHCb results for $B_s \to D_s^- \mu^+ \nu_\mu$ and $B_s \to D_s^{*-} \mu^+ \nu_\mu$ in our combination of $|V_{cb}|$.

We now proceed to combine the determinations of $|V_{cb}|$ from exclusive $B \to D$ and $B \to D^*$ semileptonic decays. To this end, we need to estimate the correlation between the lattice uncertainties in the two modes. We assume conservatively that the statistical component of the lattice error in both determinations are 100% correlated because they are based on the same MILC configurations (albeit on different subsets). We obtain:

$$N_f = 2+1 \qquad [B \to (D, D^*)\ell\nu]_{\rm BGL}: \qquad |V_{cb}| = 39.66(69) \times 10^{-3}\,, \tag{299}$$

Our results are summarized in Tab. 59, which also shows the HFLAV inclusive determination of $|V_{cb}| = 42.16(51) \times 10^{-3}$ [183] for comparison, and illustrated in Fig. 38. Finally, using the fit results in Tab. 59, we extract a value for $R(D)$ which includes both lattice and experimental information:

$$R(D)_{\rm lat+exp} = 0.2951(31)\,, \quad \text{our average.} \tag{300}$$

Note that we do not need to rescale the uncertainty on $R(D)_{\rm lat+exp}$ because, after the inclusion of experimental $B \to D\ell\nu$ ($\ell = e, \mu$) results, the shift in central value caused by using a different parameterization is negligible (see the discussion above Eq. (255)).

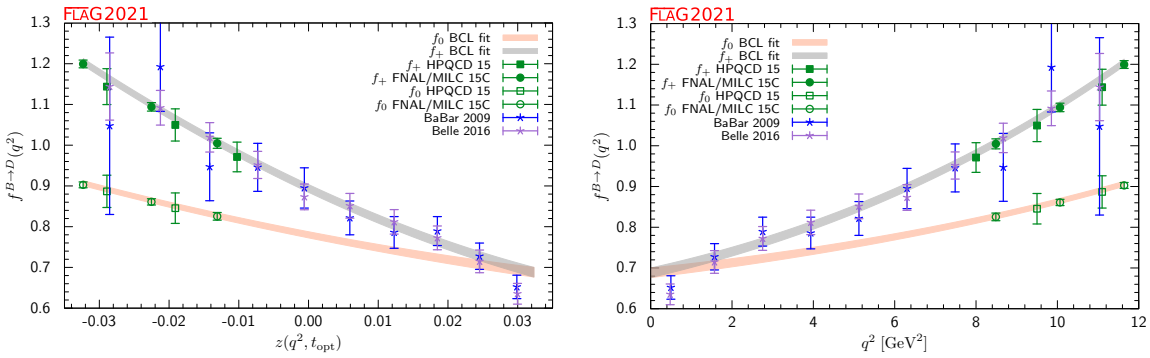

Figure 37: Lattice and experimental data for $f_+^{B\to D}(q^2)$ and $f_0^{B\to D}(q^2)$ versus z (left panel) and q^2 (right panel). Green symbols denote lattice-QCD points included in the fit, while blue and indigo points show experimental data divided by the value of $|V_{cb}|$ obtained from the fit. The grey and orange bands display the preferred $N^+ = N^0 = 3$ BCL fit (five z-parameters and $|V_{cb}|$).

8.10 Determination of $|V_{ub}/V_{cb}|$ from Λ_b decays

In 2015, the LHCb Collaboration reported a measurement of the ratio [143]

$$R_{\rm BF}(\Lambda_b) = \frac{\displaystyle\int_{15\ \rm GeV^2}^{q^2_{\rm max}} \frac{{\rm d}\mathcal{B}(\Lambda_b \to p\mu^-\bar\nu_\mu)}{{\rm d}q^2}\,{\rm d}q^2}{\displaystyle\int_{7\ \rm GeV^2}^{q^2_{\rm max}} \frac{{\rm d}\mathcal{B}(\Lambda_b \to \Lambda_c\mu^-\bar\nu_\mu)}{{\rm d}q^2}\,{\rm d}q^2}, \tag{301}$$

which, combined with the lattice QCD prediction [145] discussed in Sec. 8.6 yields a determination of $|V_{ub}/V_{cb}|$. The LHCb analysis uses the decay $\Lambda_c \to pK\pi$ to reconstruct the Λ_c and requires the branching fraction $\mathcal{B}(\Lambda_c \to pK\pi)$ of this decay as an external input. Using the latest world average of $\mathcal{B}(\Lambda_c \to pK\pi) = (6.28 \pm 0.32)\%$ [40] to update the LHCb measurement gives [166]

$$R_{\rm BF}(\Lambda_b) = (0.92 \pm 0.04 \pm 0.07) \times 10^{-2}, \tag{302}$$

and, combined with the lattice QCD prediction for $\frac{\zeta_{p\mu\bar\nu}(15{\rm GeV}^2)}{\zeta_{\Lambda_c\mu\bar\nu}(7{\rm GeV}^2)}$ discussed in Sec. 8.6,

$$|V_{ub}/V_{cb}| = 0.079 \pm 0.004_{\rm\,lat.} \pm 0.004_{\rm\,exp.}. \tag{303}$$

8.11 Determination of $|V_{ub}/V_{cb}|$ from B_s decays

More recently, LHCb reported the measurements [185]

$$R_{\rm BF}(B_s,\text{low}) = \frac{\displaystyle\int_{q^2_{\rm min}=m_\mu^2}^{7\ {\rm GeV}^2} \frac{{\rm d}\mathcal{B}(B_s\to K^-\mu^+\nu_\mu)}{{\rm d}q^2}\,{\rm d}q^2}{\mathcal{B}(B_s\to D_s^-\mu^+\nu_\mu)} = (1.66\pm0.12)\times10^{-3}, \tag{304}$$

$$R_{\rm BF}(B_s,\text{high}) = \frac{\displaystyle\int_{7\ {\rm GeV}^2}^{q^2_{\rm max}=(m_{B_s}-m_K)^2} \frac{{\rm d}\mathcal{B}(B_s\to K^-\mu^+\nu_\mu)}{{\rm d}q^2}\,{\rm d}q^2}{\mathcal{B}(B_s\to D_s^-\mu^+\nu_\mu)} = (3.25\pm0.28)\times10^{-3}, \tag{305}$$

$$R_{\rm BF}(B_s,\text{all}) = \frac{\mathcal{B}(B_s\to K^-\mu^+\nu_\mu)}{\mathcal{B}(B_s\to D_s^-\mu^+\nu_\mu)} = (4.89\pm0.33)\times10^{-3}. \tag{306}$$

Using our average of the $B_s\to K$ form factors from lattice QCD as discussed in Sec. 8.3.2, we obtain the Standard-Model predictions

$$\frac{1}{|V_{ub}|^2}\int_{q^2_{\rm min}=m_\mu^2}^{7\ {\rm GeV}^2} \frac{{\rm d}\Gamma(B_s\to K^-\mu^+\nu_\mu)}{{\rm d}q^2} = (2.51\pm0.62)\ {\rm ps}^{-1}, \tag{307}$$

$$\frac{1}{|V_{ub}|^2}\int_{7\ {\rm GeV}^2}^{q^2_{\rm max}=(m_{B_s}-m_K)^2} \frac{{\rm d}\Gamma(B_s\to K^-\mu^+\nu_\mu)}{{\rm d}q^2} = (4.02\pm0.51)\ {\rm ps}^{-1}, \tag{308}$$

$$\frac{1}{|V_{ub}|^2}\Gamma(B_s\to K^-\mu^+\nu_\mu) = (6.5\pm1.1)\ {\rm ps}^{-1}. \tag{309}$$

For the denominator, we use the $B_s\to D_s$ form factors from Ref. [123], which yields

$$\frac{1}{|V_{cb}|^2}\Gamma(B_s\to D_s^-\mu^+\nu_\mu) = (9.15\pm0.37)\ {\rm ps}^{-1}. \tag{310}$$

Combined with the LHCb measurements we obtain

$$\frac{|V_{ub}|}{|V_{cb}|}(\text{low}) = 0.0779\pm0.0098_{\,\text{lat.}}\pm0.0028_{\,\text{exp.}}, \tag{311}$$

$$\frac{|V_{ub}|}{|V_{cb}|}(\text{high}) = 0.0861\pm0.0057_{\,\text{lat.}}\pm0.0038_{\,\text{exp.}}, \tag{312}$$

$$\frac{|V_{ub}|}{|V_{cb}|}(\text{all}) = 0.0828\pm0.0070_{\,\text{lat.}}\pm0.0028_{\,\text{exp.}}. \tag{313}$$

We will use the result from the high-q^2 region in our combination in Sec. 8.12, as this is the region in which the form factor shape is most reliably constrained by the lattice data.

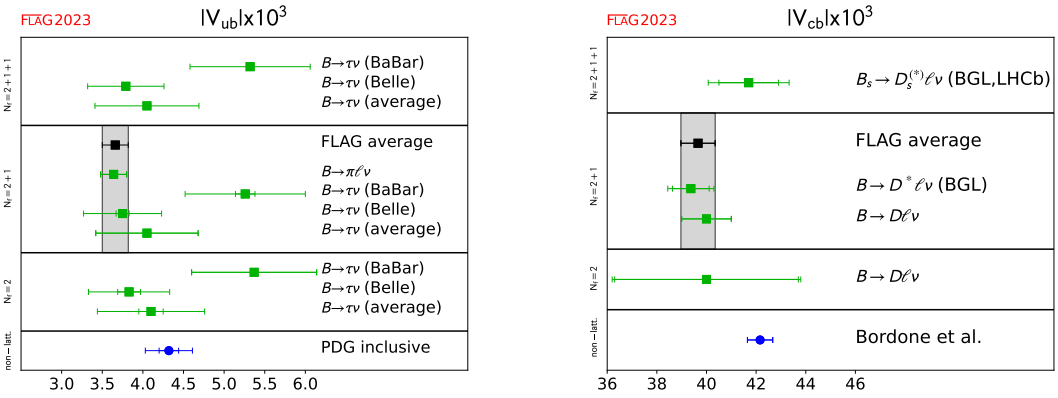

Figure 38: Left: Summary of $|V_{ub}|$ determined using: i) the B-meson leptonic decay branching fraction, $B(B^- \to \tau^- \bar{\nu})$, measured at the Belle and BaBar experiments, and our averages for f_B from lattice QCD; and ii) the various measurements of the $B \to \pi \ell \nu$ decay rates by Belle and BaBar, and our averages for lattice determinations of the relevant vector form factor $f_+(q^2)$. Right: Same for determinations of $|V_{cb}|$ using semileptonic decays. The inclusive results are taken from Refs. [132, 184].

8.12 Summary: $|V_{ub}|$ and $|V_{cb}|$

In Fig. 39, we present a summary of determinations of $|V_{ub}|$ and $|V_{cb}|$ from $B \to (\pi, D^{(*)})\ell\nu$, $B_s \to (K, D_s)\ell\nu$ (high q^2 only), $B \to \tau\nu$ and $\Lambda_b \to (p, \Lambda_c)\ell\nu$, as well as the results from inclusive $B \to X_{u,c}\ell\nu$ decays. Note that constraints on $|V_{ub}/V_{cb}|$ from baryon modes are displayed but, in view of the rating in Tab. 55, are not included in the global fit. As discussed in Sec. 8.9, experimental inputs used in the extraction of $|V_{cb}|$ from $B_s \to D_s^{(*)}\ell\nu$ decays [124, 125] given in Eq. (298) are highly correlated with those entering the global $(|V_{ub}|, |V_{cb}|)$ fit described in this section. Given these correlations and the challenges in reproducing the LHCb analysis, for the time being we do not include the result Eq. (298) into the global fit.

Currently, the determinations of V_{cb} from $B \to D^*$ and $B \to D$ decays are quite compatible; however, a sizeable tension involving the extraction of V_{cb} from inclusive decays remains. In the determination of the 1σ and 2σ contours for our average, we have included an estimate of the correlation between $|V_{ub}|$ and $|V_{cb}|$ from semileptonic B decays: the lattice inputs to these quantities are dominated by results from the Fermilab/MILC and HPQCD collaborations that are both based on MILC $N_f = 2 + 1$ ensembles, leading to our conservatively introducing a 100% correlation between the lattice statistical uncertainties of the three computations involved. The results of the fit are

$$|V_{cb}| = 39.75(69) \times 10^{-3} \,, \tag{314}$$

$$|V_{ub}| = 3.61(14) \times 10^{-3} \,, \tag{315}$$

$$p\text{−value} = 0.74 \,. \tag{316}$$

For reference, the inclusive determinations read $|V_{cb}|_{\rm incl} = (42.16 \pm 0.51) \times 10^{-3}$ [184] and $|V_{ub}|_{\rm incl} = (4.32 \pm 0.12_{\rm exp} \pm 0.13_{\rm theo} \pm 0.23_{\Delta BF}) \times 10^{-3}$ [40, 166] (the ΔBF error has been added in Ref. [40] to account for the spread in results obtained using different theoretical

models). Note that a recent Belle analysis [186] of partial $B \to X_u \ell^+ \nu_\ell$ branching fractions finds a slightly lower central value $|V_{ub}|_{\text{incl,Belle}} = (4.10 \pm 0.09_{\text{stat}} \pm 0.22_{\text{syst}} \pm 0.15_{\text{theo}}) \times 10^{-3}$.

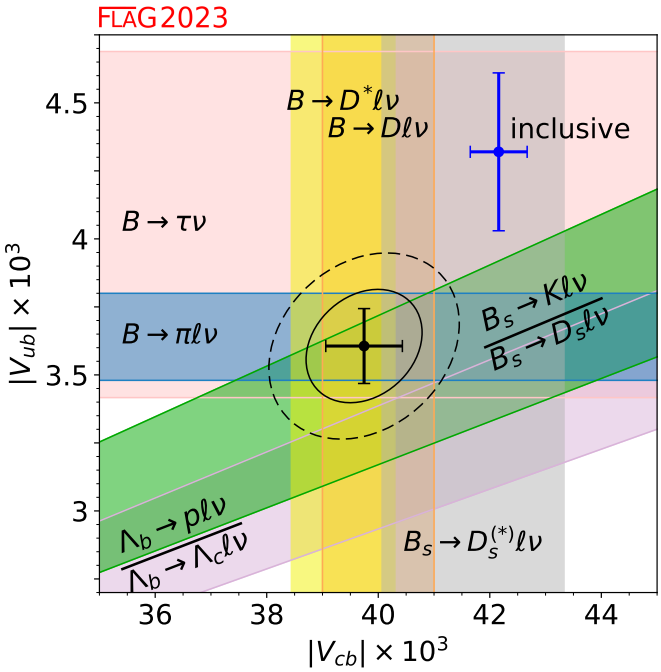

Figure 39: Summary of $|V_{ub}|$ and $|V_{cb}|$ determinations. The black solid and dashed lines correspond to 68% and 95% C.L. contours, respectively. The result of the global fit (which does not include $|V_{ub}/V_{cb}|$ from baryon modes nor $|V_{cb}|$ from $B_s \to D_s^{(*)} \ell\nu$) is $(|V_{cb}|, |V_{ub}|) = (39.75 \pm 0.69, 3.61 \pm 0.14) \times 10^{-3}$ with a p-value of 0.74. The lattice and experimental results that contribute to the various contours are the following. $B \to \pi \ell\nu$: lattice (FNAL/MILC [58], RBC/UKQCD [59], and JLQCD [60]) and experiment (BaBar [161, 162] and Belle [163, 164]). $B \to D \ell\nu$: lattice (FNAL/MILC [116] and HPQCD [117]) and experiment (BaBar [180] and Belle [669]). $B \to D^* \ell\nu$: lattice (FNAL/MILC [115]) and experiment (Belle [171]). $B \to \tau\nu$: lattice (f_B determinations in Fig 27) and experiment (BaBar [3] and Belle [2]). $B_s \to K \ell\nu / B_s \to D_s \ell\nu$: lattice (HPQCD [74], RBC/UKQCD [78], FNAL/MILC [77], HPQCD [123]) and experiment (LHCb [185]). $\Lambda_b \to p \ell\nu / \Lambda_b \to \Lambda_c \ell\nu$: lattice (Detmold 15 [145]) and experiment (LHCb [143]). $B_s \to D_s^* \ell\nu / B_s \to D_s \ell\nu$: lattice (HPQCD 19 [123] and HPQCD 19B [122]) and experiment (LHCb [124, 125]). The inclusive determinations are taken from Refs. [40, 166, 183] and read $(|V_{cb}|, |V_{ub}|)_{\text{incl}} = (42.16 \pm 0.51, 4.32 \pm 0.29) \times 10^{-3}$.

References

[1] [FLAG 19] S. Aoki et al., *FLAG Review 2019: Flavour Lattice Averaging Group (FLAG)*, *Eur. Phys. J. C* **80** (2020) 113 [1902.08191].

[2] BABAR collaboration, *Evidence of $B \to \tau\nu$ decays with hadronic B tags*, *Phys.Rev.* **D88** (2013) 031102 [1207.0698].

[3] BELLE collaboration, *Measurement of the branching fraction of $B^+ \to \tau^+\nu_\tau$ decays with the semileptonic tagging method*, *Phys. Rev.* **D92** (2015) 051102 [1503.05613].

[4] T. Inami and C.S. Lim, *Effects of superheavy quarks and leptons in low-energy weak processes $K_L \to \mu\bar{\mu}$, $K^+ \to \pi^+\nu\bar{\nu}$ and $K^0 \leftrightarrow \bar{K}^0$*, *Prog. Theor. Phys.* **65** (1981) 297.

[5] G. Buchalla and A.J. Buras, *QCD corrections to rare K and B decays for arbitrary top quark mass*, *Nucl.Phys.* **B400** (1993) 225.

[6] LHCB, CMS collaboration, *Observation of the rare $B^0_s \to \mu^+\mu^-$ decay from the combined analysis of CMS and LHCb data*, *Nature* **522** (2015) 68 [1411.4413].

[7] ATLAS collaboration, *Combination of the ATLAS, CMS and LHCb results on the $B^0_{(s)} \to \mu^+\mu^-$ decays.*, .

[8] M. Beneke, C. Bobeth and R. Szafron, *Power-enhanced leading-logarithmic QED corrections to $B_q \to \mu^+\mu^-$*, *JHEP* **10** (2019) 232 [1908.07011].

[9] [ETM 13B] N. Carrasco et al., *B-physics from $N_f = 2$ tmQCD: the Standard Model and beyond*, *JHEP* **1403** (2014) 016 [1308.1851].

[10] [ETM 16B] A. Bussone et al., *Mass of the b quark and B -meson decay constants from N_f=2+1+1 twisted-mass lattice QCD*, *Phys. Rev.* **D93** (2016) 114505 [1603.04306].

[11] [HPQCD 12] H. Na, C.J. Monahan, C.T. Davies, R. Horgan, G.P. Lepage et al., *The B and B_s meson decay constants from lattice QCD*, *Phys.Rev.* **D86** (2012) 034506 [1202.4914].

[12] R. Balasubramamian and B. Blossier, *Decay constant of B_s and B_s^* mesons from $\mathrm{N_f} = 2$ lattice QCD*, *Eur. Phys. J. C* **80** (2020) 412 [1912.09937].

[13] [HPQCD 13] R. J. Dowdall, C. Davies, R. Horgan, C. Monahan and J. Shigemitsu, *B-meson decay constants from improved lattice NRQCD and physical u, d, s and c sea quarks*, *Phys.Rev.Lett.* **110** (2013) 222003 [1302.2644].

[14] [FNAL/MILC 17] A. Bazavov et al., *B- and D-meson leptonic decay constants from four-flavor lattice QCD*, *Phys. Rev.* **D98** (2018) 074512 [1712.09262].

[15] N. Carrasco, V. Lubicz, G. Martinelli, C.T. Sachrajda, N. Tantalo, C. Tarantino et al., *QED Corrections to Hadronic Processes in Lattice QCD*, *Phys. Rev.* **D91** (2015) 074506 [1502.00257].

[16] [HPQCD 17A] C. Hughes, C.T.H. Davies and C.J. Monahan, *New methods for B meson decay constants and form factors from lattice NRQCD*, *Phys. Rev.* **D97** (2018) 054509 [1711.09981].

[17] [ETM 13E] N. Carrasco, P. Dimopoulos, R. Frezzotti, V. Giménez, P. Lami et al., *A $N_f = 2 + 1 + 1$ 'twisted' determination of the b-quark mass, f_B and f_{B_s}*, *PoS* **LATTICE2013** (2014) 313 [1311.2837].

[18] [RBC/UKQCD 14] N. H. Christ, J.M. Flynn, T. Izubuchi, T. Kawanai, C. Lehner et al., *B-meson decay constants from 2+1-flavor lattice QCD with domain-wall light quarks and relativistic heavy quarks*, *Phys.Rev.* **D91** (2015) 054502 [1404.4670].

[19] [RBC/UKQCD 14A] Y. Aoki, T. Ishikawa, T. Izubuchi, C. Lehner and A. Soni, *Neutral B meson mixings and B meson decay constants with static heavy and domain-wall light quarks*, *Phys. Rev.* **D91** (2015) 114505 [1406.6192].

[20] [RBC/UKQCD 13A] O. Witzel, *B-meson decay constants with domain-wall light quarks and nonperturbatively tuned relativistic b-quarks*, *PoS* **LATTICE2013** (2014) 377 [1311.0276].

[21] [HPQCD 11A] C. McNeile, C.T.H. Davies, E. Follana, K. Hornbostel and G.P. Lepage, *High-precision f_{B_s} and HQET from relativistic lattice QCD*, *Phys.Rev.* **D85** (2012) 031503 [1110.4510].

[22] [FNAL/MILC 11] A. Bazavov et al., *B- and D-meson decay constants from three-flavor lattice QCD*, *Phys.Rev.* **D85** (2012) 114506 [1112.3051].

[23] [HPQCD 09] E. Gamiz, C.T. Davies, G.P. Lepage, J. Shigemitsu and M. Wingate, *Neutral B meson mixing in unquenched lattice QCD*, *Phys.Rev.* **D80** (2009) 014503 [0902.1815].

[24] [ALPHA 14] F. Bernardoni et al., *Decay constants of B-mesons from non-perturbative HQET with two light dynamical quarks*, *Phys.Lett.* **B735** (2014) 349 [1404.3590].

[25] [ALPHA 13] F. Bernardoni, B. Blossier, J. Bulava, M. Della Morte, P. Fritzsch et al., *B-physics with $N_f = 2$ Wilson fermions*, *PoS* **LATTICE2013** (2014) 381 [1309.1074].

[26] [ETM 13C] N. Carrasco et al., *B-physics computations from Nf=2 tmQCD*, *PoS* **LATTICE2013** (2014) 382 [1310.1851].

[27] [ALPHA 12A] F. Bernardoni, B. Blossier, J. Bulava, M. Della Morte, P. Fritzsch et al., *B-physics from HQET in two-flavour lattice QCD*, *PoS* **LAT2012** (2012) 273 [1210.7932].

[28] [ETM 12B] N. Carrasco, P. Dimopoulos, R. Frezzotti, V. Gimenez, G. Herdoiza et al., *B-physics from the ratio method with Wilson twisted mass fermions*, *PoS* **LAT2012** (2012) 104 [1211.0568].

[29] [ALPHA 11] B. Blossier, J. Bulava, M. Della Morte, M. Donnellan, P. Fritzsch et al., *M_b and f_B from non-perturbatively renormalized HQET with $N_f = 2$ light quarks*, *PoS* **LAT2011** (2011) 280 [1112.6175].

[30] [ETM 11A] P. Dimopoulos et al., *Lattice QCD determination of m_b, f_B and f_{B_s} with twisted mass Wilson fermions*, *JHEP* **1201** (2012) 046 [1107.1441].

[31] [ETM 09D] B. Blossier et al., *A proposal for B-physics on current lattices*, *JHEP* **1004** (2010) 049 [0909.3187].

[32] [HPQCD 05B] A. Gray et al., *The upsilon spectrum and m_b from full lattice QCD*, *Phys.Rev.* **D72** (2005) 094507 [hep-lat/0507013].

[33] [RBC/UKQCD 18A] P. A. Boyle, L. Del Debbio, N. Garron, A. Juttner, A. Soni, J.T. Tsang et al., *SU(3)-breaking ratios for $D_{(s)}$ and $B_{(s)}$ mesons*, 1812.08791.

[34] [RBC/UKQCD 10C] C. Albertus et al., *Neutral B-meson mixing from unquenched lattice QCD with domain-wall light quarks and static b-quarks*, *Phys.Rev.* **D82** (2010) 014505 [1001.2023].

[35] D.J. Broadhurst and A.G. Grozin, *Matching QCD and HQET heavy - light currents at two loops and beyond*, *Phys. Rev. D* **52** (1995) 4082 [hep-ph/9410240].

[36] K. Chetyrkin and A. Grozin, *Three loop anomalous dimension of the heavy light quark current in HQET*, *Nucl.Phys.* **B666** (2003) 289 [hep-ph/0303113].

[37] S. Bekavac, A.G. Grozin, P. Marquard, J.H. Piclum, D. Seidel and M. Steinhauser, *Matching QCD and HQET heavy-light currents at three loops*, *Nucl. Phys. B* **833** (2010) 46 [0911.3356].

[38] [RBC/UKQCD 14B] T. Blum et al., *Domain wall QCD with physical quark masses*, *Phys. Rev.* **D93** (2016) 074505 [1411.7017].

[39] P. Boyle, A. Jüttner, M.K. Marinkovic, F. Sanfilippo, M. Spraggs and J.T. Tsang, *An exploratory study of heavy domain wall fermions on the lattice*, *JHEP* **04** (2016) 037 [1602.04118].

[40] Particle Data Group collaboration, *Review of Particle Physics*, *PTEP* **2020** (2020) 083C01.

[41] G. Buchalla, A.J. Buras and M.E. Lautenbacher, *Weak decays beyond leading logarithms*, *Rev. Mod. Phys.* **68** (1996) 1125 [hep-ph/9512380].

[42] F. Gabbiani, E. Gabrielli, A. Masiero and L. Silvestrini, *A Complete analysis of FCNC and CP constraints in general SUSY extensions of the standard model*, *Nucl. Phys.* **B477** (1996) 321 [hep-ph/9604387].

[43] A. Lenz and U. Nierste, *Theoretical update of $B_s - \bar{B}_s$ mixing*, *JHEP* **0706** (2007) 072 [hep-ph/0612167].

[44] M. Beneke, G. Buchalla and I. Dunietz, *Width difference in the $B_s - \bar{B}_s$ system*, *Phys.Rev.* **D54** (1996) 4419 [hep-ph/9605259].

[45] [FLAG 13] S. Aoki, Y. Aoki, C. Bernard, T. Blum, G. Colangelo et al., *Review of lattice results concerning low-energy particle physics*, *Eur.Phys.J.* **C74** (2014) 2890 [1310.8555].

[46] [FNAL/MILC 11A] C. M. Bouchard, E. Freeland, C. Bernard, A. El-Khadra, E. Gamiz et al., *Neutral B mixing from $2+1$ flavor lattice-QCD: the Standard Model and beyond*, *PoS* **LAT2011** (2011) 274 [1112.5642].

[47] [FNAL/MILC 16] A. Bazavov et al., $B^0_{(s)}$*-mixing matrix elements from lattice QCD for the Standard Model and beyond*, *Phys. Rev.* **D93** (2016) 113016 [1602.03560].

[48] [HPQCD 19A] R. J. Dowdall, C.T.H. Davies, R.R. Horgan, G.P. Lepage, C.J. Monahan, J. Shigemitsu et al., *Neutral B-meson mixing from full lattice QCD at the physical point*, *Phys. Rev.* **D100** (2019) 094508 [1907.01025].

[49] [HPQCD 06A] E. Dalgic, A. Gray, E. Gamiz, C.T. Davies, G.P. Lepage et al., $B^0_s - \bar{B}^0_s$ *mixing parameters from unquenched lattice QCD*, *Phys.Rev.* **D76** (2007) 011501 [hep-lat/0610104].

[50] [ETM 12A] N. Carrasco et al., *Neutral meson oscillations in the Standard Model and beyond from* $N_f = 2$ *twisted mass lattice QCD*, *PoS* **LAT2012** (2012) 105 [1211.0565].

[51] J.L. Rosner, S. Stone and R.S. Van de Water, *Leptonic Decays of Charged Pseudoscalar Mesons, in Review of Particle Physics [?] 2015 update*, 1509.02220.

[52] [FNAL/MILC 12] A. Bazavov, C. Bernard, C. Bouchard, C. DeTar, M. Di Pierro et al., *Neutral B-meson mixing from three-flavor lattice QCD: determination of the SU(3)-breaking ratio* ξ, *Phys.Rev.* **D86** (2012) 034503 [1205.7013].

[53] [FLAG 16] S. Aoki et al., *Review of lattice results concerning low-energy particle physics*, *Eur. Phys. J.* **C77** (2017) 112 [1607.00299].

[54] [HPQCD 11B] R. J. Dowdall et al., *The upsilon spectrum and the determination of the lattice spacing from lattice QCD including charm quarks in the sea*, *Phys.Rev.* **D85** (2012) 054509 [1110.6887].

[55] M. Della Morte, B. Jäger, T. Rae and H. Wittig, *Improved interpolating fields for hadrons at non-zero momentum*, *Eur.Phys.J.* **A48** (2012) 139 [1208.0189].

[56] [HPQCD 06] E. Dalgic et al., *B meson semileptonic form-factors from unquenched lattice QCD*, *Phys.Rev.* **D73** (2006) 074502 [hep-lat/0601021].

[57] [FNAL/MILC 08A] J. A. Bailey et al., *The* $B \to \pi\ell\nu$ *semileptonic form factor from three-flavor lattice QCD: a model-independent determination of* $|V_{ub}|$, *Phys.Rev.* **D79** (2009) 054507 [0811.3640].

[58] [FNAL/MILC 15] J. A. Bailey et al., $|V_{ub}|$ *from* $B \to \pi\ell\nu$ *decays and (2+1)-flavor lattice QCD*, *Phys. Rev.* **D92** (2015) 014024 [1503.07839].

[59] [RBC/UKQCD 15] J. M. Flynn, T. Izubuchi, T. Kawanai, C. Lehner, A. Soni, R.S. Van de Water et al., $B \to \pi\ell\nu$ *and* $B_s \to K\ell\nu$ *form factors and* $|V_{ub}|$ *from 2+1-flavor lattice QCD with domain-wall light quarks and relativistic heavy quarks*, *Phys. Rev.* **D91** (2015) 074510 [1501.05373].

[60] [JLQCD 22] B. Colquhoun, S. Hashimoto, T. Kaneko and J. Koponen, *Form factors of* $B \to \pi\ell\nu$ *and a determination of* $|V_{ub}|$ *with Möbius domain-wall fermions*, *Phys. Rev. D* **106** (2022) 054502 [2203.04938].

[61] Z. Gelzer et al., *Semileptonic B-meson decays to light pseudoscalar mesons on the HISQ ensembles*, *EPJ Web Conf.* **175** (2018) 13024 [1710.09442].

[62] [FNAL/MILC 19A] Z. Gelzer et al., *B-meson semileptonic form factors on (2+1+1)-flavor HISQ ensembles*, *PoS* **LATTICE2019** (2019) 236 [1912.13358].

[63] J. Flynn, R. Hill, A. Jüttner, A. Soni, J.T. Tsang and O. Witzel, *Semileptonic $B \to \pi\ell\nu$, $B \to D\ell\nu$, $B_s \to K\ell\nu$, and $B_s \to D_s\ell\nu$ decays*, *PoS* **LATTICE2019** (2019) 184 [1912.09946].

[64] [HPQCD 15A] B. Colquhoun, R.J. Dowdall, J. Koponen, C.T.H. Davies and G.P. Lepage, *$B \to \pi\ell\nu$ at zero recoil from lattice QCD with physical u/d quarks*, *Phys. Rev.* **D93** (2016) 034502 [1510.07446].

[65] [HPQCD 12C] C. M. Bouchard, G.P. Lepage, C.J. Monahan, H. Na and J. Shigemitsu, *Form factors for B and B_s semileptonic decays with NRQCD/HISQ quarks*, *PoS* **LAT2012** (2012) 118 [1210.6992].

[66] [HPQCD 13F] C. M. Bouchard, G.P. Lepage, J.C. Monahan, H. Na and J. Shigemitsu, *B and B_s semileptonic decay form factors with NRQCD/HISQ quarks*, *PoS* **LATTICE2013** (2014) 387 [1310.3207].

[67] [BMW 12A] S. Borsanyi, S. Dürr, Z. Fodor, C. Hoelbling, S.D. Katz et al., *High-precision scale setting in lattice QCD*, *JHEP* **1209** (2012) 010 [1203.4469].

[68] J. Bijnens and I. Jemos, *Hard Pion Chiral Perturbation Theory for $B \to \pi$ and $D \to \pi$ Formfactors*, *Nucl. Phys.* **B840** (2010) 54 [1006.1197], [Erratum: Nucl. Phys.B844,182(2011)].

[69] G. Colangelo, M. Procura, L. Rothen, R. Stucki and J. Tarrus Castella, *On the factorization of chiral logarithms in the pion form factors*, *JHEP* **09** (2012) 081 [1208.0498].

[70] P. Ball and R. Zwicky, *$|V_{ub}|$ and constraints on the leading-twist pion distribution amplitude from $B \to \pi l\nu$*, *Phys. Lett. B* **625** (2005) 225 [hep-ph/0507076].

[71] D. Bećirević and A.B. Kaidalov, *Comment on the heavy $\to$ light form-factors*, *Phys.Lett.* **B478** (2000) 417 [hep-ph/9904490].

[72] R.J. Hill, *Heavy-to-light meson form-factors at large recoil*, *Phys.Rev.* **D73** (2006) 014012 [hep-ph/0505129].

[73] C.G. Boyd, B. Grinstein and R.F. Lebed, *Constraints on form-factors for exclusive semileptonic heavy to light meson decays*, *Phys.Rev.Lett.* **74** (1995) 4603 [hep-ph/9412324].

[74] [HPQCD 14] C. M. Bouchard, G.P. Lepage, C. Monahan, H. Na and J. Shigemitsu, *$B_s \to K\ell\nu$ form factors from lattice QCD*, *Phys. Rev.* **D90** (2014) 054506 [1406.2279].

[75] C.J. Monahan, C.M. Bouchard, G.P. Lepage, H. Na and J. Shigemitsu, *Form factor ratios for $B_s \to K\,\ell\,\nu$ and $B_s \to D_s\,\ell\,\nu$ semileptonic decays and $|V_{ub}/V_{cb}|$*, 1808.09285.

[76] [FNAL/MILC 17A] Y. Liu et al., *$B_s \to K\ell\nu$ Form Factors with 2+1 Flavors*, *EPJ Web Conf.* **175** (2018) 13008 [1711.08085].

[77] [FNAL/MILC 19] A. Bazavov et al., *$B_s \to K\ell\nu$ decay from lattice QCD*, *Phys. Rev. D* **100** (2019) 034501 [1901.02561].

[78] [RBC/UKQCD 23] J. M. Flynn, R.C. Hill, A. Jüttner, A. Soni, J.T. Tsang and O. Witzel, *Exclusive semileptonic $B_s \to K\ell\nu$ decays on the lattice*, *Phys. Rev. D* **107** (2023) 114512 [2303.11280].

[79] J.M. Flynn, A. Jüttner and J.T. Tsang, *Bayesian inference for form-factor fits regulated by unitarity and analyticity*, 2303.11285.

[80] T. Blake, S. Meinel, M. Rahimi and D. van Dyk, *Dispersive bounds for local form factors in $\Lambda_b \to \Lambda$ transitions*, *Phys. Rev. D* **108** (2023) 094509 [2205.06041].

[81] F. Bahr, D. Banerjee, F. Bernardoni, M. Koren, H. Simma and R. Sommer, *Extraction of bare form factors for $\mathrm{B_s} \to \mathrm{K}\ell\nu$ decays in nonperturbative HQET*, *Int. J. Mod. Phys. A* **34** (2019) 1950166 [1903.05870].

[82] [ALPHA 14B] F. Bahr, F. Bernardoni, J. Bulava, A. Joseph, A. Ramos, H. Simma et al., *Form factors for $\mathrm{B_s} \to \mathrm{K}\ell\nu$ decays in Lattice QCD*, in *8th International Workshop on the CKM Unitarity Triangle (CKM2014) Vienna, Austria, September 8-12, 2014*, 2014, https://inspirehep.net/record/1328088/files/arXiv:1411.3916.pdf [1411.3916].

[83] M. Antonelli et al., *Flavor physics in the quark sector*, *Phys.Rept.* **494** (2010) 197 [0907.5386].

[84] Z. Liu et al., *Form factors for rare B decays: strategy, methodology, and numerical study*, *PoS* **LAT2009** (2009) 242 [0911.2370].

[85] [FNAL/MILC 15D] J. A. Bailey et al., *$B \to Kl^+l^-$ decay form factors from three-flavor lattice QCD*, *Phys. Rev.* **D93** (2016) 025026 [1509.06235].

[86] [HPQCD 13E] C. Bouchard, G.P. Lepage, C. Monahan, H. Na and J. Shigemitsu, *Rare decay $B \to K\ell^+\ell^-$ form factors from lattice QCD*, *Phys. Rev.* **D88** (2013) 054509 [1306.2384], [Erratum: *Phys. Rev.* **D88** (2013) no. 7 079901].

[87] [FNAL/MILC 15E] J. A. Bailey et al., *$B \to \pi\ell\ell$ form factors for new-physics searches from lattice QCD*, *Phys. Rev. Lett.* **115** (2015) 152002 [1507.01618].

[88] [HPQCD 13D] C. Bouchard, G.P. Lepage, C. Monahan, H. Na and J. Shigemitsu, *Standard Model predictions for $B \to Kll$ with form factors from lattice QCD*, *Phys. Rev. Lett.* **111** (2013) 162002 [1306.0434], [Erratum: *Phys. Rev. Lett.* **112** (2014) 149902].

[89] [FNAL/MILC 15F] D. Du, A.X. El-Khadra, S. Gottlieb, A.S. Kronfeld, J. Laiho, E. Lunghi et al., *Phenomenology of semileptonic B-meson decays with form factors from lattice QCD*, *Phys. Rev.* **D93** (2016) 034005 [1510.02349].

[90] LHCb collaboration, *First measurement of the differential branching fraction and CP asymmetry of the $B^\pm \to \pi^\pm\mu^+\mu^-$ decay*, *JHEP* **10** (2015) 034 [1509.00414].

[91] C.B. Lang, D. Mohler, S. Prelovsek and R.M. Woloshyn, *Predicting positive parity B_s mesons from lattice QCD*, *Phys. Lett.* **B750** (2015) 17 [1501.01646].

[92] M. Lüscher, *Volume Dependence of the Energy Spectrum in Massive Quantum Field Theories. 2. Scattering States*, *Commun. Math. Phys.* **105** (1986) 153.

[93] M. Lüscher, *Two particle states on a torus and their relation to the scattering matrix*, *Nucl. Phys.* **B354** (1991) 531.

[94] M. Lüscher, *Signatures of unstable particles in finite volume*, *Nucl. Phys.* **B364** (1991) 237.

[95] M. Lage, U.-G. Meissner and A. Rusetsky, *A Method to measure the antikaon-nucleon scattering length in lattice QCD*, *Phys. Lett.* **B681** (2009) 439 [0905.0069].

[96] V. Bernard, M. Lage, U.G. Meissner and A. Rusetsky, *Scalar mesons in a finite volume*, *JHEP* **01** (2011) 019 [1010.6018].

[97] M. Doring, U.-G. Meissner, E. Oset and A. Rusetsky, *Unitarized Chiral Perturbation Theory in a finite volume: Scalar meson sector*, *Eur. Phys. J.* **A47** (2011) 139 [1107.3988].

[98] M.T. Hansen and S.R. Sharpe, *Multiple-channel generalization of Lellouch-Luscher formula*, *Phys. Rev.* **D86** (2012) 016007 [1204.0826].

[99] R.A. Briceno and Z. Davoudi, *Moving multichannel systems in a finite volume with application to proton-proton fusion*, *Phys. Rev.* **D88** (2013) 094507 [1204.1110].

[100] [HS 14] J. J. Dudek, R.G. Edwards, C.E. Thomas and D.J. Wilson, *Resonances in coupled $\pi K - \eta K$ scattering from quantum chromodynamics*, *Phys. Rev. Lett.* **113** (2014) 182001 [1406.4158].

[101] R.A. Briceño, M.T. Hansen and A. Walker-Loud, *Multichannel $1 \to 2$ transition amplitudes in a finite volume*, *Phys. Rev. D* **91** (2015) 034501 [1406.5965].

[102] R.A. Briceño and M.T. Hansen, *Multichannel $0 \to 2$ and $1 \to 2$ transition amplitudes for arbitrary spin particles in a finite volume*, *Phys. Rev. D* **92** (2015) 074509 [1502.04314].

[103] R.R. Horgan, Z. Liu, S. Meinel and M. Wingate, *Lattice QCD calculation of form factors describing the rare decays $B \to K^* \ell^+ \ell^-$ and $B_s \to \phi \ell^+ \ell^-$*, *Phys. Rev.* **D89** (2014) 094501 [1310.3722].

[104] R.R. Horgan, Z. Liu, S. Meinel and M. Wingate, *Calculation of $B^0 \to K^{*0} \mu^+ \mu^-$ and $B_s^0 \to \phi \mu^+ \mu^-$ observables using form factors from lattice QCD*, *Phys. Rev. Lett.* **112** (2014) 212003 [1310.3887].

[105] R.R. Horgan, Z. Liu, S. Meinel and M. Wingate, *Rare B decays using lattice QCD form factors*, *PoS* **LATTICE2014** (2015) 372 [1501.00367].

[106] [RBC/UKQCD 15B] J. Flynn, A. Jüttner, T. Kawanai, E. Lizarazo and O. Witzel, *Hadronic form factors for rare semileptonic B decays*, in *Proceedings, 33rd International Symposium on Lattice Field Theory (Lattice 2015)*, vol. LATTICE2015, p. 345, 2016, http://inspirehep.net/record/1405735/files/arXiv:1511.06622.pdf [1511.06622].

[107] J. Flynn, T. Izubuchi, A. Jüttner, T. Kawanai, C. Lehner, E. Lizarazo et al., *Form factors for semi-leptonic B decays*, *PoS* **LATTICE2016** (2016) 296 [1612.05112].

[108] E. Lizarazo and O. Witzel, *Non-perturbative determinations of B-meson decay constants and semi-leptonic form factors*, *PoS* **ICHEP2016** (2016) 558 [1612.06113].

[109] A. Sirlin, *Large m_W, m_Z behavior of the $O(\alpha)$ corrections to semileptonic processes mediated by W*, *Nucl.Phys.* **B196** (1982) 83.

[110] M.E. Luke, *Effects of subleading operators in the heavy quark effective theory*, *Phys. Lett.* **B252** (1990) 447.

[111] [FNAL/MILC 04A] M. Okamoto et al., *Semileptonic $D \to \pi/K$ and $B \to \pi/D$ decays in 2+1 flavor lattice QCD*, *Nucl.Phys.Proc.Suppl.* **140** (2005) 461 [hep-lat/0409116].

[112] [FNAL/MILC 13B] S.-W. Qiu , C. DeTar, A.X. El-Khadra, A.S. Kronfeld, J. Laiho et al., *Semileptonic decays $B \to D^{(*)} l\nu$ at nonzero recoil*, *PoS* **LATTICE2013** (2014) 385 [1312.0155].

[113] M. Atoui, V. Morenas, D. Becirevic and F. Sanfilippo, *$b_s \to d_s \ell\nu_\ell$ near zero recoil in and beyond the standard model*, *Eur. Phys. J.* **C74** (2014) 2861 [1310.5238].

[114] [FNAL/MILC 08] C. Bernard et al., *The $\bar{B} \to D^* \ell\bar{\nu}$ form factor at zero recoil from three-flavor lattice QCD: a model independent determination of $|V_{cb}|$*, *Phys.Rev.* **D79** (2009) 014506 [0808.2519].

[115] [FNAL/MILC 14] J. A. Bailey et al., *Update of $|V_{cb}|$ from the $\bar{B} \to D^* \ell\bar{\nu}$ form factor at zero recoil with three-flavor lattice QCD*, *Phys. Rev.* **D89** (2014) 114504 [1403.0635].

[116] [FNAL/MILC 15C] J. A. Bailey et al., *$B \to D\ell\nu$ form factors at nonzero recoil and —V_{cb}— from 2+1-flavor lattice QCD*, *Phys. Rev.* **D92** (2015) 034506 [1503.07237].

[117] [HPQCD 15] H. Na, C.M. Bouchard, G.P. Lepage, C. Monahan and J. Shigemitsu, *$B \to D\ell\nu$ form factors at nonzero recoil and extraction of $|V_{cb}|$*, *Phys. Rev.* **D92** (2015) 054510 [1505.03925].

[118] C.J. Monahan, H. Na, C.M. Bouchard, G.P. Lepage and J. Shigemitsu, *$B_{(s)} \to D_{(s)}$ semileptonic decays with NRQCD-HISQ valence quarks*, *PoS* **LATTICE2016** (2016) 298 [1611.09667].

[119] [HPQCD 17] C. J. Monahan, H. Na, C.M. Bouchard, G.P. Lepage and J. Shigemitsu, *$B_s \to D_s \ell\nu$ Form Factors and the Fragmentation Fraction Ratio f_s/f_d*, *Phys. Rev.* **D95** (2017) 114506 [1703.09728].

[120] J. Harrison, C. Davies and M. Wingate, *$|V_{cb}|$ from the $\bar{B}^0 \to D^{*+} \ell^- \bar{\nu}$ zero-recoil form factor using $2+1+1$ flavour HISQ and NRQCD*, *PoS* **LATTICE2016** (2017) 287 [1612.06716].

[121] [HPQCD 17B] J. Harrison, C. Davies and M. Wingate, *Lattice QCD calculation of the $B_{(s)} \to D^*_{(s)} \ell\nu$ form factors at zero recoil and implications for $|V_{cb}|$*, *Phys. Rev.* **D97** (2018) 054502 [1711.11013].

[122] [HPQCD 19B] E. McLean, C.T.H. Davies, A.T. Lytle and J. Koponen, *Lattice QCD form factor for $B_s \to D_s^* l\nu$ at zero recoil with non-perturbative current renormalisation*, *Phys. Rev. D* **99** (2019) 114512 [1904.02046].

[123] [HPQCD 19] E. McLean, C.T.H. Davies, J. Koponen and A.T. Lytle, *$B_s \to D_s \ell\nu$ Form Factors for the full q^2 range from Lattice QCD with non-perturbatively normalized currents*, *Phys. Rev. D* **101** (2020) 074513 [1906.00701].

[124] LHCb collaboration, *Measurement of $|V_{cb}|$ with $B_s^0 \to D_s^{(*)-}\mu^+\nu_\mu$ decays*, *Phys. Rev. D* **101** (2020) 072004 [2001.03225].

[125] LHCb collaboration, *Precise measurement of the f_s/f_d ratio of fragmentation fractions and of B_s^0 decay branching fractions*, *Phys. Rev. D* **104** (2021) 032005 [2103.06810].

[126] [HPQCD 21B] J. Harrison and C.T.H. Davies, *$B_s \to D_s^*$ Form Factors for the full q^2 range from Lattice QCD*, *Phys. Rev. D* **105** (2022) 094506 [2105.11433].

[127] [FNAL/MILC 21] A. Bazavov et al., *Semileptonic form factors for $B \to D^*\ell\nu$ at nonzero recoil from $2+1$-flavor lattice QCD: Fermilab Lattice and MILC Collaborations*, *Eur. Phys. J. C* **82** (2022) 1141 [2105.14019], [Erratum: Eur.Phys.J.C 83, 21 (2023)].

[128] J. Harrison and C.T.H. Davies, *$B \to D^*$ vector, axial-vector and tensor form factors for the full q^2 range from lattice QCD*, 2304.03137.

[129] [JLQCD 23] Y. Aoki, B. Colquhoun, H. Fukaya, S. Hashimoto, T. Kaneko, R. Kellermann et al., *$B \to D^*\ell\nu_\ell$ semileptonic form factors from lattice QCD with Möbius domain-wall quarks*, 2306.05657.

[130] [ETM 10B] B. Blossier et al., *Average up/down, strange and charm quark masses with $N_f = 2$ twisted mass lattice QCD*, *Phys. Rev.* **D82** (2010) 114513 [1010.3659].

[131] C. Bernard and D. Toussaint, *Effects of nonequilibrated topological charge distributions on pseudoscalar meson masses and decay constants*, *Phys. Rev.* **D97** (2018) 074502 [1707.05430].

[132] [HFLAV 16] Y. Amhis et al., *Averages of b-hadron, c-hadron, and τ-lepton properties as of summer 2016*, *Eur. Phys. J.* **C77** (2017) 895 [1612.07233].

[133] R. Fleischer, N. Serra and N. Tuning, *A New Strategy for B_s Branching Ratio Measurements and the Search for New Physics in $B_s^0 \to \mu^+\mu^-$*, *Phys. Rev. D* **82** (2010) 034038 [1004.3982].

[134] LHCb collaboration, *Determination of f_s/f_d for 7 TeV pp collisions and a measurement of the branching fraction of the decay $B_d \to D^-K^+$*, *Phys. Rev. Lett.* **107** (2011) 211801 [1106.4435].

[135] [FNAL/MILC 12C] J. A. Bailey et al., *$B_s \to D_s/B \to D$ semileptonic form-factor ratios and their application to $BR(B_s^0 \to \mu^+\mu^-)$*, *Phys.Rev.* **D85** (2012) 114502 [1202.6346].

[136] L. Randall and M.B. Wise, *Chiral perturbation theory for $B \to D^*$ and $B \to D$ semileptonic transition matrix elements at zero recoil*, *Phys.Lett.* **B303** (1993) 135 [hep-ph/9212315].

[137] M.J. Savage, *Heavy meson observables at one loop in partially quenched chiral perturbation theory*, *Phys.Rev.* **D65** (2002) 034014 [hep-ph/0109190].

[138] S. Hashimoto, A.S. Kronfeld, P.B. Mackenzie, S.M. Ryan and J.N. Simone, *Lattice calculation of the zero recoil form-factor of $\bar{B} \to D^* \ell \bar{\nu}$: toward a model independent determination of $|V_{cb}|$*, *Phys.Rev.* **D66** (2002) 014503 [hep-ph/0110253].

[139] [HPQCD 20B] J. Harrison, C.T.H. Davies and A. Lytle, *$B_c \to J/\psi$ form factors for the full q^2 range from lattice QCD*, *Phys. Rev. D* **102** (2020) 094518 [2007.06957].

[140] A. Lytle, B. Colquhoun, C. Davies, J. Koponen and C. McNeile, *Semileptonic B_c decays from full lattice QCD*, *PoS* **BEAUTY2016** (2016) 069 [1605.05645].

[141] [HPQCD 16] B. Colquhoun, C. Davies, J. Koponen, A. Lytle and C. McNeile, *B_c decays from highly improved staggered quarks and NRQCD*, *PoS* **LATTICE2016** (2016) 281 [1611.01987].

[142] LHCb RICH Group collaboration, *Performance of the LHCb RICH detector at the LHC*, *Eur. Phys. J. C* **73** (2013) 2431 [1211.6759].

[143] LHCb collaboration, *Determination of the quark coupling strength $|V_{ub}|$ using baryonic decays*, *Nature Phys.* **11** (2015) 743 [1504.01568].

[144] T. Feldmann and M.W.Y. Yip, *Form Factors for Lambda$_b \to \Lambda$ Transitions in SCET*, *Phys. Rev.* **D85** (2012) 014035 [1111.1844], [Erratum: Phys. Rev.D86,079901(2012)].

[145] W. Detmold, C. Lehner and S. Meinel, *$\Lambda_b \to p \ell^- \bar{\nu}_\ell$ and $\Lambda_b \to \Lambda_c \ell^- \bar{\nu}_\ell$ form factors from lattice QCD with relativistic heavy quarks*, *Phys. Rev.* **D92** (2015) 034503 [1503.01421].

[146] A. Datta, S. Kamali, S. Meinel and A. Rashed, *Phenomenology of $\Lambda_b \to \Lambda_c \tau \overline{\nu}_\tau$ using lattice QCD calculations*, *JHEP* **08** (2017) 131 [1702.02243].

[147] S. Meinel and G. Rendon, *$\Lambda_b \to \Lambda_c^*(2595, 2625) \ell^- \bar{\nu}$ form factors from lattice QCD*, *Phys. Rev. D* **103** (2021) 094516 [2103.08775].

[148] T.D. Cohen, H. Lamm and R.F. Lebed, *Precision Model-Independent Bounds from Global Analysis of $b \to c \ell \nu$ Form Factors*, *Phys. Rev. D* **100** (2019) 094503 [1909.10691].

[149] T. Blake and M. Kreps, *Angular distribution of polarised Λ_b baryons decaying to $\Lambda \ell^+ \ell^-$*, *JHEP* **11** (2017) 138 [1710.00746].

[150] LHCb collaboration, *Angular moments of the decay $\Lambda_b^0 \to \Lambda \mu^+ \mu^-$ at low hadronic recoil*, *JHEP* **09** (2018) 146 [1808.00264].

[151] W. Detmold, C.J.D. Lin, S. Meinel and M. Wingate, *$\Lambda_b \to \Lambda \ell^+ \ell^-$ form factors and differential branching fraction from lattice QCD*, *Phys. Rev.* **D87** (2013) 074502 [1212.4827].

[152] W. Detmold and S. Meinel, *$\Lambda_b \to \Lambda \ell^+ \ell^-$ form factors, differential branching fraction, and angular observables from lattice QCD with relativistic b quarks*, *Phys. Rev.* **D93** (2016) 074501 [1602.01399].

[153] T. Blake, S. Meinel and D. van Dyk, *Bayesian Analysis of $b \to s \mu^+ \mu^-$ Wilson Coefficients using the Full Angular Distribution of $\Lambda_b \to \Lambda(\to p \pi^-) \mu^+ \mu^-$ Decays*, *Phys. Rev. D* **101** (2020) 035023 [1912.05811].

[154] LHCb collaboration, *Differential branching fraction and angular analysis of $\Lambda_b^0 \to \Lambda\mu^+\mu^-$ decays*, *JHEP* **06** (2015) 115 [1503.07138], [Erratum: JHEP 09, 145 (2018)].

[155] M. Algueró, B. Capdevila, A. Crivellin, S. Descotes-Genon, P. Masjuan, J. Matias et al., *Emerging patterns of New Physics with and without Lepton Flavour Universal contributions*, *Eur. Phys. J. C* **79** (2019) 714 [1903.09578], [Addendum: Eur.Phys.J.C 80, 511 (2020)].

[156] W. Altmannshofer and P. Stangl, *New Physics in Rare B Decays after Moriond 2021*, *Eur. Phys. J. C* **81** (2021) 952 [2103.13370].

[157] S. Meinel and G. Rendon, *$\Lambda_b \to \Lambda^*(1520)\ell^+\ell^-$ form factors from lattice QCD*, *Phys. Rev. D* **103** (2021) 074505 [2009.09313].

[158] W. Detmold, C.J.D. Lin, S. Meinel and M. Wingate, *$\Lambda_b \to p l^- \bar{\nu}_\ell$ form factors from lattice QCD with static b quarks*, *Phys. Rev.* **D88** (2013) 014512 [1306.0446].

[159] Belle collaboration, *Measurement of $B^- \to \tau^- \bar{\nu}_\tau$ with a hadronic tagging method using the full data sample of Belle*, *Phys. Rev. Lett.* **110** (2013) 131801 [1208.4678].

[160] BABAR collaboration, *A search for $B^+ \to \ell^+\nu_\ell$ recoiling against $B^- \to D^0\ell^-\bar{\nu}X$*, *Phys.Rev.* **D81** (2010) 051101 [0912.2453].

[161] BABAR collaboration, *Study of $B \to \pi\ell\nu$ and $B \to \rho\ell\nu$ Decays and Determination of $|V_{ub}|$*, *Phys.Rev.* **D83** (2011) 032007 [1005.3288], 47 pages, 26 postscript figures, accepted by Phys. Rev. D.

[162] BABAR collaboration, *Branching fraction and form-factor shape measurements of exclusive charmless semileptonic B decays, and determination of $|V_{ub}|$*, *Phys.Rev.* **D86** (2012) 092004 [1208.1253].

[163] Belle collaboration, *Measurement of the decay $B^0 \to \pi^-\ell^+\nu$ and determination of $|V_{ub}|$*, *Phys.Rev.* **D83** (2011) 071101 [1012.0090].

[164] Belle collaboration, *Study of Exclusive $B \to X_u\ell\nu$ Decays and Extraction of $\|V_{ub}\|$ using Full Reconstruction Tagging at the Belle Experiment*, *Phys. Rev.* **D88** (2013) 032005 [1306.2781].

[165] P. Gambino, P. Giordano, G. Ossola and N. Uraltsev, *Inclusive semileptonic B decays and the determination of $|V_{ub}|$*, *JHEP* **0710** (2007) 058 [0707.2493].

[166] [HFLAV 18] Y. Amhis et al., *Averages of b-hadron, c-hadron, and τ-lepton properties as of 2018*, *Eur. Phys. J. C* **81** (2021) 226 [1909.12524].

[167] P. Urquijo, *Physics prospects at the Belle II experiment*, *Nucl. Part. Phys. Proc.* **263-264** (2015) 15.

[168] E. Kou et al., *The Belle II Physics Book*, *PTEP* **2019** (2019) 123C01 [1808.10567], [Erratum: PTEP 2020, 029201 (2020)].

[169] I. Caprini, L. Lellouch and M. Neubert, *Dispersive bounds on the shape of $\bar{B} \to D^{(*)}$ lepton anti-neutrino form-factors*, *Nucl. Phys.* **B530** (1998) 153 [hep-ph/9712417].

[170] J.P. Lees et al., *A test of heavy quark effective theory using a four-dimensional angular analysis of $\overline{B} \to D^* \ell^- \overline{\nu}_\ell$*, *Phys. Rev. Lett.* **123** (2019) 091801 [1903.10002].

[171] Belle collaboration, *Measurement of the CKM matrix element $|V_{cb}|$ from $B^0 \to D^{*-} \ell^+ \nu_\ell$ at Belle*, *Phys. Rev. D* **100** (2019) 052007 [1809.03290], [Erratum: Phys.Rev.D 103, 079901 (2021)].

[172] Belle collaboration, *Measurement of differential distributions of B→D*ℓν ¯ℓ and implications on —Vcb—*, *Phys. Rev. D* **108** (2023) 012002 [2301.07529].

[173] Belle-II collaboration, *Determination of —Vcb— using B ¯0→D*+ℓ−ν ¯ℓ decays with Belle II*, *Phys. Rev. D* **108** (2023) 092013 [2310.01170].

[174] D. Bigi, P. Gambino and S. Schacht, *A fresh look at the determination of $|V_{cb}|$ from $B \to D^* \ell \nu$*, *Phys. Lett.* **B769** (2017) 441 [1703.06124].

[175] F.U. Bernlochner, Z. Ligeti, M. Papucci and D.J. Robinson, *Tensions and correlations in $|V_{cb}|$ determinations*, *Phys. Rev.* **D96** (2017) 091503 [1708.07134].

[176] B. Grinstein and A. Kobach, *Model-Independent Extraction of $|V_{cb}|$ from $\bar{B} \to D^* \ell \overline{\nu}$*, *Phys. Lett.* **B771** (2017) 359 [1703.08170].

[177] C.G. Boyd, B. Grinstein and R.F. Lebed, *Precision corrections to dispersive bounds on form-factors*, *Phys. Rev.* **D56** (1997) 6895 [hep-ph/9705252].

[178] P. Gambino, M. Jung and S. Schacht, *The V_{cb} puzzle: an update*, *Phys. Lett.* **B795** (2019) 386 [1905.08209].

[179] Belle collaboration, *Measurement of the decay $B \to D \ell \nu_\ell$ in fully reconstructed events and determination of the Cabibbo-Kobayashi-Maskawa matrix element $|V_{cb}|$*, *Phys. Rev.* **D93** (2016) 032006 [1510.03657].

[180] BaBar collaboration, *Measurement of $|V(cb)|$ and the Form-Factor Slope in $\overline{B} \to D \ell^- \overline{\nu}_\ell$ Decays in Events Tagged by a Fully Reconstructed B Meson*, *Phys. Rev. Lett.* **104** (2010) 011802 [0904.4063].

[181] D. Bigi and P. Gambino, *Revisiting $B \to D \ell \nu$*, *Phys. Rev.* **D94** (2016) 094008 [1606.08030].

[182] Particle Data Group collaboration, *Review of Particle Physics*, *Phys. Rev.* **D98** (2018) 030001.

[183] M. Bordone, B. Capdevila and P. Gambino, *Three loop calculations and inclusive Vcb*, *Phys. Lett. B* **822** (2021) 136679 [2107.00604].

[184] P. Gambino, K.J. Healey and S. Turczyk, *Taming the higher power corrections in semileptonic B decays*, *Phys. Lett.* **B763** (2016) 60 [1606.06174].

[185] LHCb collaboration, *First observation of the decay $B_s^0 \to K^- \mu^+ \nu_\mu$ and Measurement of $|V_{ub}|/|V_{cb}|$*, *Phys. Rev. Lett.* **126** (2021) 081804 [2012.05143].

[186] Belle collaboration, *Measurements of partial branching fractions of inclusive $B \to X_u \ell \nu_\ell$ decays with hadronic tagging*, *Phys. Rev. D* **104** (2021) 012008 [2102.00020].